Advanced Energy Materials

ADVANCED ENERGY MATERIALS
www.advenergymat.de

REVIEW OPEN ACCESS

Device Performance of Emerging Photovoltaic Materials (Version 6)

Osbel Almora[1,2] | Agustin O. Alvarez[3] | Derya Baran[4,5] | Carlos I. Cabrera[6] | Luigi A. Castriotta[7] | Bruno Ehrler[3] | Sule Erten-Ela[8] | Kenjiro Fukuda[9] | Fei Guo[10] | Jens Hauch[11] | Anita W.Y. Ho-Baillie[12] | T. Jesper Jacobsson[13] | Rene A. J. Janssen[14,15] | Thomas Kirchartz[16,17] | Maria A. Loi[18] | Richard R. Lunt[19] | Xavier Mathew[20] | Jie Min[21] | David B. Mitzi[22] | Mohammad K. Nazeeruddin[23] | Ana F. Nogueira[24] | Ulrich W. Paetzold[25,26] | Nam-Gyu Park[27] | Barry P. Rand[28] | Henry Snaith[29] | Takao Someya[30,31,32] | Christian Sprau[26] | Lulu Sun[31,32] | Karen Forberich[11] | Christoph J. Brabec[2,11,16]

[1]Universitat Rovira i Virgili, Tarragona43007, Spain | [2]Erlangen Graduate School of Advanced Optical Technologies (SAOT), 91052, Erlangen, Germany | [3]LMPV-Sustainable Energy Materials Department, AMOLF, Amsterdam1098 XG, The Netherlands | [4]Materials Science and Engineering, Physical Science and Engineering (PSE) Division, King Abdullah University of Science and Technology (KAUST), Thuwal23955-6900, Saudi Arabia | [5]Center for Renewable Energy and Storage Technologies (CREST), King Abdullah University of Science and Technology (KAUST), Thuwal23955-6900, Saudi Arabia | [6]Unidad Académica de Ciencia y Tecnología de la Luz y la Materia, Universidad Autónoma de Zacatecas, Zacatecas98160, Mexico | [7]Department of Electronic Engineering, CHOSE (Centre for Hybrid and Organic Solar Energy), Tor Vergata University of Rome, Rome00133, Italy | [8]Ege University, Solar Energy Institute, Bornova, Izmir 35100, Turkey | [9]Division of Electrical, Electronic and Infocommunications Engineering, Graduate School of Engineering, The University of Osaka, Suita, Osaka 565-0871, Japan | [10]Institute of New Energy Technology, College of Physics & Optoelectronic Engineering, Jinan University, Guangzhou510632, China | [11]Forschungszentrum Jülich GmbH, Helmholtz-Institut Erlangen-Nürnberg for Renewable Energy (HI ERN), 91058, Erlangen, Germany | [12]School of Physics and The University of Sydney Nano Institute, The University of Sydney, Sydney, NSW 2006, Australia | [13]Department of Physics, Chemistry and Biology (IFM), Linköping University, Linköping58339, Sweden | [14]Molecular Materials and Nanosystems & Institute for Complex Molecular Systems, Eindhoven University of Technology, Eindhoven5600 MB, The Netherlands | [15]Dutch Institute for Fundamental Energy Research, Eindhoven5612 AJ, The Netherlands | [16]IMD-3 Photovoltaics, Forschungszentrum Jülich, 52425, Jülich, Germany | [17]Faculty of Engineering and CENIDE, University of Duisburg-Essen 47057, Duisburg, Germany | [18]Zernike Institute of Advanced Materials, University of Groningen, Groningen, AG NL-9747, The Netherlands | [19]Department of Chemical Engineering and Materials Science, Department of Physics and Astronomy, Michigan State University, East Lansing, MI 48824, USA | [20]Instituto de Energías Renovables, Universidad Nacional Autónoma de México, Temixco, Morelos 62580, México | [21]The Institute for Advanced Studies, Wuhan University, Wuhan430072, China | [22]Department of Mechanical Engineering and Material Science & Department of Chemistry, Duke University, Durham, NC 27708, USA | [23]Group for Molecular Engineering and Functional Materials, Ecole Polytechnique Fédérale de Lausanne, Institut des Sciences et Ingénierie Chimiques, SionCH-1951, Switzerland | [24]Instituto de Quimica, Universidade Estadual de Campinas, Campinas, Sao Paulo 13083-859, Brazil | [25]Institute of Microstructure Technology (IMT), Karlsruhe Institute of Technology (KIT), 76344, Eggenstein-Leopoldshafen, Germany | [26]Light Technology Institute (LTI), Karlsruhe Institute of Technology (KIT) 76131, Karlsruhe, Germany | [27]School of Chemical Engineering, SKKU Institute of Energy Science and Technology (SIEST), Sungkyunkwan University, Suwon16419, Republic of Korea | [28]Department of Electrical and Computer Engineering and Andlinger Center for Energy and the Environment, Princeton University, Princeton, New Jersey 08544, USA | [29]Clarendon Laboratory, Department of Physics, University of Oxford, OxfordOX1 3PU, UK | [30]Electrical Engineering and Information Systems, The University of Tokyo, Tokyo113-8656, Japan | [31]Thin-Film Device Laboratory, RIKEN, Saitama351-0198, Japan | [32]Center for Emergent Matter Science, RIKEN, Saitama351-0198, Japan

Correspondence: Osbel Almora (osbel.almora@urv.cat) | Karen Forberich (k.forberich@fz-juelich.de) | Christoph J. Brabec (christoph.brabec@fau.de)

Received: 29 September 2025 | **Revised:** 19 November 2025 | **Accepted:** 20 November 2025

Keywords: bandgap energy | flexible photovoltaics | multijunction solar cells | photovoltaic device operational stability | power conversion efficiency | transparent and semitransparent solar cells

ABSTRACT

This 6th annual Emerging PV Report surveys peer-reviewed advances since August 2024 across perovskite, organic, kesterite, matildite, antimony seleno-sulfide, selenium, and tandem solar cell architectures. Updated graphs, tables, and analyses compile the best-performing devices from the emerging-pv.org database, benchmarking power conversion efficiency (*PCE*), flexible photovoltaic fatigue factor (*F*), light-utilization efficiency (*LUE*), and stability-test energy yield (STEY) against detailed-balance efficiency limits as functions of photovoltaic bandgap, and average visible transmittance (*AVT*) for (semi-)transparent devices. Beyond efficiency, operational stability is assessed via degradation rates (*DR*) and t_{95} lifetimes. Highlights include single-junction perovskite cells with efficiencies above 27%, organics surpassing 20%, and new Si/perovskite tandems exceeding 34%. Although multiple record efficiencies have been achieved this year, advances in mechanical robustness and operational stability remain inconsistent, especially in complex tandem stacks, emphasizing the urgent need for standardized protocols, improved large-area homogeneity, and database-driven benchmarks to accelerate the transition from laboratory demonstrations to scalable, real-world deployment.

1 | Introduction

Emerging photovoltaic (e-PV) devices (see Table 1) [1–5] hold great promise for providing cheaper, cleaner, and more versatile scalable electricity generation, serving as an alternative and/or complement to traditional photovoltaics (PVs) such as silicon devices. Both in the context of classical silicon photovoltaics as well as e-PV devices, the heterostructure architecture has emerged as the most successful approach and is used with absorber materials such as metal-halide perovskites, polymers, dyes, kesterites, and matildites. However, optimizing these devices for higher power conversion efficiency (PCE) values, larger surface areas and enhanced performance durability has been challenging, primarily due to the complexity of the interfaces within the devices and the intrinsic properties of e-PV materials.

Versatility is a key attribute of e-PV, as increasing the PCE for large-scale grid-connected electricity production is not the only research focus. Over the last decade, there has been growing research interest in potential applications such as flexible, transparent, and integrated PVs. This trend is evident in the increasing percentage of annual publications addressing these topics. However, unlike the PCE results, which can be certified by several international institutions, the standardized quantitative evaluation, and certification of other critical aspects of e-PV devices, essential for proper validation and comparison, remain a work in progress. In this context, the emerging PV initiative [6], along with its accompanying website and database, aims to establish an international framework and benchmarking system for the systematic collection, presentation, and analysis of data, serving as a reference for best practices and state-of-the-art reports.

The state-of-the-art achievements in e-PV devices, as reflected in academic publications detailing top-performing cells, have been systematically parameterized and reported since 2020 through the annual emerging PV reports (e-PVr) [1–5], of which this is the sixth edition. This report compiles the performance data of the best e-PV devices into comprehensible tables, and the PCE values are put into perspective by comparing the devices with respect to the bandgap energy of the absorber material, number of junctions, application class, and performance stability. Notably, we present performance parameters for each technology and compare the experimental data to the corresponding theoretical limit in the detailed balance (DB) model [7–9].

In this review article, we present updated graphs and tables of the best-performing research photovoltaic cells, incorporating the latest reports since August 2024. This sixth edition includes more than a hundred new research articles (Tables 3–25), selected in line with our inclusion criteria (see Section 1.1) from over 400 new entries added to the emerging-pv.org database during the past year. The following sections not only describe the updated plots and tables but also highlight and discuss the most relevant and recent achievements across each technology. Importantly, this year's report introduces mechanical and operational stability analyses through the flexible PV fatigue factor (*F*) [10] and the t_{95} operational lifetime, respectively. Additionally, we provide a commentary on broader trends and the overall progress observed in the field over the past year.

1.1 | Data Inclusion Criteria, Definitions, and Emerging-pv.org

Consistent with previous e-PVr [4, 5], to be considered for these surveys, the data must meet a set of specific criteria. First, it should be published in a peer-reviewed article in an academic journal, and the article should include a "methods" section that allows experimental replication. Second, the article should provide essential data and a clear description for experimental reproducibility and self-consistency checks (e.g., such as those at emerging-pv.org) [6].

Third, provided publication and sufficient description for reportability, data are collected for categories with established and broadly adopted characterization protocols: absolute efficiency under 1 sun, flexibility, transparency, and operational stability (Sections 2–5). These categories (i) represent primary research interests within emerging photovoltaics; (ii) rely on well-defined and comparable metrics; (iii) can be quantitatively benchmarked across technologies and against theoretical limits (e.g., the detailed-balance efficiency limit); and (iv) are implemented within the emerging-pv.org database with automated and supervised consistency checks. A detailed description of the inclusion

TABLE 1 | Abbreviations for PV technologies or material families (adapted from the e-PVr version 3) [3].

Abbreviation	Meaning and comments
Established photovoltaics	
a-Si:H	Amorphous silicon single junction photovoltaic cell (including a-SiGe:H devices).
CdTe	Cadmium telluride single junction photovoltaic cell
CIGS	Copper-indium-gallium-selenide ($CuIn_xGa_{1-x}Se_2$)-based single junction photovoltaic cell
GaAs	Gallium arsenide single junction photovoltaic cell
Si	Monocrystalline or polycrystalline silicon single junction photovoltaic cell, including homo- and heterojunction structures.
Emerging photovoltaics	
AgBiS	Silver bismuth sulfide ($AgBiS_2$)-based single junction photovoltaic cells, the so-called matildite solar cells.
CIGS/DSSC	Monolithic/2-terminal tandem photovoltaic cell: $CuIn_xGa_{1-x}Se_2$-based bottom sub-cell and dye-sensitized top sub-cell
CIGS/perovskite	Monolithic/2-terminal tandem photovoltaic cell: $CuIn_xGa_{1-x}Se_2$-based bottom sub-cell and perovskite-based top sub-cell
CIGS/AlGaAs/GaInP	Monolithic/2-terminal triple junction photovoltaic cell: $CuIn_xGa_{1-x}Se_2$-based bottom sub-cell, AlGaAs-based middle sub-cell, and GaInP-based top sub-cell
CZTS	$Cu_2ZnSn(S,Se)_4$-based single junction photovoltaic cell
DSSC	Dye-sensitized single-junction photovoltaic cell
DSSC/perovskite	Monolithic/2-terminal tandem photovoltaic cell: dye-sensitized bottom sub-cell and perovskite-based top sub-cell
GaAs/GaInP	Monolithic/2-terminal tandem photovoltaic cell: GaAs-based bottom sub-cell and GaInP-based top sub-cell
GaAs/perovskite	Monolithic/2-terminal tandem photovoltaic cell: GaAs-based bottom sub-cell and perovskite-based top sub-cell
GaAs(In,Bi,Al,P)	Monolithic/2-terminal triple junction photovoltaic cell including GaAs and no other material family specified in this table. For example: InGaAs- or GaAsBi-based bottom sub-cell, GaAs-based middle sub-cell, and GaInP- or AlGaAs-based top sub-cell
nc-Si/a-Si	Monolithic/2-terminal tandem photovoltaic cell: nanocrystalline or microcrystalline Si bottom sub-cell and amorphous Si top sub-cell
nc-Si/nc-Si/a-Si	Monolithic/2-terminal triple junction photovoltaic cell: nanocrystalline silicon-based bottom and middle sub-cells, and amorphous silicon-based top sub-cell
OPV	Organic photovoltaic material-based single junction photovoltaic cell
OPV/a-Si	Monolithic/2-terminal tandem photovoltaic cell: organic-based bottom sub-cell and amorphous silicon-based top sub-cell
OPV/perovskite	Monolithic/2-terminal tandem photovoltaic cell: the bottom and top sub-cells are organic- and perovskite-based, respectively or vice versa.
PSC, pvk, perov	Perovskite single junction photovoltaic cell. "Pvk" or "perov" may also be used in plot legends for abbreviating perovskite sub-cells in multijunction devices.
SbS	Antimony trisulfide and/or triselenide ($Sb_2(S,Se)_3$)-based single junction photovoltaic cell
Se	Selenium-based single junction photovoltaic cell
Si/DSSC	Monolithic/2-terminal tandem photovoltaic cell: Si-based bottom sub-cell and dye sensitized top sub-cell
Si/GaAsP	Monolithic/2-terminal tandem photovoltaic cell: Si-based bottom sub-cell and $GaAs_{1-x}P_x$ -based top sub-cell
Si/GaInAsP/InGaP	Monolithic/2-terminal triple junction photovoltaic cell: silicon-based bottom sub-cell, GaInAsP-based middle sub-cell and GaInP-based top sub-cell

(Continues)

TABLE 1 | (Continued)

Abbreviation	Meaning and comments
Si/perov/perov	Monolithic/2-terminal triple junction photovoltaic cell: Si-based bottom sub-cell and perovskite-based middle and top sub-cells
Si/perovskite	Monolithic/2-terminal tandem photovoltaic cell: Si-based bottom sub-cell and perovskite-based top sub-cell
TLSC	Transparent luminescent solar concentrator, including a lightguide, luminophore, and mounted solar cell(s).

criteria per category is included in Sections S1.5–S1.6 of the Supporting Information, including Table S2, which summarizes the minimal mandatory data. Further categories are under active consideration for future inclusion in the emerging-pv.org database and subsequent editions of this annual survey. For example, indoor photovoltaics has gained significant momentum and has recently advanced in standardized measurement protocols and quantitative figures of merit [11–13], making it a strong candidate for future implementation of dedicated self-consistency checks within the emerging-pv.org database.

Notable updates to the inclusion criteria relate to the description of mechanical stability bending tests of flexible solar cells. New mandatory requirements for these reports include the number of bending cycles, bending strain, and PCE values before and after the bending test [10, 14]. For the bending strain, the estimation of the device thickness (including substrate and encapsulation, if appropriate) and bending radius is the minimum requirement in the single-layer strain model. Importantly, while Section 3 will address "notable exceptions" concerning high PCE values and the most relevant bending test results, our general rule, consistent with the definition of the fatigue factor (F, see Equation 5 in table 2), is to include only those studies where bending tests result in *PCE* retention below 99%. In this way, performance losses greater than 1% can be more reliably attributed to genuine degradation processes rather than measurement artifacts. As the fatigue factor reflects both *PCE* retention and bending test conditions, it is recommended to report clear quantitative correlations between test parameters and *PCE* losses to better define the mechanical performance limits of the device. Bending tests that show no *PCE* decrease, likely due to insufficient applied strain, offer limited insight into the actual mechanical stability.

A discussion on the "emergence" labeling for PV devices and its relation with the PV technology generations and research can be found in version 4 of the e-PVr [4]. The equations, definitions, and useful references already presented in the previous e-PVr [5] and updated in the current version are summarized in Table 2. Notably, we here emphasize the use of the definition of the photovoltaic bandgap energy as the inflection point of the absorption threshold of the EQE spectrum (see Figure S1) [15, 16]. This definition not only characterizes the operational response of the entire device (rather than an independent absorber layer or a combination of sub-layers), but also provides a framework for comparing different emerging technologies, in particular where a single optical bandgap energy is not directly defined [1], such as in organic photovoltaics.

Following the previous e-PVr [5], each section highlights the best-performing cells reported in the literature, grouped by technology, material family, or application (abbreviations in Table 1). For multijunction PV cells (see Figure S2), we define the top sub-cell as that which receives the full incident photon flux and typically has the highest bandgap ($E_{g,top}$) while the bottom sub-cell receives the residual flux and typically has the lowest bandgap ($E_{g,bottom}$). Two-junction (tandem) devices include only top and bottom sub-cells, whereas triple-junction cells feature a middle sub-cell typically with a bandgap ($E_{g,mid}$) between those of the top and bottom layers.

Significant upgrades to the Emerging-PV website and database [6] since August 2024 include the enhancement of the flexible photovoltaic form with the calculation of fatigue factor (Equation 5 in Table 2), and the generation of digitally signed data report certificates. The latter functionality enables users to download a comprehensive summary of their personal uploaded data, encompassing all derived parameters and automatically generated messages related to the implemented calculations and consistency checks.

2 | Highest Power Conversion Efficiency Photovoltaic Cells

To introduce the recent progress in the e-PV field, we plotted the reported *PCE* values of all emerging-pv.org database entries versus publication date for the two most widely studied single-junction technologies: perovskite (Figure 1a,b) and organic (Figure 1c,d) solar cells, with data points colored according to their bandgap energy. This dataset includes, but is not limited to, the records listed in Tables 3–25 and represents, to the best of our knowledge, the subset of publications on emerging photovoltaics that report device progress in line with our inclusion criteria. This list excludes manuscripts focused primarily on materials, theory, or reviews.

Several trends emerge. First, the number of publications has markedly increased in the past three years for both PSCs and OPV technologies. This surge in high-performance reports reflects the growing maturity of these systems as they move closer industrial deployment. Other factors may also contribute, such as improvements in database screening and a shift in research focus from fundamental science during the early stages of development toward material and device engineering aimed primarily at performance optimization. This trend aligns with the relatively stable annual publication rate for solar cells overall,

TABLE 2 | Equations and definitions (updated after e-PVr version 3) [4].

No.	Equation	Definitions and comments	Refs.
(1)	$PCE = \frac{P_{out}}{P_{in}} = \frac{V_{oc} \cdot J_{sc} \cdot FF}{P_{in}}$	PCE, power conversion efficiency; P_{out}, output power density; P_{in}, incoming power density; V_{oc}, open-circuit voltage; J_{sc}, short-circuit current density; *FF*, fill factor	[1]
(2)	$EQE = \frac{Q_m}{1+\exp[\kappa \frac{(\lambda - \frac{hc}{E_g})}{\lambda_s}]}$	Procedure to determine E_g from the EQE(λ) spectrum: EQE, external quantum efficiency; λ, wavelength; Q_m, maximum EQE value just above the bandgap absorption threshold; h, Planck's constant; c, speed of light; E_g, photovoltaic bandgap energy; λ_s, sigmoid wavelength width parameter (EQE onset quality wavelength), $\kappa = \ln[7+4\sqrt{3}] \approx 2.63$, dimensionless coefficient related to the second derivative of the sigmoid.	[15]
(3)	$J_{sc,EQE} = \frac{q}{hc} \int EQE(\lambda) \lambda \, \Gamma_{AM1.5G}(\lambda) d\lambda$	$J_{sc,EQE}$, short-circuit current density as integrated from the EQE for the standard 1 sun illumination intensity AM1.5G spectrum $\Gamma_{AM1.5G}$ (typically in units of $W \cdot m^{-2} \cdot nm^{-1}$); q is the elementary charge.	
(4)	$EDBL = \frac{PCE^{real}}{PCE^{ideal}} = \frac{J_{sc}^{real}}{J_{sc}^{ideal}} \frac{V_{oc}^{real}}{V_{oc}^{ideal}} \frac{FF^{real}}{FF^{ideal}}$	*EDBL*, experiment-to-detailed balance-limit ratio, the "real" superscript refers to the experimental values; the "ideal" superscript refers to the theoretical limit of each performance parameter as in the detailed-balance (DB) models [7–9], e.g., the highest efficiency for a single junction cell with absorber material of bandgap energy E_g at a temperature T_c under a spectral irradiance Γ. The proper application of a detailed-balance performance limit model on an experiment implies $EDBL \leq 1$.	[16, 17]
(5)	$F = \frac{PCE_{final} - PCE_{initial}}{PCE_{initial} \cdot \varepsilon \cdot \log_{10}[N_{BC}]}$	*F*, flexible photovoltaic fatigue factor; $PCE_{initial}$(PCE_{final}) power conversion efficiency before (after) the mechanical bending test; ε, strain applied to the sample and; N_{BC}, the number of bending cycles during the bending test.	[10]
(6)	$AVT = \frac{\int T(\lambda) P(\lambda) \lambda \Gamma_{AM1.5G}(\lambda) d\lambda}{\int P(\lambda) \lambda \, \Gamma_{AM1.5G}(\lambda) d\lambda}$	*AVT*, average visible transmittance; *T*, transmittance; *P*, photopic response of the human eye.	[18]
(7)	$LUE = AVT \cdot PCE$	*LUE*, light utilization efficiency	[19]
(8)	$PBCC = EQE(\lambda) + T(\lambda) + R(\lambda)$	The photon balance consistency check implies PBCC ≤ 1	[18]
(9)	$E_{\Delta\tau} = \int_0^{\Delta\tau} P_{out} dt = \int_0^{\Delta\tau} P_{in} PCE dt$	$\Delta\tau$, operational stability test time; $E_{\Delta\tau}$, operational stability test energy yield (STEY) for a test of duration $\Delta\tau$; t, time; STEY is taken for 200 h and 1 000 h of stability tests as E_{200h} and E_{1000h}, respectively.	[1]
(10)	$DR_{\Delta\tau} = \frac{PCE(\tau) - PCE(0)}{\Delta\tau}$	$DR_{\Delta\tau}$, effective overall degradation rate for an operational stability test of duration $\Delta\tau$; DR_{200h} and DR_{1000h} are taken as the overall degradation rates for 200 h and 1000 h of stability tests, respectively.	[1]
(11)	$PCE\,(t_{95}) = 0.95\, PCE(0)$	t_{95}, time for which the power conversion efficiency reaches 95% of their initial value $PCE(0)$ during an operational stability test.	

and specifically for OPV devices, while perovskite publications continue to rise (see Figure S3).

Before 2020, reported bandgap values were broadly distributed, despite some clustering. After 2020, however, a noticeable narrowing of focus is visible: OPV records centered almost exclusively on absorber blends with ~1.4 eV bandgaps (Figure 1c,d), while PSCs increasingly concentrated on compositions close to $FAPbI_3$ with ~1.55 eV bandgaps (Figure 1a,b). For perovskites, higher and lower bandgaps remain represented, typically for devices designed for multijunction or transparent applications. Entries for OPVs, by contrast, show almost no variation, indicating that the community has converged on a narrow set of material systems with bandgaps of around 1.4 eV since the invention of the Y-series of non-fullerene acceptors [20]. Importantly, whereas only a handful of entries exceeded 26% *PCE* for perovskites and 20% for OPVs in e-PV Report 5 [5], such values are now routinely observed in the present dataset.

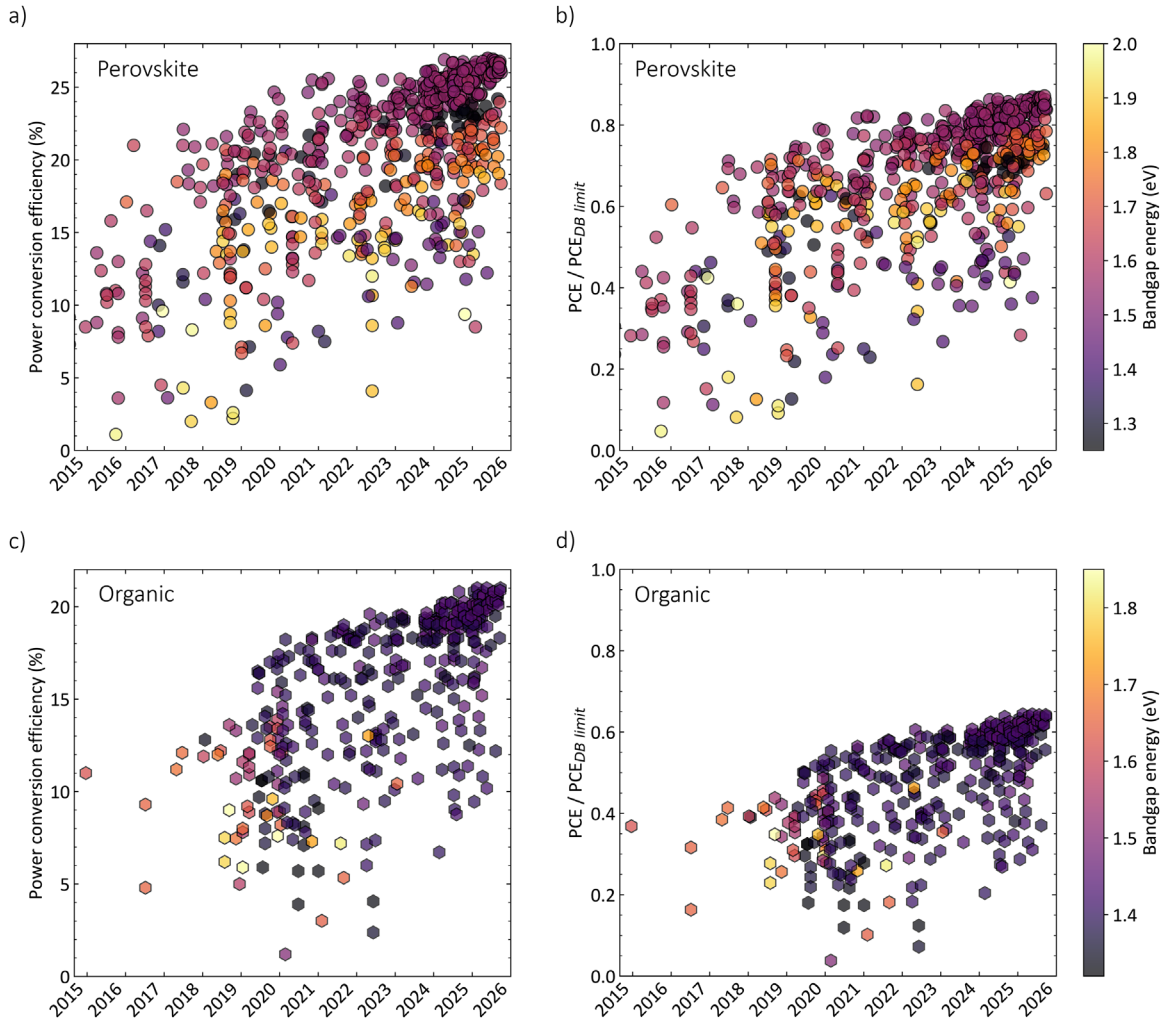

FIGURE 1 | Power conversion efficiency of publications recorded in the emerging-pv.org database over publication date and colored according to the bandgap energy, displayed for perovskite (top, a-b) and organic (bottom, c-d) solar cells. From left to right: (a,c) efficiency, and (b,d) experiment-to-detailed balance-limit ratio (Equation 4 in Table 2) corresponding to each bandgap energy, over publication date.

To benchmark against theoretical limits, the same data are replotted in Figure 1b (PSCs) and Figure 1d (OPVs) as experiment-to-detailed balance-limit ratio (*EDBL*, Equation 4 in Table 2). This representation highlights that perovskite devices have reached nearly 90% of the DB limit, while OPVs remain at around 65%. The origin of this discrepancy becomes clear in Figure S4, which shows V_{oc}, *FF*, and J_{sc} as percentages of their respective DB limits. Perovskites achieve 90–100% across all three parameters, whereas OPVs are lower (80–90%), with V_{oc} particularly limited (~80%). Notably, high relative performance values are also observed for perovskites with bandgaps above 1.55 eV, underscoring that this technology is optimized across a range of absorber compositions rather than being confined to a single high-performing material system.

2.1 | Single Junction Devices

The single-junction solar cells with the highest power conversion efficiencies reported in peer-reviewed articles since August 2024 are summarized in Tables 3–7 and illustrated in Figures 2 and 3. In Figure 2, the updated data are shown as opaque symbols, while lighter-colored symbols represent previous records. For reference, solid lines indicate the single-junction detailed balance [7] (DB) theoretical efficiency limits, calculated under the assumption of radiative emission from both the front and rear surfaces of the photovoltaic cell [7, 21]. The percentage ratios for the experimental performance compared to their corresponding DB theoretical limit are presented in Figure 3b,c.

Perovskite solar cells continue to deliver the highest PCE, V_{oc}, and *FF* values among e-PV devices (see Figure 2 and Table 3), particularly those based on **FAPbI$_3$** and mixed cations perovskite absorbers with photovoltaic bandgap energies around 1.54 ± 0.02 eV. The current certified records are 27.3% and 26.9% for devices with designated illumination areas of 0.1065 cm^2 and 1.017 cm^2, respectively, as listed in the efficiency tables by Green et al. [22]. Among the peer-review published studies, Qu et al. [23] reported a device with 26.8% *PCE* (0.11 cm^2, certified 26.0% at 0.07 cm^2). They attributed this performance to a binary synergistic post-treatment, blending 4-tert-butyl-benzylammonium iodide with phenylpropylammonium iodide and spin-coating onto the FAPbI$_3$ surface. This treatment formed a passivation layer with enhanced crystallinity, improving hole extraction and transfer.

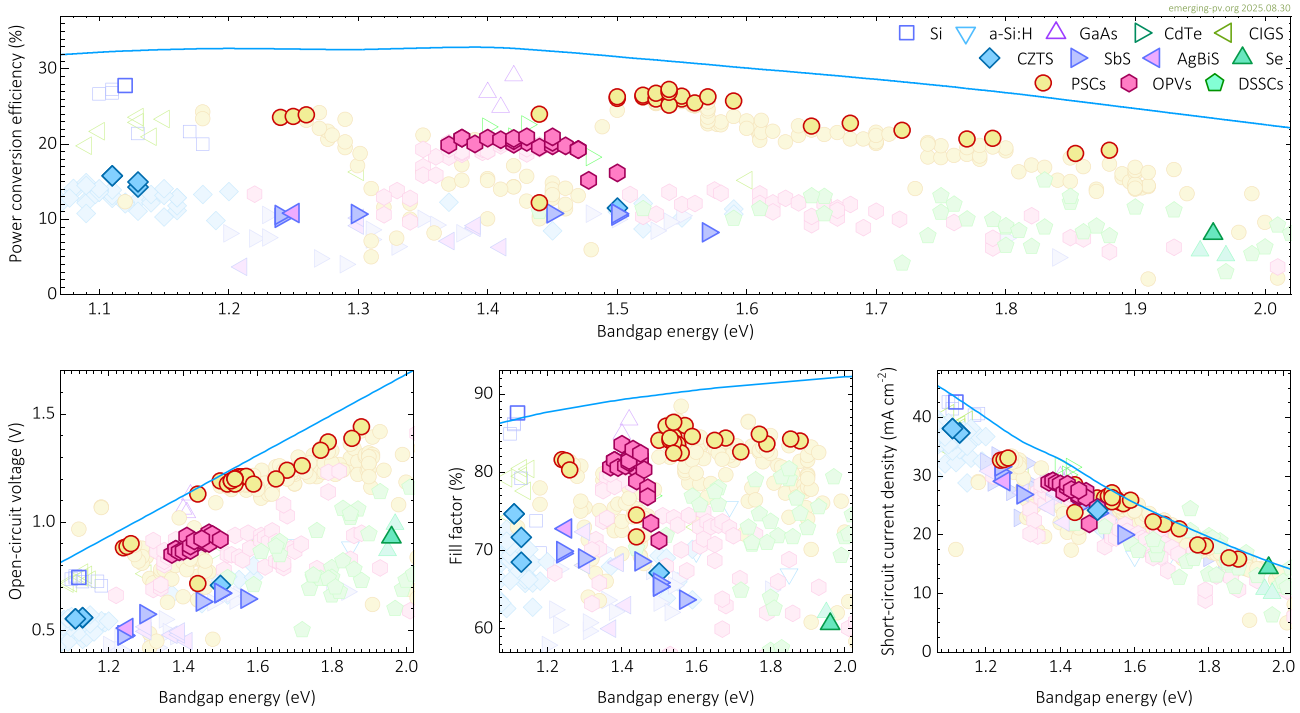

FIGURE 2 | Highest PCE single junction photovoltaic cells. Performance parameters as a function of effective absorber bandgap for different photovoltaic technologies: PCE (top) V_{oc} (bottom left), *FF* (bottom center), and J_{sc} (bottom right). Experimental data are summarized in Section 7.1, with the lighter and more opaque dots corresponding to reports before and after August 2024, respectively. The solid lines indicate the corresponding theoretical detailed-balance efficiency limit [21].

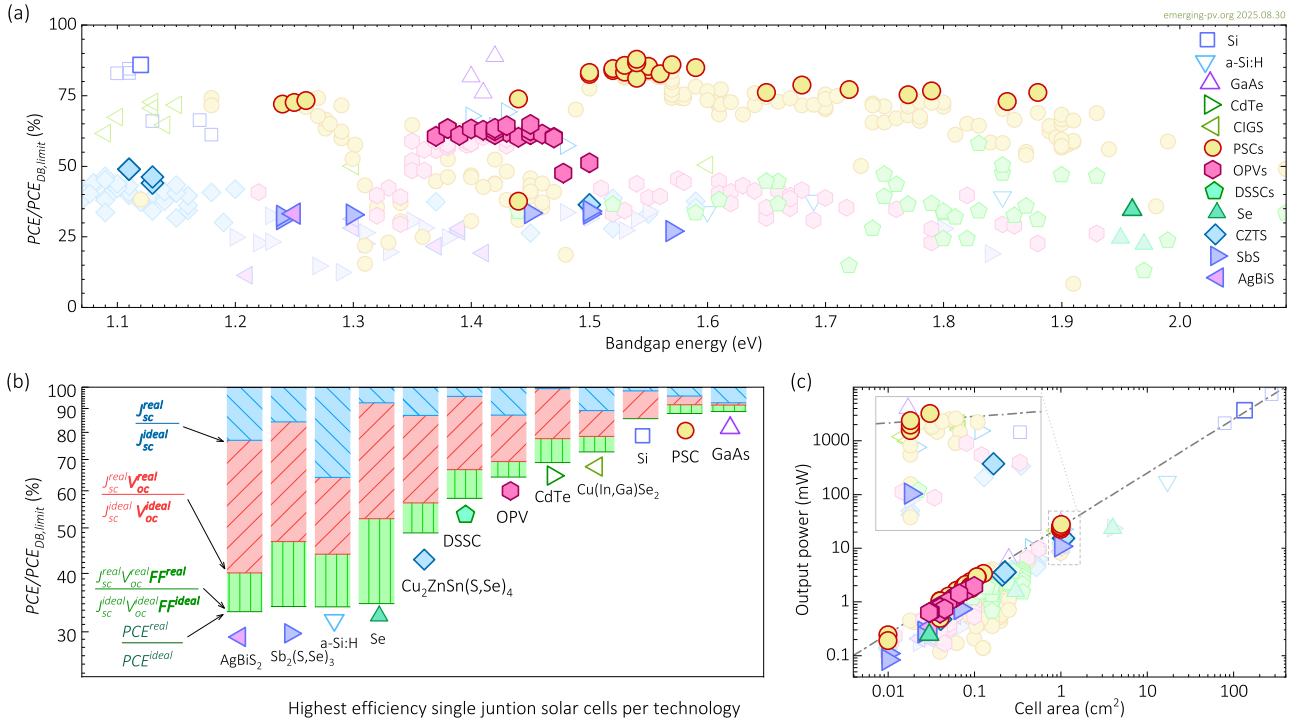

FIGURE 3 | Detailed balance efficiency limit analysis (a, b) and output power (c). (a) Experiment-to-detailed balance efficiency-limit ratio (EDBL, Equation 4, and in Table 2) as a function of the bandgap energy, based on the data in Figure 2. (b) Logarithmic loss analysis [16, 17] for the device with the highest PCE of each PV technology. (c) Output power versus device area, where the dash-dotted line represents the efficiency isoline for PCE = 25%. In (a) and (c), opaque symbols correspond to reports published after August 2024, while light symbols denote earlier reports.

For devices exceeding 1 cm^2 area (inset of Figure 3c), the new output power record was set by Wang et al. [24], achieving 25.2 mW (certified 24.35% *PCE* for 24.35 mW). Their approach improved the growth homogeneity of the $Cs_{0.1}FA_{0.9}PbI_3$ surface by controlling amorphous phases of self-assembled monolayers (SAMs), thereby reducing trap-assisted recombination losses. Recent high *PCE* perovskite solar cells were reported to depend on precursor chemistry, perovskite compositions and device configurations [25]. Other new records were also reported for narrow- and wide-bandgap devices mostly associated with demonstrations of high-efficiency multi-junction solar cells (see Section 2.2).

Organic solar cells with efficiencies above 20% have been systematically reported over the past year, primarily from small-area devices (≤0.1 cm^2) with photovoltaic bandgap energies of 1.43 ± 0.04 eV (see Table 4). No new efficiency records have been reported for devices with bandgap values <1.37 eV or >1.5 eV. Two studies by Li et al. [26] and Wang et al. [27] recently published 21% *PCE*. Notably, Li et al. [26] has reported the highest certified *PCE* value (20.8%) with devices based on D18:L8-BO:BTP-eC9 as active layer and AZnO-F3N as cathode interfacial layer (CIL). In this work, the inorganic-organic hybrid CIL was developed through a two-component synergistic strategy by combining the organic material PNDIT-F3N with two-dimensional amorphous zinc oxide, reducing interface defects and surface while improving charge extraction and transport. Moreover, Wang et al. [27], also achieved 21.0% *PCE* (certified 20.25%) with the second highest *FF* (82.9%) in our records from a device based on D18 (PY-IT diluted)/L8-BO:C5-16 (D18 diluted). In this work, the authors demonstrated that diluting the electron donor with an electron acceptor of opposite electrostatic potential promotes stronger intermolecular interactions and enhanced structural order. They further showed that a polymeric diluent is more effective than a small-molecule counterpart due to its extended conjugated backbone. The ternary heterojunction of C5-16:L8-BO binary acceptors diluted with D18 exhibited the highest degree of structural order, resulting in improved light absorption, charge transport, and suppressed recombination, particularly when prepared via layer-by-layer deposition of diluted p-type and n-type heterojunctions.

Kesterite solar cells also achieved new certified *PCE* records, as listed in the efficiency tables by Green et al. [22] with 15.8% and 14.1% for devices with active areas of 0.225 and 1.075 cm^2, respectively. These devices also set new records for the technology in terms of *FF* (74.7%) and output power (15.2 mW) (see Table 6). Among peer-reviewed publications, Yao et al. [28] reported a device PCE of 14.99% (certified 14.38%) for a 0.4 cm^2 cell. In their study, the authors regulated the phase evolution from Cu_2ZnSnS_4 to $Cu_2ZnSn(S,Se)_4$ during the initial selenization stage to obtain high-quality absorber layers with reduced defects and suppressed secondary phases. By incorporating mercaptopropionic acid into the 2-methoxyethanol precursor solution, they produced large Cu_2ZnSnS_4 colloidal particles and dense precursor films. During selenization, the reduced nucleation sites decreased selenium-molecule interactions and extended the phase evolution process, leading to more controllable heterogeneous nucleation, uniform elemental distribution, and improved large-grain growth throughout the absorber layer.

Antimony seleno-sulfide solar cells have achieved efficiencies slightly above previous records in several recent studies. Zhao et al. [29] reported 10.81% PCE in a 0.01 cm^2 device by introducing Na_2SeSO_3 into the $Sb_2(S,Se)_3$ precursor solution as a passivator for Sb_{Se} antisite defects. Independently, Liu et al. [30] achieved 10.76% PCE (certified 10.5%) in a 0.07 cm^2 device by incorporating lithium fluoride into the precursor solution. This approach improved the conductivity, morphology, and n-type properties of the cadmium sulfide transport layer while simultaneously passivating selenium vacancies and Sb_S antisite defects in the $Sb_2(S,Se)_3$ absorber. Notably, Dong et al. [31] reported a certified 10.7% PCE for a 1 cm^2 device, setting a new record for output power at 10.7 mW. Their strategy focused on charge-carrier management through the use of a textured fluorine-doped tin oxide substrate as the front contact to enhance light scattering and maximize charge generation. To mitigate voids and shunt pathways introduced by the textured surface, a SnO_2 layer was inserted by atomic layer deposition, resulting in improved charge transport and reduced recombination losses.

A new PCE record for matildite solar cells was reported by Li et al. [32], achieving 10.8% PCE with $AgBiS_2$ nanocrystals in devices with an active area of 0.03 cm^2. In this work, the authors developed a post-deposition in situ passivation strategy using a multifunctional molecular agent that both enhanced the colloidal dispensability of the $AgBiS_2$ nanocrystal ink and passivated nanocrystal surfaces after film formation. The latter was achieved through in situ dissociation of chloride ions, which acted as atomic-scale surface passivators. This approach reduced morphological defects, lowered trap-state density, and balanced charge-carrier mobilities, leading to improved device performance.

Selenium solar cells were the first photovoltaic devices ever demonstrated [33], and their intrinsically wide bandgap makes them attractive candidates for multijunction and indoor applications. However, optimizing crystalline Se films for efficient charge-carrier transport has remained a longstanding challenge. The most recent record for this technology was reported by Liu et al. [34], achieving 8.1% PCE in devices with an active area of 0.03 cm^2. In their work, the authors employed a substrate-heating strategy to enhance interfacial bonding between Se and the underlying substrate, which promoted the growth of Se films with a standing orientation (chains aligned perpendicular to the substrate). This orientation significantly improved carrier mobility by facilitating charge transport along the covalently bonded Se chains, in contrast to the less favorable lying-oriented films.

Figure 3a compares the *PCE* data from Figure 2 with the DB efficiency limit, expressed as the experiment-to-detailed-balance limit ratio (*EDBL*, Equation 4, Table 2). Among PSCs, the best-performing devices reach 87.9% EDBL, with the most recent results exceeding 83% for absorbers with 1.50 eV < E_g < 1.60 eV, and above 73% for the latest records using narrow- and wide-bandgap perovskites. For OPVs, the top-performing devices achieve 64.3% of the DB limit, and most new records within the 1.37 eV < E_g < 1.47 eV range reach values above 60% EDBL. In addition, the most recent record devices for $Cu_2ZnSn(S,Se)_4$, Se,

$Sb_2(S,Se)_3$, and $AgBiS_2$ solar cells reach 48.8%, 34.5%, 34.0%, and 33.2% of their respective DB efficiency limits.

A closer examination of the EDBL ratio is shown in Figure 3b, which presents the updated logarithmic loss analysis [35] for the highest-PCE devices of each technology. From left to right, matildite, antimony selenide, selenium, kesterite, organic, and perovskite record cells exhibit progressively smaller overall losses. For all technologies except perovskites, the dominant contribution arises from the V_{oc} deficit, likely linked to excess non-radiative recombination. In the case of selenium solar cells, significant additional losses are observed in the *FF*, which may be attributed to contact-related series resistance issues [36]. By contrast, the new record perovskite solar cells continue to display a more balanced distribution of losses across V_{oc}, J_{sc}, and *FF*.

The output power in milliwatts, corresponding to the data in Figure 2, is shown in Figure 3c as a function of illuminated area. In this plot, the PCE isolines (e.g., the dash-dot grey line for $PCE = 25\%$) appear as diagonal contours, with points closer to the top-right region indicating higher output power. Overall, studies on e-PV technologies continue to focus predominantly on devices with active areas between 0.01 and 0.2 cm^2. Notable exceptions listed in the efficiency tables by Green et al. [22] include a silicon solar cell (3.72 W, 133 cm^2), a perovskite solar cell (27.4 mW, 1.02 cm^2), and a kesterite solar cell (15.2 mW, 1.075 cm^2). Among PSCs reported in published manuscripts, the highest output power during the last year was achieved by Wang et al. [24], with 25.2 mW from a 1.0 cm^2 device. Another notable result is the antimony selenosulfide solar cell reported by Dong et al. [31], which delivered 10.7 mW from a 1.0 cm^2 device.

2.2 | Multijunction Devices (Monolithic)

The performance parameters of monolithic (two-terminal) multijunction photovoltaic research cells are summarized in Figure 4, where opaque symbols represent reports published since August 2024, and lighter-colored symbols correspond to earlier results. The complete dataset is provided in Tables 8–10, and Figure 4a also includes the performance parameters in the optimized bandgap detailed balance (DB) efficiency limit for devices with up to three junctions, including radiative coupling [37].

This year's survey highlights an apparent perovskite predominance in the multijunction subfield: to the best of our knowledge, all but one new record PCE values reported involve at least one perovskite-based sub-cell. In other words, almost no new records have been reported for perovskite-free multijunction devices (see Figure 4a). Notably, the latest record efficiencies from CIGS/perovskite, all-OPV, and OPV/perovskite tandems mark their first demonstrations of tandem efficiencies surpassing their respective single-junction perovskite counterparts. Nevertheless, these values remain below those of the best-performing all-perovskite tandems, which themselves still underperform relative to the single-junction DB efficiency limit. The only exception is Si/perovskite tandems, which continue to exceed the absolute efficiency limits for single junction solar cells.

Among double-junction devices, the record PCE remains with the Si/perovskite tandem. Jia et al. [38], from LONGi, have once again surpassed their previous results, achieving 34.58% PCE on a 1.0 cm^2 device. This milestone was enabled by the introduction of an asymmetric SAM ((3-((9-ethyl-9H-carbazol-3-yl)oxy)propyl)phosphonic acid, HTL201) as a hole-selective layer in the perovskite top sub-cell. The asymmetric design minimized steric hindrance and provided more uniform coverage on the textured silicon substrate, thereby reducing non-radiative recombination. At the same time, optimized energy-level alignment improved carrier extraction. Together, these advances unlocked an outstanding V_{oc} of 1.996 V, which is only second to the new V_{oc} = 2.01 V record for the Si/perovskite tandems reported by Er-Raji et al. [39].

For all-perovskite tandems, we highlight two new records reporting 29.6% (29.5% certified) by Wang et al. [40] and the certified 29.1% reported by Liu et al. [41] (although both studies are still outperformed by the "certified-but-not-published" 30.1% in Green's tables) [42]. The best cell from Wang and co-workers also achieved a record V_{oc} = 2.179 V (see Figure 4b), attributed to the introduction of a mercapto-functionalized mesoporous silica layer as a superstructure at the buried interface to modulate the crystallization. This was associated with a decrease in nanovoids, defect passivation, and suppression of the Sn(II) oxidation in the tin–lead perovskite films, contributing substantially to reduced charge carrier losses and improved stability. On the other hand, Liu and co-workers developed wide-bandgap perovskite films with improved (100) crystal orientation, the introduction of which was associated with suppression of non-radiative recombination. They claim that using a two-dimensional perovskite as an intermediate phase on the film surface promotes heterogeneous nucleation along the (100) three-dimensional perovskite facets during crystallization. These two studies [40, 41] report nearly the highest values for $J_{sc} > 16$ mA cm^{-2} (see Figure 4c) and $FF > 81\%$ (see Figure 4d). However, the output power of these devices was $P_{out} < 1.5$ mW due to their relatively small active areas <0.05 cm^2 (see Figure 4e).

The latest output power record for all-perovskite tandem solar cells is presented in the inset of Figure 4e, and it was reported by Tan and co-workers [43], achieving P_{out} = 29.9 mW (certified 29.6 mW) from 1.05 cm^2 devices with efficiencies of 28.5% (certified 28.2%). The authors attributed this performance to the mitigation of inhomogeneity in the wide-bandgap perovskite sub-cells during upscaling. To address this issue, they introduced a mixed additive strategy combining 4-fluorophenethylammonium chloride (F-PEACl) and 4-trifluoromethylphenylammonium chloride (CF_3-PACl) to form a tailored two-dimensional (2D) perovskite interfacial layer (TTDL). In this configuration, F-PEACl promoted the formation of a 2D perovskite at the surface, reducing contact losses and improving uniformity during deposition of the C_{60} electron transport layer, while CF_3-PACl enhanced charge extraction and transport.

For CIGS/perovskite tandems, a new record PCE of 28.05% (certified 27.22%) was reported by Pei et al. [44]. In this work, the introduction of 4-(2-aminoethyl)-benzenesulfonyl fluoride hydrochloride (TAR 3) was found to inhibit passivation failures, enabling multisite defect passivation and promoting charge-carrier transport of the wide-bandgap perovskite. This also led to

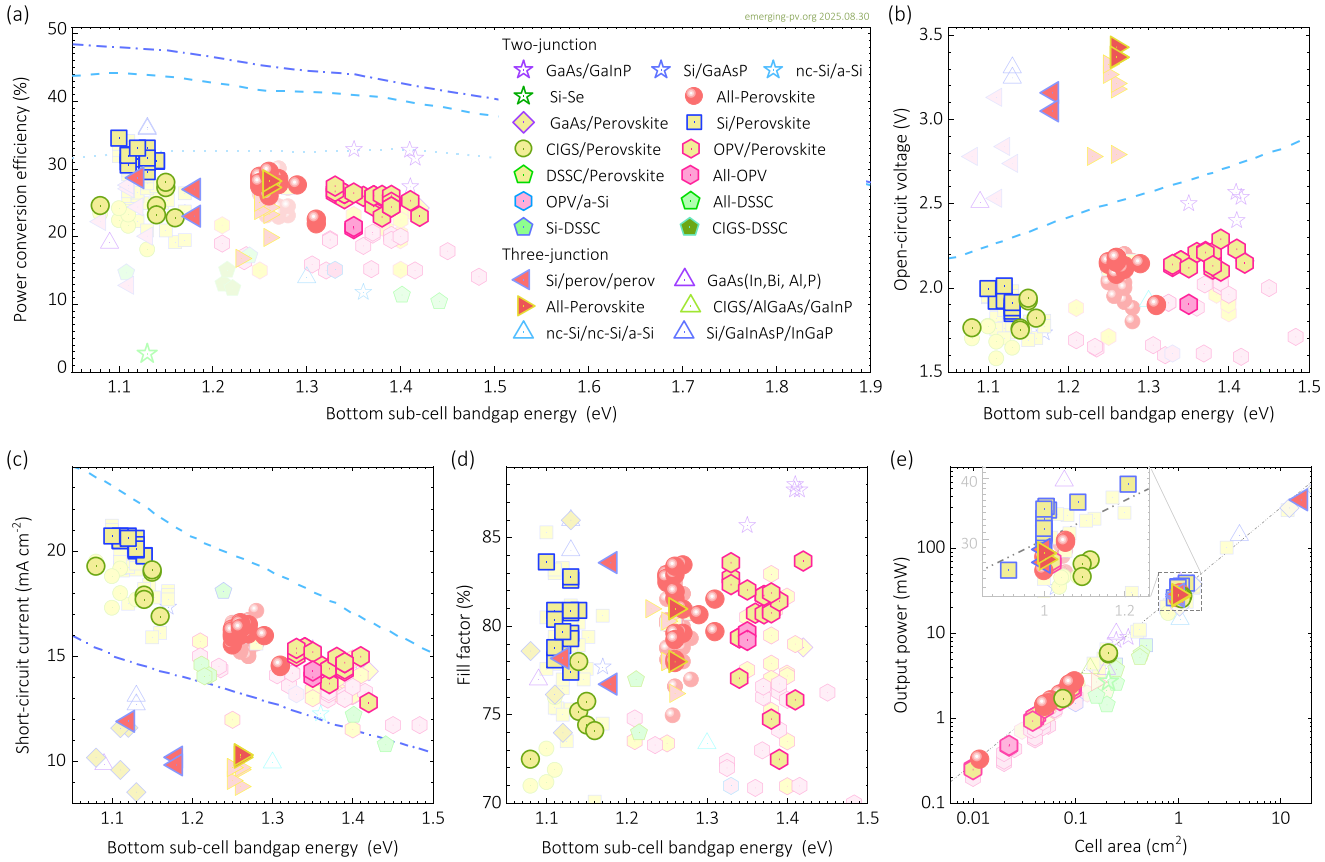

FIGURE 4 | Highest-PCE values for monolithic (two-terminal) multijunction photovoltaic research cells with up to three junctions. Performance parameters are shown as a function of the absorber bandgap energy of the bottom sub-cell for different photovoltaic technologies: (a) PCE, (b) open-circuit voltage, (c) short-circuit current density, and (d) fill factor, along with (e) output power versus device area. The dotted, dashed, and dash-dotted lines in (a-c) represent the detailed balance efficiency limits for single-junction, double-junction (optimized top sub-cell), and triple-junction (optimized top and middle sub-cells) devices, respectively [37, 31]. In (e), the dash-dot-dot line corresponds to the efficiency isoline for PCE = 30% and the inset magnifies the ~1 cm^2-area results. Data points are represented by light-colored symbols for reports published before August 2024 and by opaque symbols for those published thereafter.

a new photovoltage record of V_{oc} = 1.938 V for CIGS/perovskite devices (see Figure 4b), although the small active area of these cells, ~0.21 cm^2, limited their output power (see Figure 4e).

Among CIGS/perovskite cells with active areas >1 cm^2, a new output power record of P_{out} = 26.8 mW (certified 25.3 mW) was reported by Ying et al. [45], corresponding to devices with efficiencies of 24.6% (certified 23.2%). Their approach employed an antisolvent-seeding strategy designed to decouple SAM adsorption from dissolution, while simultaneously promoting perovskite seeding. The authors further suggested that a high-polarity solvent prevents clustering of SAM molecules during dissolution, whereas a low-polarity antisolvent promotes high-density SAMs formation during adsorption. In addition, a pre-mixed seed layer was introduced to further improve perovskite wettability, crystallinity, and adhesion. Notably, these devices were fabricated on flexible substrates, achieving performance values second only to the best rigid CIGS/perovskite tandems listed in the efficiency tables from Green et al. [22], which exhibit similar *PCE* but with a slightly larger mask aperture area.

The main performance limitation for the CIGS/perovskite tandems remains the *FF*. As shown in Figure 4d, the reported values (*FF*<80%) are the lowest among all the multijunction devices published in the last year. In fact, the current *FF* record for this technology was also achieved in the flexible cells reported by Ying et al. [45] with a value of 78%.

An unprecedented number of OPV/perovskite tandem entries is included in this year's survey. Among them, the work by Jia et al. [46] stands out, reporting several record-breaking achievements: the highest device PCE of 27.5% and a *FF* of 83.6% for small-area devices (0.05 cm^2), as well as the highest output power of P_{out} = 27.2 mW (certified 26.9 mW) from a 1.019 cm^2 device with a PCE of 26.7% (certified 26.4%). In this study, the authors optimized the organic narrow-bandgap sub-cell by introducing an asymmetric non-fullerene acceptor, P2EH-1 V, featuring a unilateral conjugated π-bridge that reduced the optical bandgap to 1.27 eV while maintaining efficient exciton dissociation and favorable nanomorphology. Transient absorption spectroscopy confirmed efficient hole transfer from P2EH-1 V to the polymer donor PM6, leading to reduced non-radiative recombination losses.

Tandems based on OPV and perovskite sub-cells face the challenge that the lower bandgap partner (the organic sub-cell)

is limited to high PCE materials in the 1.3 to 1.4 eV range (close to the single junction efficiency maxima). This, therefore, requires also a higher upper band gap for current matching (as compared to other perovskite-based tandems) and leads to the unsurprising situation that OPV/perovskite tandems have arisen with the highest V_{oc} values among the different e-PV tandem technologies. Several studies report $V_{oc} > 2.2$ V, second only to GaAs/GaInP devices (Figure 4b). The highest V_{oc} of 2.230 V was reported by Tian et al. [47], although this cell exhibited a low *FF* (75.8%), leading to a *PCE* = 25.3%. In their study, efforts focused on reducing optical losses in Au-embedded interconnection layers by tailoring the shape and size distribution of Au nanoparticles. By achieving fewer, smaller, and more uniform spherical nanoparticles, the authors minimized localized surface plasmon resonance absorption while maintaining efficient electron–hole recombination within the interconnection layers.

Despite these record V_{oc} values, OPV/perovskite tandems still reach only ~83% of their maximum V_{oc}, according to the DB efficiency limit for the corresponding bottom sub-cell bandgaps (see dashed line in Figure 4b). This value lags behind all-perovskite and Si/perovskite tandems, which approach ~87% and ~89%, respectively. A similar trend is observed for J_{sc}, where OPV/perovskite tandems reach up to ~88.8% of their maximum J_{sc}, compared with ~91.2% for all-perovskite and ~91.3% for Si/perovskite tandems (see dashed line in Figure 4c).

All-OPV tandems were recently reported by Wang et al. [48], achieving a *PCE* of 21.5% (certified 21.2%). These results represent the first perovskite-free OPV tandems to surpass the current record for single-junction OPV cells, while also delivering improved *FF*, with the first values exceeding 79% among OPV tandems. In this work, the authors incorporated a narrow-bandgap acceptor, BTA-4F, based on a 2-methyl-2H-benzotriazole (BTA) central core. This acceptor was composed the PBDB-TF:BTA-4F blend in the bottom sub-cell and, combined with a wide-bandgap top sub-cell comprising a PB3:FTCC-Br blend, resulted in reduced recombination for a decrease of V_{oc} loss.

The triple-junction all-perovskite devices reported by Hu et al. [49] achieved a new record PCE of 28.4% (certified 27.28%) for 1cm^2 devices. These devices outperform all previously reported all-perovskite triple-junction cells across every performance metric (*PCE*, V_{oc}, J_{sc}, *FF*, P_{out}), representing the first instance of this device type surpassing the PCE of single-junction perovskite solar cells. This remarkable performance was attributed by the authors to the optimization of the narrow-bandgap tin-lead perovskites in the bottom sub-cell. They highlight that Sn(II) species dominate interactions with precursors and additives, revealing the unique role of carboxylic acids in regulating solution colloidal properties and film crystallization, and of ammonium chloride salts in improving the optoelectronic properties of the films. Building on this insight, they introduced materials combining these two functional groups, amino acid salts, which significantly enhance the semiconducting quality and homogeneity of the perovskite films, surpassing the effect observed when the individual functional groups are introduced separately. Moreover, Snaith and co-workers [49] also demonstrated a quadruple-junction all-perovskite device achieving 27.9% *PCE* and an unprecedented high V_{oc} of 4.94 V.

For silicon-perovskite-perovskite triple-junction solar cells, a new record power conversion efficiency of 28.7% was reported by Fuzong et al. [50] for a 1 cm^2 aperture area. In this study, 3-ammonium propionic acid iodide was incorporated into the perovskite lattices, which enhanced the phase stability of both the $FAPbI_3$ middle sub-cell and the bromide-rich top sub-cell, by suppressing the α-to-δ transition and reducing light-induced phase segregation, respectively. Moreover, a 16 cm^2 triple-junction silicon-perovskite-perovskite solar cell was reported by Zheng et al. [51], achieving a certified steady-state *PCE* of 23.3%, along with a 1 cm^2 device reaching 27.06% *PCE*. The authors attributed this performance enhancement and remarkable upscaling to the use of a piperazine-1,4-diium chloride surface treatment, which effectively replaced the less stable lithium fluoride as a passivator of surface defects in the top perovskite sub-cell. Additionally, they optimized the size of gold nanoparticles deposited on atomic layer–deposited tin oxide, improving ohmic contact while minimizing optical losses at the interface between the top and middle perovskite sub-cells. This approach enabled a more efficient and monolithic perovskite–perovskite integration, contributing to the overall high device performance.

3 | Flexible Photovoltaic Cells

The performance parameters of relevant flexible solar cells are summarized in Tables 11–16 and illustrated in Figure 5a,b, which highlight the steady increase in *PCE* records across nearly all flexible solar cell technologies. However, when considering recent recommendations for best practices in bending test protocols by Fukuda et al. [14], and the introduction of the flexible photovoltaic fatigue factor (*F*) by Sun et al. [10], Figure 5c–h presents the subset of the data focused on mechanical stability and including bending tests. These results indicate that progress in this area over the past year has remained relatively limited.

The fatigue factor *F* (see Equation 5 in Table 2), expressed as a percentage, quantifies mechanical stability relative to "*a reference sample defined as having 99% PCE retention after 10 bending cycles with 1% strain (ε)*". Within this framework, smaller absolute values of |*F*| correspond to lower photovoltaic "fatigue," while $F < 0$ denotes performance loss and $F > 0$ denotes performance gain after bending tests.

Although most e-PV technologies now report new record efficiencies and output powers for 1 cm^2 flexible solar cells (Figure 5a,b), the parameterization of bending test results (Figure 5c–h) reveals little substantive progress in mechanical durability. This is reflected in modest *PCE* retentions and fatigue factors. Moreover, when comparing the total number of *PCE* records (Figure 5a,b) with those that also report *PCE* retention data (Figure 5c–e), the latter is markedly smaller, which evidences that many publications on flexible solar cells still omit bending tests. Even among the studies that do include such tests, only a small fraction report fatigue factors with |*F*| < 100% (Figure 5f–h). This limitation can be attributed to the frequent use of bending radii that correspond to strain values below 1%. Such mild testing conditions fail to impose significant stress on the devices, typically yielding results with very large numbers of bending cycles accompanied by only minimal *PCE* loss, or, in some cases, even apparent efficiency gains.

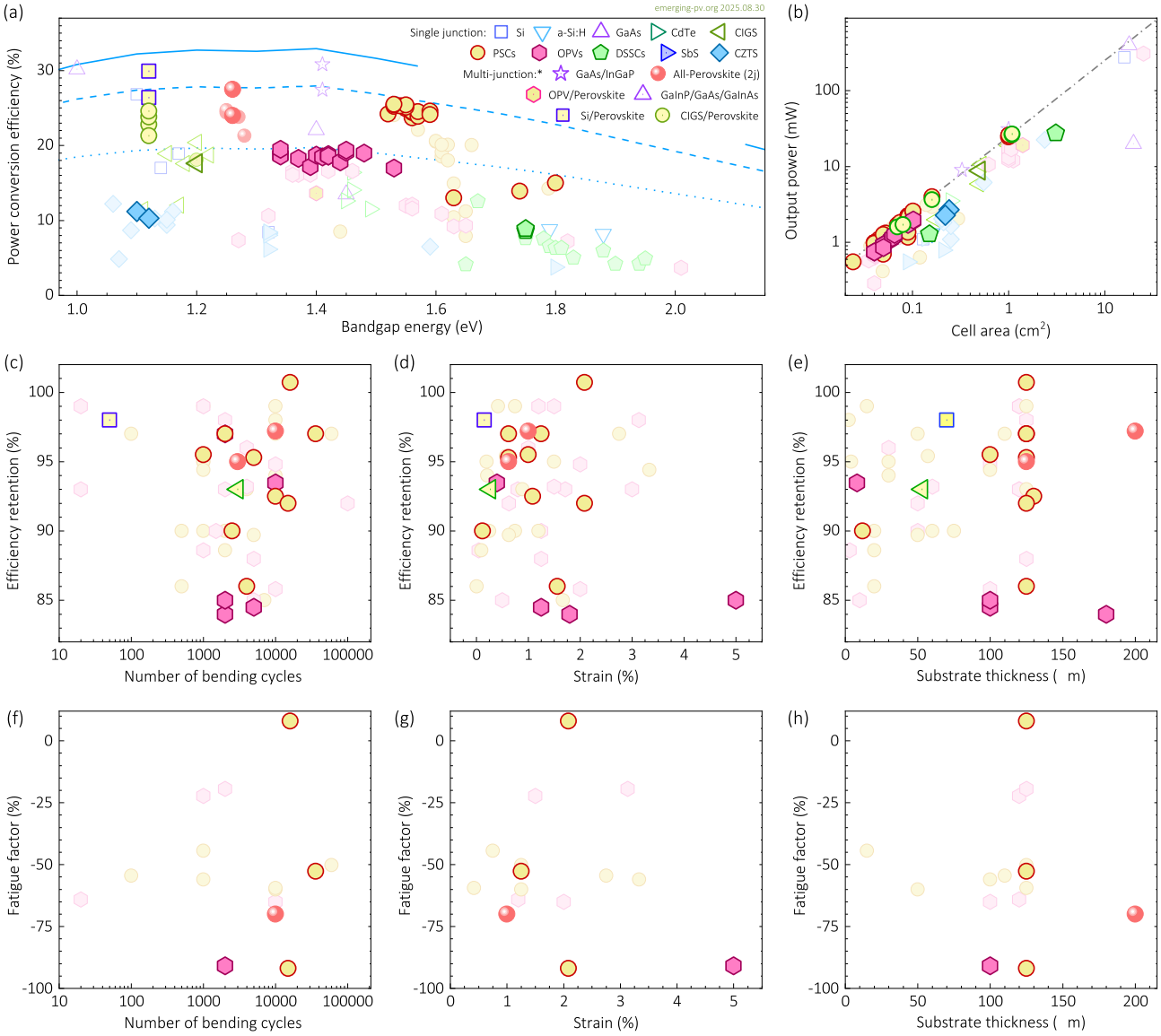

FIGURE 5 | Flexible solar cells with the highest performance among e-PV technologies: (a) PCE and (b) output energy as functions of the absorber (or bottom sub-cell absorber in case of multijunction devices) bandgap energy for various photovoltaic technologies. Bending test performance is provided: (c) power conversion efficiency retention as a function of (c) number of bending cycles, (d) strain, and (e) substrate thickness; and fatigue factor (Equation 5 in Table 2) [10] values as functions of (f) number of bending cycles, (g) strain and (h) substrate thickness. The experimental data are summarized in Section 7.2. In (a), the solid, dashed, and dotted lines indicate 100%, 85%, and 60% of the theoretical single junction DB efficiency limit [21], respectively. In (b), the dash-dot line in the output power-area plot is the efficiency isoline for PCE = 25%. The lighter and opaque symbols are reports before and after August 2024, respectively.

In terms of raw *PCE*, record 25.54% (certified 25.44% on 1.01 cm^2) flexible perovskite solar cells were demonstrated by Chu et al. [52] by suppressing island/coffee-ring instabilities via an elastic porous meniscus printing regime. This study also showed 90% of PCE retention after 2 500 bending cycles with bending radius (R) of 5 mm. This mechanical test applied a 0.12% strain to the sample with over 12 μm-thick ITO/PEN substrates. Notably, the same methodology delivered 100 cm^2 flexible modules at certified 15.65% efficiencies, correlating mesoscale flow control to device-level uniformity.

At the buried interface, two complementary strategies stand out. On the one hand, Tang et al. [53] reported a linear polymer, heparin sodium, "heterointerface bridge" that pushes flexible n–i–p devices to 25.23% with exceptional mechanical durability with 95.5% *PCE* retention after 1 000 bending cycles with 1.25% strain (R = 5 mm). On the other hand, Liang et al. [54] reported a multifunctional boronic-acid additive (4-BBA) that nucleates a stress-relaxed, SAM-bridged buried interface in inverted (p–i–n) stacks, yielding 25.30% (certified 25.13%), record V_{oc} of 1.21 V, and 95.3% PCE retention after 5000 bends with 0.63% strain (R = 10 mm), suggesting a co-optimization of recombination kinetics and interfacial mechanics. Moreover, Cai et al. [55] reported a buried-interface "fastening" strategy for flexible perovskite solar cells with a top PCE of 24.16% and *PCE* retention over 86% after 4000 bending cycles. In this bending test, a 1.56% strain (R = 4 mm) was applied to the sample, fabricated on 125 μm PEN substrate. These results were enabled by the introduction

of hexamethylene diisocyanate into the perovskite precursor and ethylene glycol on the SnO_2 electron transport layer, which simultaneously relaxes gradient residual stress and improves adhesion.

Ning et al. [56] reported highly oriented acryloyloxy-ethyltrimethyl ammonium chloride-acrylamine (DAC-AA)-doped SnO_2 nanocrystals enabling air-processed flexible PSCs reaching PCE values of 23.87% (0.092 cm^2) and 22.41% (1 cm^2). This approach was also found to decrease the formation of micro-strain inside the perovskite, leading to 92.5% *PCE* retention after 10 000 bends with 1.08% strain ($R = 6$ mm, 130 μm PEN/ITO/SnO_2 substrate).

The highest (and lowest absolute) values of fatigue factor in our database over the last year were reported by Guo et al. [57] who demonstrated $CsPbI_3$-based PSCs on 125 μm-thick PEN/ITO substrates. In their study, the authors introduced an organic sulfonate additive, 1-propylsulfonate-3-methylimidazolium chloride (SMCl), to lower the crystallization temperature of $CsPbI_3$. This strategy significantly enhanced mechanical stability in bending tests, yielding 97% *PCE* retention after 36 000 bending cycles with 1.25% strain (R = 5 mm), corresponding to a fatigue factor of −53%. This is the smallest absolute value for F among all cells in this report. As a notable exception, we also highlight that this study also reported the devices retaining 100.7% of their initial PCE after 16 000 bending cycles at 2.08% strain (R = 3 mm), corresponding to an impressive fatigue factor of 7.99%. Notably, since these results correspond to devices with efficiencies up to 13.86%, whereas $CsPbI_3$ cells have already demonstrated efficiencies above 21% [58], they raise questions about the fundamental stability of higher-performing devices, which may be more susceptible to strain-induced impurities, defects, and morphological changes.

The next best results in terms of fatigue factor are attributed to the "self-welding" process induced by visible light enabled by the incorporation of a functional diselenide polymer, which was reported by Li et al. [59]. The diselenide was found to accumulate at the surface and grain boundaries, where it effectively repaired defects and cracks in perovskite films. As a result, record flexible PSC PCE values of 24.85% were achieved, with 92% PCE retention after 15 000 bending cycles under 2.08% strain (R = 3 mm, 125 μm-thick PEN/ITO substrate). This experiment led to a fatigue factor of −91.95% (see Figure 5f–h). Furthermore, a 15.82 cm^2 flexible module demonstrated 21.65% PCE with >93% retention after 15 000 bending cycles.

The highest PCE among flexible organic solar cells was reported by Chen et al. [60] with values of 19.51% (18.69% certified) over devices with 0.0625 cm^2 of active area. In this study, the hole charge extraction was optimized by combining Ag-nanowire flexible transparent electrodes and BCzBN:NiO_x interlayers correlated with compensation of plasmon energy losses, while boosting electrode transmittance by 10.74%. These devices were fabricated over 180 μm-thick PET substrates and recorded a *PCE* retention of 84% after 2000 bending cycles with 1.8% strain (R = 5 mm). Moreover, Li et al. [61] added a thermoplastic elastomer material (polyurethane, PU) to PM6:PBQx-TF:PY-IT-based active layer films, resulting in a PCE of 19.40% (certified 19.07%) for devices with an effective area of 0.102 cm^2. Furthermore, they also presented module-scale demonstrations, with 25 cm^2 area flexible modules with efficiencies of 15.48%.

Silver nanowire flexible transparent electrodes with a "smart targeting layer" including a thiol group that facilitates self-assembling molecules via S–Ag bonds on the Ag-nanowires were reported by Xia et al. [62], leading to flexible organic solar cells with 18.84% PCE (certified 18.56%) on ITO-free flexible cells. In this study, the effect of bending radius was explored, resulting in an 85% *PCE* retention after 2 000 bending cycles with $R = 1$ mm.

Among flexible tandem solar cells, the highest PCE to date was reported by Sun et al. [63], who achieved a certified 29.88% in a device with 1.04 cm^2 aperture area, consisting of a perovskite top sub-cell over a 70 μm-thick heterojunction silicon bottom sub-cell. This performance was attributed to the high phase homogeneity of single-cation FA perovskite films, which, unlike mixed-cation FAMA, facilitated charge transfer across all facets of the textured Si pyramids while also relieving residual stress at the silicon/perovskite interface. The devices showed no performance loss after 2000 bending cycles at 0.11% strain (R = 3.2 cm), with *PCE* retention >101% ($F > 0$). Under higher strain conditions (ε = 0.16%, R = 2.25 cm), the cells retained 98% of their initial PCE after 50 bending cycles.

Flexible monolithic 1.09 cm^2-area CIGS/perovskite tandems by Ying et al. [45] reached 24.6% PCE (certified 23.8%), developing an antisolvent-seeding strategy that decouples SAMs adsorption from dissolution, while integrating perovskite seeding. These devices were fabricated over 50 μm-thick stainless steel and retained 93% of their initial efficiencies after 3000 bending cycles with 0.27% strain ($R = 10$ mm).

Finally, flexible all-perovskite tandems reported by Li et al. [64] achieved a 27.5% PCE cell (area 0.049 cm^2) and a 23.0% certified PCE module (area 20.26 cm^2). The module also showed 97.2% retention after 10 000 bending cycles with 1% strain (R = 10 mm), leading to a fatigue factor value of −70%. This is the smallest absolute value for F among multijunction cells in this report. This achievement was attributed to a scalable fabrication strategy based on pretreating the wet perovskite films with an in situ additive coating under continuous gas quenching. Moreover, slot-die trials toward ∼804 cm^2 aperture area show that strain-accommodating interlayers are now scalable.

4 | Transparent and Semitransparent Photovoltaic Cells

With respect to (semi-)transparent solar cells, progress over the last year can be clearly observed in terms of two reports achieving light utilization efficiencies (*LUE*, see Equation 7 in Table 2) beyond 6%. Both are based on semitransparent organic solar cells and constitute new *LUE* records among all technologies in the emerging-pv.org database. Overall, 21 new reports have been entered in this e-PVr, 13 from organic photovoltaics, five perovskite solar cells, one semitransparent solar cell based on SbS, and two transparent luminescent solar concentrators (see Figure 6 and Tables 17–22).

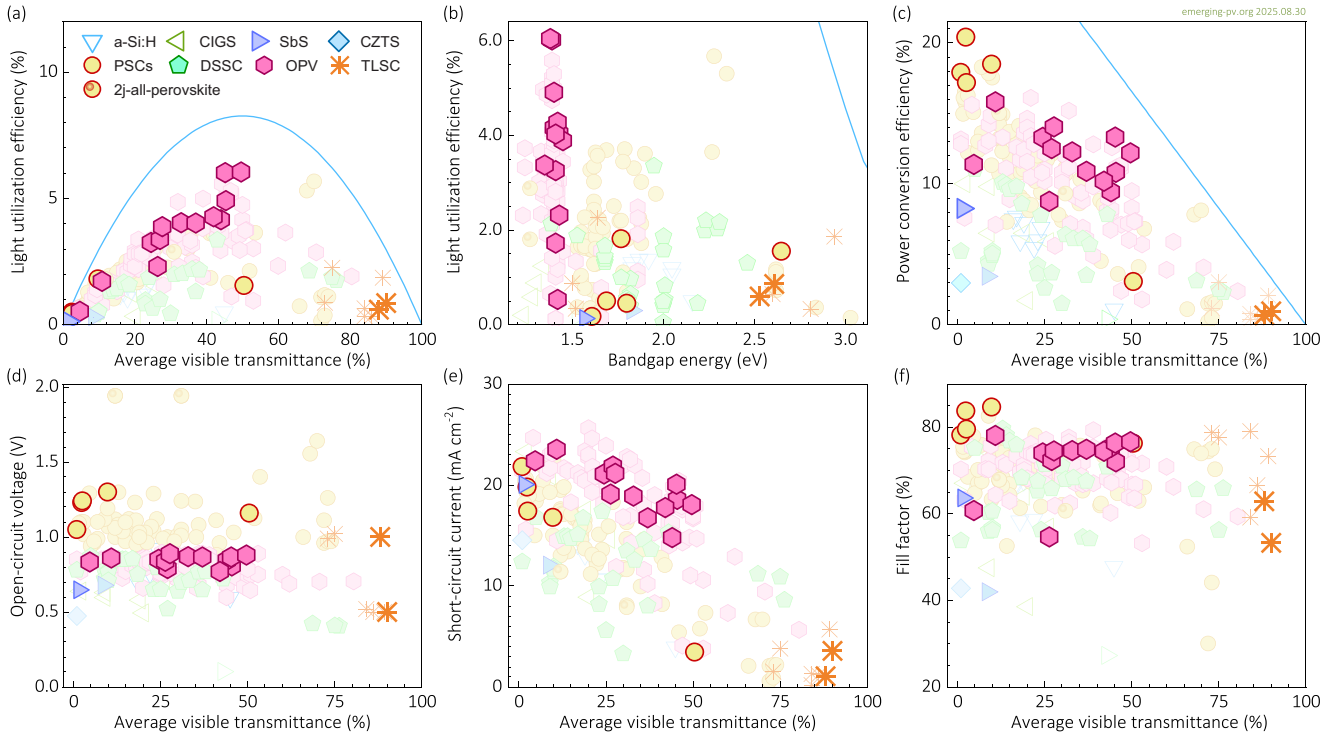

FIGURE 6 | Best performing transparent and semitransparent PVs: *LUE* versus (a) *AVT* and (b) E_g; and (c) PCE, (d) V_{oc}, (e) J_{sc}, and (f) *FF* as a function of *AVT*. The experimental data are summarized in Section 7.3. The blue solid lines indicate the corresponding theoretical detailed balance efficiency limit for non-wavelength-selective PVs. In (b), the multijunction cells are potted as a function of the bandgap energy of the absorber material in the bottom sub-cell. The lighter and more opaque symbols are reports before and after August 2024, respectively.

We again emphasize the importance of consistently reporting the EQE and transmittance spectra for (semi-)transparent devices in order to allow accurate estimations and cross-checking of the critical parameters: *AVT* (see Equation 6 in Table 2), *LUE* (Equation 7 in Table 2)), and the photon balance consistency check (*PBCC*, see Equation 8 in Table 2). These parameters are key for comparison and performance assessment in (semi-)transparent solar cells.

In the field of semitransparent OPVs, Yu et al. [65] reported 6.05% *LUE*. Their devices employed a novel ternary blend combining the wide-bandgap donor PBOF with the acceptors eC9 and $PC_{61}BM$, deposited on a SAM hole-transport layer atop a high-transparency indium tin oxide (ITO) electrode. Together with an aperiodic dichroic mirror of LiF/TeO_2 layers on top of an 11 nm thin silver electrode, record cells achieved a *PCE* of 12.2% and an *AVT* of 49.6%. Such semitransparent organic solar modules could serve as smart windows to provide energy and to save energy due to reduced cooling needs, especially in climates with hot summers and warm winters.

In another study, Ding et al. [66] added a third component, BTO-BO, into the D18:BTP-eC9 photoactive layer, which was processed from non-halogenated toluene. This improved the stacking of the donor polymer from H-type to J-type aggregates, which reduced absorption in the visible while improving charge transport. With a *PCE* of 13.3% and an *AVT* of 45%, an *LUE* of 6.02% was achieved when a thin Ag electrode was complemented with TeO_2. Without this layer, an *LUE* of 3.86% at a *PCE* of 13.3% and *AVT* of 26% was achieved. Interestingly, the authors also showed semitransparent solar cells on flexible PET substrates (*LUE* 3.42%) and a 15 cm^2 mini module (*LUE* 4.53%), highlighting efforts in transparent solar design combined with upscaling. Considering the selective transparency in the 400–700 nm wavelength range, where plant pigments primarily absorb light, experiments growing sprouts under semitransparent solar modules showed no adverse effects on plant growth compared with glass. These results demonstrate the potential of integrating photovoltaics with agriculture (agrivoltaics), particularly in applications such as greenhouses [67].

A notable example of semitransparent organic solar modules was shown by Han et al. [68], which used *o*-xylene processed absorber layers that combined PCE10 with a modified BTP-eC9 acceptor (eC9-2Cl). On the cell level, they reached 10.2% *PCE* and 42% *AVT* leading to an *LUE* of 4.3% in the best performing device, in which a thin Ag electrode was complemented by a LiF/MoO_3 outcoupling double layer. On the minimodule level, this approach led to almost 4% LUE in 25 cm^2 devices, highlighting the progress towards visibly transparent energy-generating windows. In a similar device architecture, Yang et al. [69] investigated layer-by-layer processed PCE10-2F/4FY, in which the fluorophenyl outer groups of 4FY led to tighter packing as compared to using Y6 as the acceptor. As a result, an *AVT* of 45% together with 10.8% *PCE* resulted in 4.91% LUE in semitransparent OPVs. Moreover, an 18 cm^2 mini module also showed a noteworthy *LUE* value of 3.1%.

Thin Ag electrodes can also be used to build Fabry-Pérot microcavities, in which a dielectric is placed between two Ag layers. Based on the refractive index of the dielectric and by

tuning the layer thicknesses, wavelength-specific transmission through the microcavity can be tuned, allowing adjustable colors of such semitransparent devices. Based on this approach, colorful semitransparent organic solar cells have been shown by Khandelwal et al. [70] in violet, blue, green, red, and magenta, with efficiencies over 11%. Inherently, due to transmittance peaks at certain wavelengths, the overall *AVT* of these devices with less than 10% is rather low, and so is the LUE (<1%). Using a similar approach, Deng et al. [71] have shown how to combine power with art. Based on high-throughput optical computing and experimental optimization, they realized navy, sky blue, azure, yellow, vermilion, and brown colors in order to replicate an iconic modern artwork, "Composition C" of Piet Mondrian, over a slot-die coated semitransparent organic solar module. In their work, the highest *LUE* of 1.7% was achieved for a green colored semitransparent cell with a *PCE* of 15.8% and 11% *AVT*.

As an alternative electrode, silver nanowires (AgNW) can be solution-processed, and compared with thin Ag layers, they generally offer higher transparency without the need for additional optical outcoupling. Wu et al. [72] developed a sandwich electrode of AgNW and PDINN to achieve PM6:BTP-eC9:L8-BO semitransparent OPVs with 44% *AVT* and 9.5% PCE, leading to an LUE of 4.2%. Interestingly, complementing the AgNW electrode with a 30 nm TeO_2 layer, the ratio between the PCE values of rear- and front-side illumination (i.e., the bifaciality factor) exceeded 95% on average at an LUE of 3.7%.

From the developments in semitransparent perovskite solar cells, the most noteworthy addition in the last year is a new *LUE* record for the lead-free $Cs_2AgBiBr_6$ absorber in the work of Barichello et al. [73]. Semitransparent solar cells with the 2.65 eV wide-bandgap perovskite, blade-coated with 400 nm thickness, achieved a *PCE* of 3.1% with an *AVT* of 51%, leading to 1.55% of *LUE*. Notably, a 6 cm^2 semitransparent mini module was also fabricated with a *PCE* of 1%.

Highest transparencies are typically achieved with TLSCs. In the last year, Chonlateeroj et al. [74] reported a new class of self-absorption-free luminophores of which, embedded in a PMMA matrix, HBTM achieved an LUE of 0.60% with an AVT of 88% and an overall PCE of 0.68% with Si solar cells mounted to the edges. An even higher *AVT* of 90% was achieved by Xia et al. [75] based on $MAPbBr_3$ luminophores directly synthesized in a PVDF–HFP matrix. With a PCE of 0.96% based on edge-mounted Si solar cells, an LUE of 0.86% was achieved. Interestingly, the high mid-infrared emission of the luminescent film could at the same time be used for radiative cooling and, thanks to a back ITO electrode, cooling properties can either be regulated by flipping the TLSC or even active heating can be applied, demonstrating the possibilities towards functionalized windows and zero-energy buildings.

5 | Operational Stability in Emerging Research Solar Cells

The operational stability of e-PV technologies remains a critical issue for both scientific research and industrial deployment. We have updated the latest literature reporting stability tests conducted under continuous 1 sun illumination for 200 h and/or 1000 h, as summarized in Tables 23–25 and Figure 7. Importantly, in this update, we incorporated datasets and plots for t_{95} (see Equation 11 in Table 2), as a new figure of merit for systematic quantitative assessment of performance stability in the e-PV reports. From this expanded dataset, several notable trends and characteristics are evident, reflecting the latest progress as well as the persistent challenges in the field.

Among the general trends that remain unchanged compared with previous editions of the e-PV surveys, we highlight the still limited availability of data on performance stability. Most stability tests in the literature continue to follow procedures similar to the ISOS-D dark storage experiments [76], rather than the recommended ISOS-L protocols [76]. This trend is particularly critical for emerging technologies other than perovskite-based devices, as illustrated by the fact that only a single non-perovskite performance study was reported for an OPV. This work by Liu et al. [77] introduced an in situ-derived inorganic SiO_xN_y interlayer to passivate surface defects in the ZnO electron transport layer through the formation of Zn–O–Si bonds. The SiO_xN_y layer, prepared by curing a solution-deposited perhydropolysilazane (PHPS) film, enhanced charge extraction from the active layer and effectively suppressed the decomposition of non-fullerene acceptors at the ZnO interface. As a result, the ZnO/SiO_xN_y-based devices retained 94% of their initial *PCE* after 2 000 h of aging, representing one of the most stable and best-performing OPVs reported to date.

Another persistent trend is the greater availability of stability tests lasting over 200 h (Figure 7a–c), compared with experiments extending beyond 1000 h (Figure 7d–f). However, the inclusion of the newly reported t_{95} values (Figure 7g–i) now provides further insight: most of these t_{95} values fall below 1000 h. This observation is consistent with the higher absolute degradation rates observed for 200 h of stability tests (up to 0.3% loss per day, Figure 7c) compared with those reported beyond 1000 h (up to 0.07% loss per day, Figure 7f). Moreover, despite the still limited number of results with $t_{95} > 1\ 000$ h, the apparently increasing trend shown in the publication time evolution of Figure 7i suggests significant progress could be reported within the next two to five years.

In terms of bandgap energy, both the energy yield (Figure 7a,d) and the t_{95} values (Figure 7g) continue to show the typical clustering around E_g values corresponding to the most efficient devices—for example, 1.55 eV for perovskite and 1.44 eV for OPV cells. This clustering is likely a practical outcome: researchers tend to prioritize the time-consuming stability tests only after strong indications of high device quality, such as record-breaking PCE results. However, this raises a question: could there be materials with potentially higher operational stability—and therefore greater long-term energy yield—even if their initial performance is not state-of-the-art? Exploring this possibility would be particularly relevant for perovskite and organic solar cells with narrower or wider bandgaps.

Comparing energy yields and PCE values in Figure 7b,e, one can see that perovskite single-junction devices now commonly achieve initial efficiencies exceeding 26%, delivering energy yields

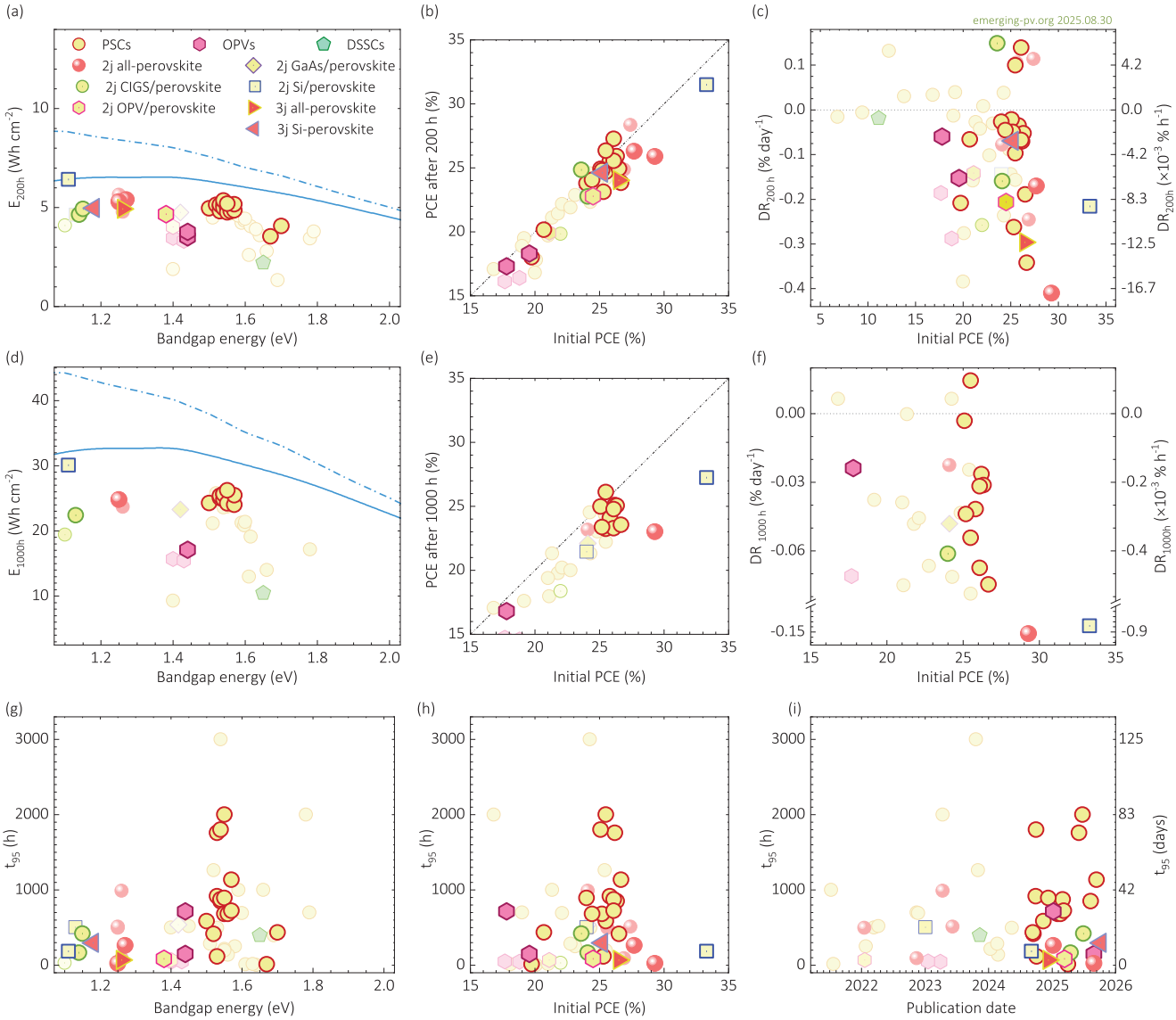

FIGURE 7 | Operational stability under 100 mW cm^{-2} illumination at MPP conditions during 200 h (a-c) and 1 000 h (d-f) of testing. Analysis parameters include: (a,d) stability test energy yield (STEY, Equation 9, Table 2) as a function of bandgap energy, (b, e) final as a function of initial power conversion efficiency, and (c, f) degradation rate (Equation 10 in Table 2) as a function of initial efficiency. The characteristic **t_{95} times** are also plotted as a function of bandgap energy (g), initial efficiency (h), and publication date (i). Experimental data are summarized in Section 7.4. The solid and dot–dashed blue lines in the STEY plots (a, d) represent the detailed balance theoretical limits for single-junction and double-junction devices, respectively. In (b, e), the diagonal dot–dot–dashed lines indicate where the final and initial efficiencies are equal. In (c, f), positive values above the horizontal dotted line denote devices where the PCE increased relative to the initial value.

>5 Wh cm^{-2} after 200 h (Figure 7a) and >24 Wh cm^{-2} after 1000 h (Figure 7d) of operational stability test. Notably, efficiencies measured after 200 h and 1000 h are in some cases higher than the initial values, consistent with the positive degradation rates observed in Figure 7c,f.

Multijunction devices, particularly silicon/perovskite tandems, have reached initial efficiencies above 34%, while also delivering the highest energy yield in the e-PV database, surpassing 30 Wh cm^{-2} after 1000 h of testing. Xu et al. [78] attributed this performance to a bilayer interfacial passivation strategy, which incorporated ultrathin LiF layers followed by deposition of diammonium diiodide molecules at the perovskite/transport layer interface. This approach effectively suppresses non-radiative recombination, enhances charge extraction, and the tandem cell achieves a certified stabilized *PCE* of 33.89%, with a high *FF* (83%) and a V_{oc} of 1.97 V. However, this multilayer design also resulted in an accelerated degradation rate of 0.16% per day—more than twice the value reported for the most stable single-junction perovskite solar cells. Similarly, high absolute degradation rates (>0.2% loss per day) have been observed in other tandem devices tested for less than 1000 h (Figure 7c). This early-stage decline is likely associated with the complex interfacial engineering required in tandem architectures.

The lowest degradation rate for a device with initial PCE over 25% is calculated for the operational stability test reported by Zhu et al. [79] with a value of −0.003% per day. In their work, tris(2,4,6-

trimethyl-3-(pyridin-3-yl)phenyl)borane (3TPYMB) was incorporated through hydrogen bonding and Lewis acid–base interactions with perovskite surfaces and grain boundaries. As a result, their unencapsulated devices maintained 97.8% of the initial PCE after 1,800 h of continuous maximum power point operation under N_2 atmosphere, 1 sun illumination, and 60°C conditions. Rather than relying on external surface passivation, this strategy leverages hydrogen bonding and Lewis acid–base interactions to directly modulate perovskite grain surfaces and interfacial energy levels. This approach enhances charge transport while mitigating interfacial degradation from ionic migration, thereby enabling the simultaneous achievement of high PCE and long-term stability.

The highest values E_{1000h} (Figure 6d) and t_{95} among cells with PCE>25% (Figure 7h) were reported by Wu et al. [80], for an encapsulated perovskite solar cell that retained 97% of its initial 25.5% PCE after 2000 h, corresponding to an energy yield of 26.2 Wh cm^{-2} under maximum power point (MPP) tracking at 1 sun white LED, ∼45°C, ∼60% relative humidity in air. In this work, the authors designed diradical SAMs via a coplanar donor–acceptor conjugation strategy to facilitate hole transport across the interface. The diradical SAMs simultaneously enhanced hole conductivity, chemical stability, and large-area processability by combining the intrinsic diradical character with sterically hindered molecular design. These synergistic improvements represent a significant advance toward scalable and durable PSCs.

Notably, caution is warranted when interpreting records obtained from operational stability tests conducted at temperatures close to room temperature under white LED illumination, rather than following the ISOS-L-2 protocol, which recommends testing at a minimum of 65°C with solar simulators [76]. In such cases, uncertainties remain regarding the impact of thermal stress and ultraviolet (UV) or near-infrared (NIR) photon fluence on device stability. Consequently, it is unclear whether these results represent a genuine breakthrough in stability or are primarily specific to the reported testing conditions.

6 | Conclusions

The 2025 (and sixth) edition of the Emerging PV Report highlights significant progress across nearly all e-PV material families and device architectures, while also underscoring persistent challenges that must be addressed before widespread deployment. Perovskite devices remain the clear front-runners, approaching 90% of their detailed balance efficiency limit and exceeding 27% certified *PCE* in single junctions, with Si/perovskite tandem configurations achieving >34%. Organic photovoltaics have consolidated record efficiencies above 20%, although their relative proximity to the detailed balance efficiency limit remains lower (∼65%), constrained by non-radiative recombination losses that limit their V_{oc}. Other material classes, such as kesterites, matildites, antimony seleno-sulfides, and selenium, continue to advance incrementally, setting new efficiency and output power benchmarks but still lagging behind in absolute performance.

In terms of applications, flexible and transparent PVs show encouraging progress in efficiency, module scaling, and interfacial engineering strategies, yet their mechanical durability remains underexplored. The introduction of the fatigue factor (*F*) [10] metric and adoption of best practices for bending test protocols [14] are critical steps toward standardizing evaluation and comparability in this area. Likewise, operational stability remains a bottleneck: while some single-junction perovskites have demonstrated >2000 h of near-stable operation, tandem devices exhibit higher early-stage degradation, likely linked to interfacial complexity.

Looking ahead, three main priorities are highlighted for the e-PV community: (i) broadening stability and durability studies across technologies and operating conditions, particularly beyond perovskites; (ii) scaling device areas without sacrificing homogeneity and reproducibility; and (iii) advancing standardized protocols and database-driven benchmarks to accelerate cross-comparison and transparent reporting. By addressing these gaps, e-PV technologies can transition from laboratory success to reliable, versatile contributors in the global photovoltaic landscape.

7 | Tables

The tables below list the reports on the best achievements in most of the established and emerging PV technologies as a function of the device bandgap E_g. Unless otherwise noted, the E_g values were estimated by fitting the absorption threshold region of the corresponding EQE spectra to (Equation 2 in Table 2). Note that, for some absorber materials, this definition may result in a value slightly larger (typically on the order of the thermal energy) than that of the optical bandgap [6]. The new reports from articles published since August 2024 are highlighted in bold. The older reports from articles published before August 2024, which were already included in our previous surveys, are referenced to the corresponding e-PVr version. In contrast, each older report that was missed in the corresponding previous e-PVr is now included with its corresponding individual citation. All citations, further data, and visualization tools can be found on the emerging-pv.org website. This website and database are the main and recommended data collection path for inclusion in the e-PVr and a useful instrument that complements the tables below.

In the case of *PCE* reports of PSCs showing hysteresis behavior in the *J–V* characteristic, while sweeping the voltage in different directions and/or scan rates, the lower *PCE* value has been considered in each case. This is discussed in detail in Section S1.1.

For transparent/semitransparent cells, note that the *AVT* values may differ from those reported in the original manuscripts when a definition different from that of (Equation 6), in Table 2, is used in the original published article.

7.1 | Highest Efficiency Research Solar Cells Tables

TABLE 3 | Perovskite single-junction solar cells with the highest efficiency: performance parameters as a function of device absorber bandgap energy (from the EQE spectrum) [15].

E_g [eV]	PCE [%]	V_{oc} [mV]	J_{sc} [mA cm^{-2}]	FF [%]	Absorber perovskite	Refs.
1.12	12.4	967	17.5	72.9	$MAPb_{0.5}Sn_{0.5}Br_3$:Bi^{3+}:$BA_2MA_4Sn_5I_{16}$	[3]
1.18	24.3	1070	29.1	78.0	$FA_{0.7}MA_{0.3}Pb_{0.7}Sn_{0.3}I_3$/BTBTI:PCBM	[3]
1.18	23.4	1067	28.9	75.8	$FA_{0.7}MA_{0.3}Pb_{0.7}Sn_{0.3}I_3$/BTBTI:PCBM	[3][a]
1.24	**23.5**	**882**	**32.7**	**81.6**	**$Cs_{0.1}FA_{0.6}MA_{0.3}Pb_{0.5}Sn_{0.5}I_3$**	[81]
1.25	**23.7**	**887**	**32.8**	**81.7**	**$Cs_{0.1}FA_{0.6}MA_{0.3}Pb_{0.5}Sn_{0.5}I_3$**	[40]
1.26	**23.9**	**900**	**33.1**	**80.0**	**$Cs_{0.1}FA_{0.6}MA_{0.3}Pb_{0.5}Sn_{0.5}I_3$**	[49]
1.26	23.4	871	33.0	81.4	$FA_{0.7}MA_{0.3}Pb_{0.5}Sn_{0.5}I_3$	[4]
1.26	23.2	880	32.8	80.1	$FA_{0.7}MA_{0.3}Pb_{0.5}Sn_{0.5}I_3$	[5]
1.27	24.2	894	33.4	80.9	$Cs_{0.2}FA_{0.76}Rb_{0.04}Pb_{0.5}Sn_{0.5}I_3$	[82]
1.27	22.1	850	32.3	80.3	$FA_{0.7}MA_{0.3}Pb_{0.5}Sn_{0.5}I_3$	[5]
1.28	20.6	842	30.6	80.1	FSA: $FA_{0.7}MA_{0.3}Pb_{0.5}Sn_{0.5}I_3$	[2][a]
1.28	21.7	850	31.6	80.8	FSA: $FA_{0.7}MA_{0.3}Pb_{0.5}Sn_{0.5}I_3$	[2]
1.28	21.2	820	32.5	79.3	$Cs_{0.2}FA_{0.8}Pb_{0.5}Sn_{0.5}I_3$	[4]
1.29	23.3	880	32.8	80.8	$Cs_{0.025}FA_{0.475}MA_{0.5}Pb_{0.5}Sn_{0.5}Br_{0.075}I_{2.925}$	[3]
1.29	20.3	842	31.6	76.3	$Cs_{0.17}FA_{0.83}Pb_{0.5}Sn_{0.5}I_3$	[4]
1.29	19.5	810	32.1	75.0	$Cs_{0.25}FA_{0.75}Pb_{0.5}Sn_{0.5}I_3$	[4]
1.30	18.8	820	29.6	77.3	$FA_{0.6}MA_{0.4}Pb_{0.4}Sn_{0.6}I_3$	[2]
1.30	17.1	840	27.9	73.0	$Cs_{0.05}FA_{0.8}MA_{0.15}Pb_{0.5}Sn_{0.5}I_3$	[2]
1.31	5.0	420	23.8	50.3	$CsSnI_3$	[2][b]
1.31	7.1	486	22.9	64.0	$MASnI_3$	[2][b]
1.31	14.1	740	26.7	71.4	$Cs_{0.25}FA_{0.75}Pb_{0.5}$ $Sn_{0.5}I_3$	[2]
1.32	11.6	720	23.4	68.9	$MAPb_{0.4}Sn_{0.6}$ $Br_{0.2}I_{2.8}$	[2]
1.33	7.5	450	24.9	67.0	$CsSnI_3$:MBAA	[2]
1.34	10.0	767	20.5	63.6	$MAPb_{0.4}Sn_{0.6}I_3$	[2]
1.34	12.1	780	20.7	75.1	$MAPb_{0.4}Sn_{0.6}Br_{0.4}I_{2.6}$	[2]
1.35	21.1	846	31.4	79.5	$FAPb_{0.5}Sn_{0.5}I_3$	[5]
1.35	16.3	780	26.5	79.0	$FAPb_{0.7}Sn_{0.3}I_3$	[2]
1.36	8.2	630	19.7	66.1	$CsSnI_3$	[2]
1.37	14.7	737	27.1	73.6	$FA_{0.3}MA_{0.7}Pb_{0.7}Sn_{0.3}I_3$	[2]
1.38	17.3	810	28.2	75.4	$FAPb_{0.75}Sn_{0.25}I_3$	[2]
1.38	15.2	800	26.2	72.5	$MAPb_{0.75}Sn_{0.25}I_3$	[2]
1.39	20.6	1020	26.6	76.0	$FA_{0.7}MA_{0.3}Pb_{0.7}Sn_{0.3}I_3$	[2]
1.40	15.4	856	24.8	72.4	$FA_{0.85}PEA_{0.15}SnI_3$	[5]
1.40	15.1	815	25.2	73.6	$FA_{0.85}PEA_{0.15}SnI_3$	[5][a]
1.40	8.2	745	17.8	61.8	$MAPb_{0.6}Sn_{0.4}I_3$	[2]
1.40	10.1	655	22.1	69.6	$FASnI_3$ + DipI + $NaBH_4$	[3]
1.41	14.0	780	23.6	76.3	$FASnI_3$	[5]
1.42	17.1	830	26.9	76.7	$CsPb_{0.6}Sn_{0.4}I_3$	[5]
1.42	14.3	920	20.4	76.2	$FASnI_3$	[3]
1.42	14.4	820	22.4	78.0	$MAPb_{0.75}Sn_{0.25}I_3$	[2]
1.42	13.2	840	20.3	78.0	$EA_{0.098}EDA_{0.01}FA_{0.882}SnI_3$	[2]
1.43	15.7	974	21.7	74.1	$FASnI_3$	[5]

(Continues)

TABLE 3 | (Continued)

E_g [eV]	PCE [%]	V_{oc} [mV]	J_{sc} [mA cm^{-2}]	FF [%]	Absorber perovskite	Refs.
1.43	12.4	949	17.4	74.9	$FA_{0.85}PEA_{0.15}SnI_3$:NH_4SCN	[2][a]
1.44	**24.0**	**1130**	**28.5**	**75.4**	**PM6:Y7:$PC_{61}BM$/$MAPbCl_xI_{3-x}$**	[83]
1.44	**12.2**	**716**	**23.8**	**71.9**	**$EA_{0.098}EDA_{0.01}FA_{0.882}Ge_{0.05}Sn_{0.95}I_3$**	[84]
1.44	12.3	750	21.7	75.3	$EA_{0.098}EDA_{0.01}FA_{0.882}SnI_3$	[3]
1.44	10.1	642	22.2	70.8	$Cs_{0.2}FA_{0.8}SnI_3$	[2][a]
1.44	10.2	638	22.0	72.5	$FASnI_3$:FOEI	[2][a]
1.45	14.8	820	25.2	71.69	$FASnI_3$:FPEABr	[5]
1.45	14.0	828	24.0	69.3	$FASnI_3$:FPEABr	[3][a]
1.45	13.3	907	21.2	69.2	$FA_{0.75}MA_{0.25}SnBr_{0.25}I_{2.75}$	[5]
1.45	13.6	840	22.9	70.8	$FASnI_3$	[3]
1.45	12.8	869	19.6	74.5	$FARbSn(Br,Cl,I)_3$	[4]
1.46	14.2	821	23.3	74.1	$FASnI_3$	[5]
1.46	12.0	774	22.6	69.24	$FASnI_3$	[5][b]
1.46	11.4	700	22.6	72.3	$FASnI_3$	[5]
1.47	13.1	770	22.9	74.4	$Cs_{0.05}FA_{0.95}SnI_3$	[4]
1.48	6.0	460	23.9	53.9	$CsSnI_3$	[2]
1.49	22.3	1090	26.3	78.0	$FA_{0.6}MA_{0.4}PbI_3$ (sc)	[2]
1.50	**26.3**	**1190**	**26.3**	**84.1**	**$FAPbI_3$**	[85]
1.50	**26.1**	**1100**	**26.0**	**84.0**	**$FAPbI_3$**	[85][a]
1.50	24.5	1166	25.7	82.0	$FA_{0.95}Rb_{0.05}PbI_3$	[5]
1.51	25.6	1193	24.9	85.9	$Cs_{0.025}FA_{0.90}MA_{0.075}PbI_3$	[5]
1.52	**26.5**	**1175**	**26.3**	**85.9**	**$FAPbI_3$**	[86]
1.52	**26.2**	**1172**	**25.7**	**82.0**	**$FAPbI_3$**	[86][a]
1.52	26.1	1164	26.1	85.7	$Cs_{0.05}FA_{0.95}PbI_3$	[5]
1.53	**26.8**	**1191**	**26.6**	**84.4**	**$FAPbI_3$**	[23]
1.53	**26.0**	**1190**	**26.0**	**84.0**	**$FAPbI_3$**	[23][a]
1.53	26.5	1180	26.4	86.2	$Cs_{0.05}FA_{0.85}MA_{0.1}PbI_3$	[5]
1.53	26.2	1174	26.1	85.2	$Cs_{0.05}FA_{0.85}MA_{0.1}PbI_3$	[5][a]
1.54	**26.9**	**1203**	**27.1**	**82.3**	[c]	[22][a]
1.54	**27.3**	**1200**	**26.3**	**85.4**	[c]	[22][a]
1.54	**26.5**	**1182**	**26.5**	**84.5**	**$FAPbI_3$**	[87]
1.54	**26.2**	**1179**	**26.4**	**84.3**	**$FAPbI_3$**	[87][a]
1.54	26.0	1170	26.2	84.8	$Cs_{0.2}FA_{0.8}PbI_{1.9}Br_{1.1}$	[5]
1.54	**25.2**	**1175**	**25.6**	**83.8**	**$Cs_{0.1}FA_{0.9}PbI_3$**	[24][b]
1.55	**26.4**	**1210**	**26.1**	**83.3**	**$Cs_{0.2}FA_{0.8}$ Pb $Br_{1.1}I_{1.9}$**	[88]
1.55	**26.0**	**1207**	**25.9**	**83.3**	**$Cs_{0.2}FA_{0.8}$ Pb $Br_{1.1}I_{1.9}$**	[88][a]
1.55	26.0	1171	25.6	86.5	$Cs_{0.05}FA_{0.931}MA_{0.019}PbI_3$	[5]
1.55	26.0	1193	26.0	84.0	$FA_{0.97}MA_{0.03}PbBr_{0.09}I_{2.91}$	[5]
1.55	25.7	1184	25.7	84.2	$Cs_{0.05}FA_{0.931}MA_{0.019}PbBr_{0.06}I_{2.94}$	[5]
1.55	25.7	1188	25.7	84.2	$Cs_{0.05}FA_{0.931}MA_{0.19}PbBr_{0.06}I_{2.948}$	[5][a]
1.55	25.7	1170	25.7	85.3	$Cs_{0.1}FA_{0.9}PbI_3$	[5][a]
1.56	**25.5**	**1209**	**25.5**	**82.5**	**$Cs_{0.05}FA_{0.85}MA_{0.10}PbBr_{0.09}I_{2.91}$**	[89]
1.56	25.4	1185	25.4	84.6	$Cs_{0.01}FA_{0.9603}MA_{0.0297}PbBr_{0.09}I_{2.91}$	[5][a]

(Continues)

TABLE 3 | (Continued)

E_g [eV]	PCE [%]	V_{oc} [mV]	J_{sc} [mA cm^{-2}]	FF [%]	Absorber perovskite	Refs.
1.56	25.2	1201	24.8	84.5	$Cs_{0.05}FA_{0.9025}MA_{0.0475}PbBr_{0.15}I_{2.85}$	[4]
1.56	25.1	1209	24.7	83.9	$Cs_{0.05}FA_{0.9025}MA_{0.0475}PbBr_{0.15}I_{2.85}$	[4][a]
1.56	25.1	1195	24.9	84.4	$FA_{0.995}MA_{0.005}PbBr_{0.015}I_{0.985}$	[3]
1.56	25.2	1180	24.1	84.8	[c]	[2][a]
1.56	25.2	1181	25.1	84.8	$FAMAPb(I,Br,Cl)_3$	[2][a]
1.56	25.3	1193	25.1	84.6	$FAMAPb(I,Br,Cl)_3$	[2]
1.57	**26.3**	**1211**	**25.3**	**86.0**	**$Cs_{0.05}FA_{0.9}MA_{0.05}PbBr_{0.15}I_{2.85}$**	[90]
1.57	25.8	1194	25.5	84.9	$Cs_{0.05}FA_{0.9025}MA_{0.0475}PbBr_{0.15}I_{2.85}$	[5]
1.57	25.7	1190	26.0	83.2	$FAPbI_3$	[5]
1.57	25.6	1190	25.0	86.0	$Cs_{0.2}FA_{0.8}PbBr_{0.9}I_{2.1}$	[5]
1.57	24.7	1175	26.0	80.8	$FAPbI_3$	[5][a]
1.57	24.4	1190	25.6	80.2	$FAPb(I,Cl)_3$	[4]
1.57	23.6	1179	24.3	82.4	$FAPb(I,Cl)_3$	[4][a]
1.57	23.1	1170	23.8	82.7	$Cs_{0.05}$ $FA_{0.9025}MA_{0.475}PbBr_{0.15}I_{2.85}$	[4]
1.57	23.0	1170	24.1	81.6	$Cs_{0.05}FA_{0.88}MA_{0.07}PbBr_{0.24}I_{2.76}$	[2]
1.57	23.0	1147	25.1	79.9	$FA_{0.95}MA_{0.05}PbBr_{0.15}I_{2.85}$	[3][a]
1.57	23.4	1153	25.2	80.6	$Cs_{0.05}FA_{0.75}MA_{0.15}Rb_{0.05}PbBr_{0.15}I_{2.85}$	[3]
1.58	22.9	1173	23.4	80.0	$Cs_{0.05}FA_{0.9}MA_{0.05}PbBr_{0.26}I_{2.74}$	[3]
1.58	22.6	1186	24.2	78.6	$FA_{0.92}MA_{0.08}PbBr_{0.24}I_{2.76}$	[2][a]
1.58	22.6	1178	22.73	84.4	[c]	[2][a]
1.59	**25.7**	**1176**	**25.9**	**84.6**	**$Cs_{0.05}FA_{0.847}MA_{0.076}PbBr_{0.24}I_{2.76}$**	[91]
1.59	23.7	1216	23.9	81.6	$Cs_{0.05}FA_{0.82}MA_{0.13}PbBr_{0.39}I_{2.61}$	[5]
1.59	21.0	1140	23.7	77.7	$FA_{0.85}MA_{0.15}PbBr_{0.45}I_{2.55}$	[2][a]
1.60	23.1	1162	24.1	82.5	$Cs_{0.05}FA_{0.85}MA_{0.1}PbBr_{0.1}I_{0.9}$	[5]
1.60	22.1	1150	24.1	79.8	$Cs_{0.05}FA_{0.85}MA_{0.1}PbBr_{0.1}I_{0.9}$	[5][b]
1.60	20.3	1130	23.2	77.4	$MAPb(Cl,I)_3$	[2][a]
1.61	21.4	1120	23.1	82.9	$MAPbI_3$	[2][b]
1.61	21.5	1192	21.6	83.6	$Cs_{0.05}FA_{0.88}MA_{0.07}PbBr_{0.44}I_{2.56}$	[2][a]
1.61	23.2	1240	22.1	84.5	$Cs_{0.05}FA_{0.88}MA_{0.07}PbBr_{0.44}I_{2.56}$	[2]
1.61	22.6	1200	24.0	78.5	$Cs_{0.07}FA_{0.765}MA_{0.135}Rb_{0.03}PbBr_{0.45}I_{2.55}$	[2]
1.62	21.7	1180	22.5	81.7	$MAPbI_3$-DAP	[2]
1.63	20.3	1130	23.4	76.8	$Cs_{0.05}FA_{0.76}MA_{0.19}PbBr_{0.6}I_{2.4}$	[2]
1.64	22.4	1130	23.7	83.8	$Cs_{0.05}MA_{0.1425}FA_{0.8075}PbBr_{0.45}I_{2.55}$	[3]
1.64	20.4	1140	23.6	75.8	$Cs_{0.05}FA_{0.79}MA_{0.16}PbBr_{0.51}I_{2.49}$	[2]
1.65	**22.4**	**1200**	**22.2**	**84.3**	**$Cs_{0.17}FA_{0.83}PbBr_{1.8}I_{1.2}$**	[45]
1.65	21.9	1256	21.0	83.0	$Cs_{0.15}FA_{0.8}MA_{0.05}PbBr_{0.6}I_{2.4}$	[5]
1.65	21.9	1230	21.2	84.0	$Cs_{0.1}FA_{0.2}MA_{0.7}PbBr_{0.45}I_{0.2.55}$	[3]
1.66	21.3	1260	20.5	82.6	$Cs_{0.15}FA_{0.65}MA_{0.2}PbBr_{0.6}I_{2.4}$	[5]
1.67	21.6	1240	21.3	81.8	$Cs_{0.213}FA_{0.757}MA_{0.03}PbBr_{0.437}Cl_{0.09}I_{2.473}$	[5]
1.68	**22.8**	**1240**	**21.8**	**84.3**	**$Cs_{0.05}$ $FA_{0.8}MA_{0.15}PbBr_{0.75}I_{2.25}$**	[92]
1.68	22.7	1200	22.5	84.1	$Cs_{0.05}FA_{0.8}MA_{0.15}$ Pb $Br_{0.75}I_{2.25}$	[5][a]
1.68	20.7	1220	21.3	79.7	$Cs_{0.05}$ $FA_{0.8}MA_{0.15}PbBr_{0.75}I_{2.25}$	[2]
1.69	20.7	1220	20.6	82.1	$CsPbI_3$	[4]

(Continues)

TABLE 3 | (Continued)

E_g [eV]	PCE [%]	V_{oc} [mV]	J_{sc} [mA cm^{-2}]	FF [%]	Absorber perovskite	Refs.
1.70	21.6	1220	21.7	81.5	$CsPbI_3$	[4]
1.70	21.2	1244	20.6	82.5	$CsPbI_3$	[4]
1.70	20.3	1230	20.3	81.5	$CsPbI_3$	[4]
1.70	20.2	1176	20.8	82.5	$CsPbI_3$	[3]
1.71	21.3	1300	19.7	83.4	$Cs_{0.1}FA_{0.8}MA_{0.1}PbBr_{0.9}I_{2.1}$	[5]
1.72	**21.9**	**1260**	**21.0**	**82.6**	**$CsPbI_3$**	[58]
1.73	14.1	1230	15.9	72.7	$Cs_{0.1}FA_{0.9}PbBrI_2$	[5]
1.74	18.3	1269	18.9	76.3	$Cs_{0.095}MA_{0.1425}FA_{0.7125}Rb_{0.05}PbBrI_2$	[2]
1.74	20.0	1274	18.2	86.3	$Cs_{0.16}FA_{0.80}MA_{0.04}PbBr_{0.96}I_{2.04}$	[4]
1.74	20.2	1210	19.3	86.5	$Cs_{0.2}FA_{0.8}PbBr_{0.9}I_{2.1}$	[3]
1.75	19.8	1310	19.4	78.0	$Cs_{0.17}FA_{0.83}PbBr_{1.2}I_{1.8}$	[2]
1.76	18.5	1210	20.0	76.4	$Cs_{0.05}FA_{0.79}MA_{0.16}PbBr_{1.2}I_{1.8}$	[2]
1.77	**20.7**	**1332**	**18.3**	**84.8**	**$Cs_{0.2}FA_{0.8}PbBr_{1.2}I_{1.8}$**	[93]
1.77	19.5	1340	17.6	83.0	$Cs_{0.1}FA_{0.8}MA_{0.1}PbBr_{1.2}I_{1.8}$	[5]
1.78	19.8	1350	17.7	83.1	$Cs_{0.2}FA_{0.8}PbBr_{1.2}I_{1.8}$	[5]
1.79	**20.8**	**1370**	**18.1**	**83.6**	**$Cs_{0.2}FA_{0.8}PbBr_{1.2}I_{1.8}$**	[94]
1.79	19.6	1324	17.9	83.0	$Cs_{0.4}DMA_{0.1}FA_{0.5}PbBr_{0.72}Cl_{0.12}I_{2.16}$	[5]
1.79	19.3	1330	17.3	83.9	$Cs_{0.2}FA_{0.8}PbBr_{1.2}I_{1.8}$	[4][a]
1.80	19.5	1330	17.8	82.7	$Cs_{0.2}FA_{0.8}PbBr_{1.2}I_{1.8}$	[5]
1.80	19.1	1274	17.7	84.5	$Cs_{0.2}FA_{0.8}PbBr_{1.2}I_{1.8}$	[4]
1.81	16.3	1220	17.0	78.6	$Cs_{0.4}FA_{0.6}PbBr_{1.05}I_{1.95}$	[2]
1.82	17.2	1266	16.8	80.9	$Cs_{0.35}FA_{0.65}PbBr_{1.2}I_{1.8}$	[3]
1.83	16.9	1240	16.9	80.7	$FA_{0.6}MA_{0.4}PbBr_{1.2}I_{1.8}$	[3]
1.84	15.2	1260	15.6	77.3	$Cs_{0.2}FA_{0.8}PbBr_{1.2}I_{1.8}$-DAP	[2]
1.85	**18.8**	**1387**	**16.1**	**84.2**	**$Cs_{0.25}FA_{0.75}PbBr_{1.5}I_{1.5}$**	[95]
1.85	18.1	1360	16.0	83.0	$Cs_{0.1}FA_{0.8}MA_{0.1}PbBr_{1.5}I_{1.5}$	[5]
1.86	17.0	1340	15.9	79.8	$CsPbBr_{0.75}I_{2.25}$-0.5FAOAc	[2]
1.87	14.0	1280	14.0	78.1	$CsBa_{0.2}Pb_{0.8}BrI_2$	[2]
1.87	13.7	1220	14.6	76.8	$CsEu_{0.05}Pb_{0.95}BrI_2$	[2]
1.88	**19.2**	**1440**	**15.9**	**84.0**	**$CsPbBrI_2$**	[94]
1.88	17.4	1420	15.0	81.4	$CsPbBrI_2$	[3]
1.89	16.0	1310	15.8	77.5	$CsPbBrI_2$	[2]
1.89	15.6	1300	15.3	78.3	$CsPbBr_xI_{2-x}$	[2]
1.90	15.0	1240	16.0	75.6	$InCl_3$:$CsPbI_2Br$	[2][a]
1.90	16.5	1242	16.3	81.3	$CsPbBrI_2$	[4]
1.90	16.1	1320	15.3	79.7	$CsPbBrI_2$	[2]
1.90	14.5	1300	14.3	78.1	$CsPbBrI_2$	[4]
1.90	14.7	1302	14.2	79.6	$CsPbBrI_2$	[4]
1.90	14.2	1210	14.8	79.0	$CsPbBrI_2$	[5]
1.90	14.0	1269	14.9	73.8	$CsPbBrI_2$	[4]
1.91	16.2	1393	14.0	83.5	$Cs_{0.1}FA_{0.8}MA_{0.1}PbBr_{1.8}I_{1.2}$	[5]
1.91	14.5	1300	14.3	77.8	$CsPbBrI_2$	[4]
1.91	14.4	1312	15.6	70.1	$Cs_{0.83}FA_{0.17}PbBr_{1.8}I_{1.2}$	[2]

(Continues)

TABLE 3 | (Continued)

E_g [eV]	PCE [%]	V_{oc} [mV]	J_{sc} [mA cm^{-2}]	FF [%]	Absorber perovskite	Refs.
1.91	14.2	1160	15.7	77.9	$CsPbBrI_2$	[2]
1.91	2.0	620	5.4	60.8	$MA_3Sb_2I_9$+HI	[2][b]
1.93	16.6	1417	14.2	82.7	$Cs_{0.25}FA_{0.60}MA_{0.15}PbBr_{1.5}I_{1.35}OCN_{0.15}$	[5]
1.94	13.4	1240	14.2	76.0	$CsPbBr_{1.2}I_{1.8}$	[3]
1.98	8.3	1080	12.3	62.0	$CsPbBr_2I$	[2]
1.99	13.4	1312	13.4	76.3	$Cs_{0.85}Rb_{0.15}PbBr_{1.25}I_{1.75}$	[4]
2.00	9.6	1185	11.2	72.3	$Cs_{0.15}FA_{0.85}PbBr_{2.1}I_{0.9}$	[2]
2.03	2.8	836	6.4	52.7	$MAPbBr_{1.77}I_{1.23}$	[2]
2.04	10.3	1340	9.7	79.2	$MAPbBr_{2.1}I_{0.9}$	[2]
2.05	6.1	1450	5.4	77.1	$MAPbBr_2I$	[2]
2.09	10.2	1270	11.5	69.4	$CsPbBr_2I$	[2]
2.10	10.7	1261	11.8	72.0	$CsPbBr_2I$	[2]
2.11	9.2	1200	10.2	74.6	GAI-DEE-$CsPbBr_2I$	[2]
2.20	8.9	1639	7.7	70.6	$FAPbBr_3$	[3]
2.27	10.6	1552	8.9	76.5	$FAPbBr_3$	[2]
2.28	8.1	1640	6.7	74.0	$FAPbBr_3$	[5][b]
2.28	10.5	1520	8.3	83.0	$CsPbBr_3$	[3]
2.29	10.2	1650	8.7	71.1	$MAPbBr_3$	[3]
2.30	11.2	1574	8.5	83.7	$CsPbBr_3$	[4]
2.31	9.7	1458	8.1	81.9	$CsPbBr_3$	[2]
2.32	10.1	1653	7.7	79.1	$MAPbBr_3$	[2]
2.33	8.5	1580	6.6	82.0	$CsPbBr_3$	[2]
2.33	8.2	1470	7.3	76.1	$CsPbBr_3$	[2]
2.34	10.7	1635	7.8	84.1	$CsPbBr_3$	[3]
2.34	10.1	1602	7.9	80.0	$CsPbBr_3$	[2]
2.34	9.7	1584	7.4	82.8	$CsPbBr_3$	[2]
2.35	10.7	1622	7.9	83.5	$CsPbBr_3$	[2]
2.35	10.6	1610	7.8	84.4	$CsSnBr_3$	[2]
2.35	10.2	1611	7.8	81.0	$CsPbBr_3$	[3]
2.36	10.3	1570	8.2	79.6	$CsPb_{0.97}Tb_{0.03}Br_3$	[3]
2.36	4.0	1130	5.5	63.6	$CsPbBr_{2.9}I_{0.1}$	[2]
2.37	2.2	690	5.0	63.5	$MA_3Sb_2Cl_xI_{9-x}$	[2]
2.38	8.1	1490	6.9	78.8	$CsPbBr_3$	[2]
2.41	2.7	1020	5.2	51.2	$Cs_2AgBiBr_6$	[2]
2.42	1.1	870	2.9	43.0	$BdAPbI_4$	[2]
2.43	2.8	820	5.7	60.3	$CsPb_2Br_5$	[2]
2.44	2.4	1140	3.4	60.9	$FAPbBr_{2.1}Cl_{0.9}$	[2]
2.45	2.9	1010	4.1	70.9	$Cs_2AgBiBr_6$	[2]
2.46	1.7	1060	3.9	40.2	$Cs_2AgBiBr_6$	[2]
2.47	3.3	1278	3.3	77.5	$Cs_2AgBiBr_6$	[3]
2.48	1.4	1060	2.5	52.0	$FAPbBr_2Cl$	[2]

[a]Certified power conversion efficiency.
[b]Notable exception included as a material and/or large-area highlight.
[c]Notable exception included as a PCE highlight without the absorber information.
[d]PCE from *J-V* with significant hysteresis and MPP tracking closer to the listed value; sc, single crystal.

TABLE 4 | Organic single-junction solar cells with the highest efficiency: performance parameters as a function of device absorber bandgap energy (from the EQE spectrum) [15].

E_g [eV]	PCE [%]	V_{oc} [mV]	J_{sc} [mA cm^{-2}]	FF [%]	Absorber blend	Refs.
1.22	13.4	663	30.0	67.1	PTB7-Th:ATT-9	[3]
1.32	13.0	916	20.2	70.1	BTR:Y6:bisPC$_{71}$BM	[3]
1.32	10.6	690	24.3	63.2	PTB7-Th:IEICO-4F	[2]
1.33	13.9	865	22.4	71.4	BTR:MeIC:Y11	[3]
1.34	12.8	712	27.3	65.9	PTB7-Th:IEICO-4F	[2]
1.35	19.3	870	28.6	77.9	PM6:BTP-eC9:L8-BO	[4]
1.35	17.0	804	27.2	76.4	PM6:mBzS-4F	[2]
1.35	15.9	820	26.3	73.4	PM6:Y6	[2]
1.36	15.9	846	25.4	74.1	PM6:Y11	[2][a]
1.36	18.3	840	27.4	79.4	D18:NFAs	[4]
1.37	**19.9**	**852**	**29.0**	**80.6**	**PM6:BTA-E3**	[96]
1.37	20.2	863	29.1	80.5	PM6:BTP-eC9:SMA	[5]
1.37	19.4	858	28.3	79.7	PM6:BTP-eC9:Y6-1O:PC$_{71}$BM	[5]
1.37	18.3	856	26.9	79.4	PM6:BTP-eC9:PC$_{71}$BM	[2]
1.38	**20.8**	**876**	**29.2**	**81.5**	**D18-Cl:N3:AT-β2O**	[97]
1.38	18.9	880	26.9	79.8	PBDB-TCl:AITC:BTP-eC9	[4][a]
1.38	18.7	862	27.4	79.3	PM6:BTP-eC9:BTP-S9	[3][a]
1.39	**20.1**	**863**	**28.8**	**80.6**	**PM6:BTP-eC9**	[98]
1.39	**19.2**	**860**	**28.6**	**78.4**	**PM6:BTP-eC9**	[98][a]
1.40	**20.8**	**867**	**28.7**	**83.6**	**D18-Cl:BTP-C3F**	[99]
1.40	19.1	869	27.5	79.9	PBDB-TF:L8-BO:BTP-eC9	[3][a]
1.41	**20.6**	**937**	**27.2**	**80.8**	**D18:AQx-2F:eC9**	[100]
1.41	20.2	880	28.4	80.9	PBDB-TF:L8-BO:BTP-eC9	[5]
1.41	19.8	880	27.9	80.7	PBDB-TF:L8-BO:BTP-eC9	[5][a]
1.42	**20.5**	**890**	**28.1**	**1.42**	**D18:L8-BO:BTP-eC9**	[101][a]
1.42	**20.8**	**890**	**28.7**	**1.42**	**D18:L8-BO:BTP-eC9**	[101]
1.42	**20.0**	**870**	**28.3**	**81.2**	**PM6:P(BTzE-BDT):BTP-eC9**	[102]
1.43	**20.3**	**906**	**27.7**	**80.7**	**D18 (PY-IT)/L8-BO:C5-16 (D18)**	[27][a]
1.43	**21.0**	**914**	**27.7**	**82.9**	**D18 (PY-IT)/L8-BO:C5-16 (D18)**	[27]
1.43	20.9	923	27.9	80.8	D18-Cl:BTP-4F-P2EH	[5]
1.43	20.2	920	27.2	80.8	D18:Z8:L8-BO	[5]
1.43	19.8	900	27.0	81.0	D18:Z8:L8-BO	[5][a]
1.44	**19.6**	**907**	**27.4**	**78.7**	**D18:L8-BO**	[103]
1.44	19.9	900	27.5	80.4	D18:PM6:L8-BO	[5]
1.44	19.4	901	26.5	81.0	D18:L8-BO	[5]
1.45	**21.0**	**923**	**27.6**	**82.5**	**D18:L8-BO:BTP-eC9**	[26]
1.45	**20.8**	**918**	**27.6**	**81.9**	**D18:L8-BO:BTP-eC9**	[26] [a]

(Continues)

TABLE 4 | (Continued)

E_g [eV]	PCE [%]	V_{oc} [mV]	J_{sc} [mA cm^{-2}]	FF [%]	Absorber blend	Refs.
1.45	**19.8**	**920**	**26.5**	**81.2**	**N3-BO/F-BTA3**	[104][a]
1.45	**20.3**	**924**	**26.8**	**81.9**	**N3-BO/F-BTA3**	[104]
1.46	**19.8**	**903**	**27.3**	**80.2**	**PM6:L8-BO(TZ-3Cl)**	[105]
1.46	19.7	937	26.1	80.4	D18:AQx-2F	[5]
1.47	**19.3**	**951**	**26.4**	**76.9**	**PM6:3QY**	[106]
1.47	**19.3**	**902**	**27.5**	**78.1**	**PM6/L8-BO(BBS+CN)**	[107]
1.48	**15.2**	**944**	**21.91**	**73.5**	**PM6:CH-PHE**	[108]
1.50	15.4	920	22.6	74.1	PM6:DTTC-4Cl	[2]
1.51	13.3	780	22.9	75.0	PM6:SeTlC4Cl-DIO	[2]
1.52	10.4	850	18.0	68.0	PBDB-T:IDT-EDOT:$PC_{71}BM$	[2]
1.53	10.7	850	22.2	56.7	PM6:SeTlC4Cl	[2]
1.54	13.6	940	19.5	73.8	BTR:NITI:$PC_{71}BM$	[2]
1.55	12.0	840	19.5	73.3	PM6:IT-4F	[2]
1.56	12.1	826	20.9	70.1	PM6:IT-4F	[2]
1.58	13.9	950	21.7	67.4	PM6:DTTC-4F	[2]
1.58	13.5	880	20.6	74.53	PBDB-T-SF:IT-4F	[2]
1.61	13.4	940	20.2	70.5	PM6:DTC-4F	[2]
1.61	12.1	916	18.1	73.0	PBDB-T-2Cl:MF1	[2]
1.62	11.0	793	19.4	71.5	[c]	[2][a]
1.62	12.2	930	17.5	75.0	PTQ10:IDTPC	[2]
1.63	12.8	910	19.1	73.6	PTQ10:IDIC-2F	[2]
1.64	12.9	960	17.4	71.3	PTQ10:IDIC	[2]
1.65	10.4	910	16.2	70.6	PBDB-T:ITIC	[4]
1.66	12.1	815	20.3	73.2	[c]	[2][a]
1.67	11.2	1080	16.3	63.6	PvBDTTAZ:O-IDTBR	[4]
1.67	11.5	791	19.7	73.7	[c]	[2][a]
1.68	12.0	1030	18.5	63.0	PBDTTT-EFT:EH-IDTBR	[2]
1.69	8.9	878	13.9	72.9	PBT1-C:NFA	[2]
1.70	11.1	867	17.8	71.9	[c]	[2][a]
1.72	10.0	899	16.8	66.4	[c]	[2][a]
1.76	9.6	786	17.0	72.0	PPDT2FBT:$PC_{70}BM$	[2]
1.79	7.5	1140	10.6	62.1	BDT-ffBX-DT:PDI4	[2]
1.79	6.2	1230	8.9	56.6	BDT-ffBX-DT:SFPDI	[2]
1.85	9.0	900	13.8	72.9	BTR:$PC_{71}BM$	[2]
1.85	7.6	830	13.3	69.1	PBDB-T:$PC_{71}BM$	[2]
1.86	7.4	940	12.7	61.9	PBDB-T:NDP-Se-DIO	[2]
1.88	5.7	950	10.7	55.9	PBDB-T-2Cl:PC61BM	[2]
1.93	6.3	790	12.2	65.3	P3HT:TCBD14	[2]
2.01	3.7	592	10.4	59.2	P3HT:PCBM	[2]

[a]Certified power conversion efficiency.
[b]Notable exception included as a large-area highlight.
[c]Notable exception included as a PCE highlight without the absorber information.

TABLE 5 | Dye-sensitized single-junction solar cells with the highest efficiency: performance parameters as a function of device absorber bandgap energy (from the EQE spectrum) [15].

E_g [eV]	PCE [%]	V_{oc} [mV]	J_{sc} [mA cm^{-2}]	FF [%]	Sensitizing dye	Refs.
1.44	11.0	714	21.9	70.3	[b]	[2][a]
1.52	11.4	743	21.3	71.9	[b]	[2][a]
1.59	10.1	710	18.5	76.9	TF-tBu_C_3F_7	[2]
1.61	11.4	864	17.3	75.8	YS7	[5]
1.62	12.1	860	17.6	80.3	SGT-021	[5]
1.65	13.2	889	19.1	77.5	SGT-021/HC-A6+ThCA	[5]
1.66	13.0	910	18.1	78.0	SM315	[3]
1.66	10.7	849	16.6	75.9	BJS2	[2]
1.72	4.2	503	12.7	64.9	NP2	[4]
1.74	7.8	694	15.4	72.7	YD2	[2]
1.75	10.9	745	20.7	70.8	YKP-88/YKP-137 (6/4)	[2]
1.75	13.1	755	24.4	71.0	N719	[5]
1.76	12.0	960	15.9	79.0	SM371	[3]
1.77	10	740	18.1	74.7	N719	[2]
1.79	9.9	740	19.0	70.5	PI-COF:N719	[3]
1.80	9.1	744	19.0	64.0	N719	[2]
1.80	9.0	790	19.8	57.2	N719	[2]
1.80	6.5	663	13.3	74.5	SK7	[2]
1.81	8.5	700	19.4	62.6	N719	[3]
1.82	6.4	680	13.1	71.8	AN-11	[2]
1.83	15.2	1063	18.0	79.4	SL9 + SL10 /BPHA	[3][a]
1.83	8.9	820	19.0	57.5	N719	[2]
1.85	12.3	1020	15.2	79.1	[b]	[2][a]
1.85	13.4	1040	15.6	80.4	[b]	[4][a]
1.86	8.3	782	14.8	71.7	N719	[2]
1.87	9.1	1060	11.2	76.7	L351	[2]
1.88	7.8	730	14.3	74.7	TY4	[2]
1.90	11.6	946	16.9	72.9	ZL004	[4]
1.93	11.2	1140	13.0	75.6	L350	[2]
1.97	3.0	600	6.3	79.4	AN-14	[2]
1.99	5.4	689	11.3	69.5	SK6	[2]
2.00	6.3	732	12.0	71.7	CW10+SK6	[2]
2.01	9.2	1160	11.0	72.1	L349	[2]
2.02	8.1	760	14.3	75.0	TY6	[2]
2.05	3.9	680	7.4	77.5	AN-12	[2]
2.09	6.9	780	11.6	76.3	TY3	[2]
2.12	5.8	739	10.8	72.7	CW10	[2]
2.15	4.1	640	8.76	73.6	PS1	[3]
2.23	5.8	760	10.2	74.8	MS3	[2]
2.32	5.3	1170	6.4	70.8	L348	[2]

[a]Certified power conversion efficiency.
[b]Notable exception included as a PCE highlight without the absorber information.

TABLE 6 | Inorganic emerging single-junction solar cells with the highest efficiency: performance parameters as a function of device photovoltaic absorber bandgap energy (from the EQE spectrum) [15].

E_g [eV]	PCE (%)	V_{oc} [mV]	J_{sc} [mA cm^{-2}]	FF [%]	Absorber material/technology	Refs.
0.98	11.2	430	39.2	66.8	$Cu_2ZnSn(Se,S)_4$	[2]
1.02	11.6	441	39.2	67.4	$Cu_2ZnSnSe_4$	[2]
1.03	11.6	423	40.6	67.3	$Cu_2ZnSnSe_4$	[2][a]
1.04	9.6	425	34.9	64.5	$Cu_2ZnSnSe_4$	[2]
1.05	9.4	457	32.5	63.3	$Cu_2ZnSnSe_4$	[2]
1.05	13.8	514	38.7	69.3	$Cu_2ZnSn(S,Se)_4$	[5][b),c]
1.05	9.0	410	34.3	64.0	$Cu_2ZnSn(S,Se)_4$	[5]
1.06	9.5	460	31.1	66.4	$Cu_2ZnSnSe_4$	[2]
1.06	13.8	526	39.3	66.5	$Cu_2ZnSn(S,Se)_4$	[5]
1.06	13.2	477	40.1	69.0	$Cu_2ZnSn(S,Se)_4$	[2]
1.06	12.7	461	40.4	68.3	$Cu_2ZnSn(S,Se)_4$	[2][a]
1.07	12.5	491	37.4	68.2	$Cu_2ZnSnSe_4$	[2][a]
1.07	12.1	538	35.3	63.7	$Cu_2ZnSn(S,Se)_4$	[4][a]
1.08	13.8	546	36.3	69.4	$Cu_2ZnSn(S,Se)_4$	[4][a]
1.08	14.1	551	35.7	71.8	$Cu_2ZnSn(S,Se)_4$	[4]
1.09	15.1	530	38.4	74.0	$Cu_2ZnSn(S,Se)_4$	[5][a]
1.09	14.5	555	36.7	71.2	$Cu_2ZnSn(S,Se)_4$	[5]
1.09	14.9	555	36.9	72.7	$Cu_2ZnSn(S,Se)_4$	[4][a]
1.10	13.5	511	37.9	69.5	$Cu_2ZnSn(S,Se)_4$	[5][a,d]
1.10	14.1	565	35.4	70.3	$(Ag,Cu)_2ZnSn(S,Se)_4$	[5]
1.10	14.0	542	39.1	66.0	$Cu_2ZnSn(S,Se)_4$	[5]
1.10	13.8	545	36.8	68.7	$(Ag,Cu)_2ZnSn(S,Se)_4$	[5][a]
1.10	13.6	546	35.9	69.4	$Cu_2ZnSn(S,Se)_4$	[5]
1.10	13.6	538	36.2	69.9	$Cu_2ZnSn(S,Se)_4$	[3]
1.11	**14.1**	**535**	**39.0**	**67.6**	**$Cu_2ZnSn(S,Se)_4$**	[22][a,b]
1.11	**15.8**	**554**	**38.1**	**74.7**	**$Cu_2ZnSn(S,Se)_4$**	[22][a]
1.11	13.9	550	35.8	71.0	$Cu_2ZnSn(S,Se)_4$	[5]
1.11	13.1	547	34.3	70.0	$Cu_2ZnSn(S,Se)_4$	[3]
1.11	12.8	526	35.3	68.9	$Cu_2ZnSn(S,Se)_4$	[3][a]
1.12	12.1	494	36.2	67.5	$Cu_2ZnSn(S,Se)_4$	[4][a]
1.12	12.3	527	32.3	72.3	$Cu_2Zn(Sn_{0.78}Ge_{0.22})Se_4$	[2]
1.13	**15.0**	**560**	**37.4**	**71.7**	**$Cu_2ZnSn(S,Se)_4$**	[28]
1.13	**14.3**	**559**	**37.4**	**68.5**	**$Cu_2ZnSn(S,Se)_4$**	[28][a]
1.14	13.3	531	37.8	66.2	$Cu_2ZnSn(S,Se)_4$	[5]
1.14	12.6	541	35.4	65.9	$Cu_2ZnSn(S,Se)_4$	[2][a]
1.15	14.1	573	35.1	70.1	$Cu_2ZnSn(S,Se)_4$	[5]
1.15	13.2	531	37.5	66.3	$Cu_2ZnSn(S,Se)_4$	[5]
1.15	10.3	522	28.9	68.5	$Cu_2ZnSn(S,Se)_4$	[4][a]
1.16	11.2	539	33.1	62.8	$Cu_2ZnSn(S,Se)_4$	[2]
1.16	12.9	494	38.2	68.3	$Cu_2ZnSn(S,Se)_4$	[5]
1.16	12.9	546	35.9	65.8	$Cu_2ZnSn(S,Se)_4$	[4][b]
1.16	11.8	498	36.3	66.5	$Cu_2ZnSn(S,Se)_4$	[4][b]
1.18	13.3	546	36.9	66.1	$Cu_2ZnSn(S,Se)_4$	[5]

(Continues)

TABLE 6 | (Continued)

E_g [eV]	PCE (%)	V_{oc} [mV]	J_{sc} [mA cm^{-2}]	FF [%]	Absorber material/technology	Refs.
1.19	9.8	537	32.6	56.3	$Cu_2ZnSn(S,Se)_4$	[4]
1.2	13.7	544	36.7	68.5	$Cu_2ZnSn(S,Se)_4$	[5]
1.20	8.12	432	35.5	57.9	Sb_2Se_3	[5]
1.21	3.7	280	30.9	41.9	$AgBiS_2$	[5]
1.22	7.5	413	28.9	62.4	Sb_2Se_3	[2]
1.23	7.6	410	30.5	60.5	Sb_2Se_3	[5]
1.23	10.6	467	33.5	67.6	Sb_2Se_3	[4][b]
1.24	**10.6**	**478**	**31.7**	**69.9**	**Sb_2Se_3**	[109]
1.24	**10.2**	**477**	**30.6**	**69.6**	**Sb_2Se_3**	[109][a]
1.25	**10.8**	**511**	**29.2**	**72.8**	**$AgBiS_2$**	[32]
1.27	4.8	370	27.3	47.3	Sb_2Se_3	[2]
1.29	4.0	340	22.9	51.0	Sb_2Se_3	[2]
1.30	10.2	518	27.2	72.4	$AgBiS_2$	[5]
1.30	9.2	496	27.1	68.1	$AgBiS_2$	[5][b]
1.30	**10.7**	**576**	**26.9**	**69.0**	**$Sb_2(S,Se)_3$**	[31][a,d]
1.31	8.6	440	32.2	60.8	Sb_2Se_3	[5]
1.31	7.3	420	29.2	59.7	Sb_2Se_3	[2]
1.33	8.6	520	27.8	59.8	Sb_2Se_3	[3]
1.35	10.1	551	26.0	70.1	$Sb_2(S,Se)_3$	[4]
1.36	9.2	492	29.5	63.7	Sb_2Se_3	[5][b),c]
1.37	12.3	668	27.1	67.9	Cu_2ZnSnS_4	[5][c]
1.37	7.1	480	24.7	60.0	$AgBiS_2$	[3]
1.38	8.1	474	27.7	62.2	Sb_2Se_3	[5]
1.39	8.9	482	26.8	68.5	$AgBiS_2$	[3][a]
1.39	9.2	495	27.1	68.4	$AgBiS_2$	[3]
1.41	6.3	450	22.1	63.0	$AgBiS_2$	[4]
1.45	8.5	625	24.4	55.7	$Cu_2ZnGeSe_4$	[3]
1.45	**10.8**	**633**	**24.9**	**68.6**	**$Sb_2(S,Se)_3$**	[29]
1.48	10.8	631	25.3	67.4	$Sb_2(S,Se)_3$	[4]
1.50	**11.5**	**709**	**24.2**	**67.2**	**Cu_2ZnSnS_4**	[110][a]
1.50	11.0	731	21.7	69.3	Cu_2ZnSnS_4	[2][a]
1.50	**10.8**	**673**	**24.5**	**65.4**	**$Sb_2(S,Se)_3$**	[30]
1.50	**10.5**	**672**	**23.7**	**65.9**	**$Sb_2(S,Se)_3$**	[30][a]
1.50	10.0	655	24.1	63.3	$Sb_2(S,Se)_3$	[3][a]
1.52	12.1	749	23.4	68.9	Cu_2ZnSnS_4	[5][a]
1.52	8.7	664	20.6	63.9	$(Cu_{0.99}Ag_{0.01})_{1.85}(Zn_{0.8}Cd_{0.2})_{1.1}SnS_4$	[2]
1.53	8.5	670	20.4	62.1	$Sb_2(S,Se)_3$	[4]
1.54	10.7	673	23.7	66.8	$Sb_2(S,Se)_3$	[3]
1.54	9.7	638	23.2	65.5	$Sb_2(S,Se)_3$	[3]
1.55	10.2	736	21.0	65.8	Cu_2ZnSnS_4	[4]
1.55	10.5	664	23.8	66.3	$Sb_2(S,Se)_3$	[3]
1.57	**8.3**	**647**	**20.0**	**63.7**	**$Sb_2(S,Se)_3$**	
1.59	10.7	801	21.0	63.7	Cu_2ZnSnS_4	[5]

(Continues)

TABLE 6 | (Continued)

E_g [eV]	PCE (%)	V_{oc} [mV]	J_{sc} [mA cm^{-2}]	FF [%]	Absorber material/technology	Refs.
1.59	11.4	746	21.8	70.1	Cu_2ZnSnS_4	[4][a]
1.73	8.0	757	60.5	17.4	Sb_2S_3	[3]
1.80	7.5	711	16.1	65.0	Sb_2S_3	[2]
1.84	4.9	680	13.7	53.0	Sb_2S_3	[4]
1.95	5.8	870	10.8	62.1	Se	[4]
1.96	**8.1**	**930**	**14.4**	**60.6**	**Se**	[34]
1.97	5.2	991	10.0	52.4	Se	[4]

[a]Certified power conversion efficiency.
[b]Notable exception included missing the illuminated aperture/mask area information.
[c]"Effective" area subtracting that of the busbars and finger electrodes was used for the PCE calculation.
[d]Large-area cell highlight.

TABLE 7 | Single-junction solar cells with the highest efficiency among established technologies: performance parameters as a function of device absorber bandgap energy (from the EQE spectrum) [15].

E_g [eV]	PCE [%]	V_{oc} [mV]	J_{sc} [mA cm^{-2}]	FF [%]	Absorber material/technology	Refs.
1.09	19.8	716	34.9	79.2	$Cu(In,Ga)Se_2$	[2][a]
1.10	21.7	718	40.7	74.3	$Cu(In,Ga)Se_2$	[2][a]
1.11	26.7	751	41.2	86.5	Si	[4][a]
1.11	26.7	738	42.7	84.9	Si	[2][a]
1.13	21.4	725	37.3	79.2	Si	[5]
1.13	22.9	744	38.8	79.5	$Cu(In,Ga)Se_2$	[2][a]
1.13	23.6	767	38.3	80.5	$Cu(In,Ga)Se_2$	[4][a]
1.14	21.0	757	35.7	77.6	$Cu(In,Ga)Se_2$	[2][a]
1.15	23.4	734	39.6	80.4	$Cu(In,Ga)Se_2$	[2][a]
1.17	21.7	727	40.4	73.8	Si	[5]
1.18	20.0	706	40.7	69.7	Si	[3]
1.30	16.3	762	31.4	68.1	$Cu(In,Ga)Se_2$	[2]
1.40	22.3	898	31.7	78.9	CdTe	[4][a]
1.41	25.0	1045	28.7	83.0	GaAs	[5]
1.42	29.1	1127	29.8	86.7	GaAs	[2][a]
1.43	22.6	898	31.6	79.6	CdTe	[5]
1.42	21.0	876	30.3	79.4	CdTe	[2][a]
1.48	18.3	857	27.0	77.0	CdTe	[2][a]
1.60	15.2	902	23.1	73	$Cu(In,Ga)Se_2$	[2]
1.60	10.2	896	16.4	69.8	Si (amorphous)	[2][a]
1.69	10.6	896	16.1	75.6	Si (amorphous)	[2]
1.85	10.1	886	16.8	67.0	Si (amorphous)	[2][a]

[a]Certified power conversion efficiency.

TABLE 8 | Monolithic multijunction perovskite-based research solar cells with the highest efficiency: performance parameters as a function of the device photovoltaic bandgap energies (from the EQE spectra) of the sub-cells.

$E_{g,bottom}$ [eV]	$E_{g,middle}$, $E_{g,top}$ [eV]	PCE [%]	V_{oc} [mV]	J_{sc} [mA cm^{-2}]	FF [%]	Bottom absorber material	Middle, top absorber material[s]	Refs.
						Si/perovskite		
1.10	**1.67**	**34.6**	**1996**	**20.7**	**83.6**	**Si**	**$Cs_{0.02}FA_{0.75}MA_{0.23}PbBr_{0.69}I_{2.31}$**	[38][a]
1.10	1.68	33.7	1996	21.0	85.3	Si	$Cs_{0.05}FA_{0.8}MA_{0.15}PbBr_{0.75}I_{2.25}$	[5]
1.10	**1.68**	**34.9**	**1997**	**21.1**	**82.8**	**Si**	[a,b]	[22]
1.10	1.69	32.8	1949	20.9	80.5	Si	$Cs_{0.05}FA_{0.8}MA_{0.15}PbBr_{0.75}I_{2.25}$	[5]
1.10	1.69	31.9	1943	22.1	77.6	Si	$Cs_{0.05}FA_{0.8}MA_{0.15}PbBr_{0.75}I_{2.25}$	[5][a]
1.11	**1.66**	**32.1**	**1920**	**20.7**	**80.9**	**Si**	**$Cs_{0.22}FA_{0.63}MA_{0.15}PbBr_{0.42}Cl_{0.09}I_{2.49}$**	[111]
1.11	1.67	33.7	1974	21.0	81.3	Si	[b]	[4][a]
1.11	1.67	30.1	1903	20.1	78.6	Si	$Cs_{0.14}FA_{0.86}PbBr_{0.66}\ I_{2.34}$	[5]
1.11	1.67	29.8	1920	19.5	79.4	Si	$Cs_{0.209}FA_{0.741}MA_{0.05}PbBr_{0.4275}Cl_{0.15}I_{2.4225}$	[4]
1.11	1.67	26.7	1756	19.2	79.2	Si	$Cs_{0.15}FA_{0.65}MA_{0.2}PbBr_{0.6}I_{2.4}$:PEA($I_{0.25}SCN_{0.75}$)	[2]
1.11	1.68	34.1	1980	20.7	83.2	Si	$Cs_{0.05}FA_{0.8}MA_{0.15}PbBr_{0.72}I_{2.28}$	[5, 78]
1.11	1.68	33.9	1966	20.8	83.0	Si	$Cs_{0.05}FA_{0.8}MA_{0.15}PbBr_{0.72}I_{2.28}$	[5][a]
1.11	1.68	25.7	1781	19.1	75.4	Si	$Cs_{0.05}FA_{0.8}MA_{0.15}PbBr_{0.75}\ I_{2.25}$	[2][a]
1.11	1.69	29.8	1190	19.5	79.8	Si	[b]	[3][a]
1.11	1.69	29.2	1929	19.5	77.6	Si	$Cs_{0.05}FA_{0.703}MA_{0.247}PbBr_{0.78}I_{2.22}$	[4]
1.11	**1.69**	**32.0**	**1980**	**20.5**	**78.8**	**Si**	**$Cs_{0.05}FA_{0.8}MA_{0.15}PbBr_{0.75}$** [112]**$I_{2.25}$**	[112]
1.11	**1.70**	**31.0**	**1880**	**20.5**	**80.4**	**Si**	**$CsPbI_3$**	[113]
1.11	**1.70**	**30.6**	**1897**	**20.7**	**78.1**	**Si**	**$CsPbI_3$**	[113][a]
1.12	1.55	22.3	1700	17.5	75.0	Si	$FAMAPbI_3$	[4]
1.12	1.64	26.0	1760	19.2	76.5	Si	$FA_{0.83}MA_{0.17}PbI_3$	[2]
1.12	1.65	26.5	1760	19.4	77.0	Si	$Cs_{0.05}\ FA_{0.79}MA_{0.16}PbBr_{0.51}\ I_{2.49}$	[2]
1.12	**1.68**	**33.1**	**2011**	**20.6**	**79.7**	**Si**	**$Cs_{0.13}FA_{0.87}PbBr_{0.78}\ I_{2.22}$**	[39]
1.12	1.68	28.8 (29.2)[c]	1895	19.2	78.9	Si	$Cs_{0.05}FA_{0.73}MA_{0.22}\ Pb\ Br_{0.69}I_{2.31}$	[2]
1.12	1.70	32.1	1867	20.7	83.3	Si	$CsFAPb(Br,I)_3$	[5]
1.12	**1.70**	**31.5**	**1925**	**20.7**	**78.9**	**Si**	**$Cs_{0.05}FA_{0.8}MA_{0.15}PbBr_{0.75}I_{2.25}$**	[114]
1.13	1.65	30.9	1953	19.8	79.9	Si	$Cs_{0.05}FA_{0.855}MA_{0.095}PbBr_{0.6}I_{2.4}$	[5][a]

(Continues)

TABLE 8 | (Continued)

$E_{g,bottom}$ [eV]	$E_{g,middle}$, $E_{g,top}$ [eV]	PCE [%]	V_{oc} [mV]	J_{sc} [mA cm^{-2}]	FF [%]	Bottom absorber material	Middle, top absorber material[s]	Refs.
1.13	1.67	28.3	1776	20.1	79.6	Si	$FAMAPb(Br,Cl,I)_3$	[3][a]
1.13	1.67	27.1	1886	19.1	75.3	Si	$CsFAMAPb(Br,Cl,I)_3$	[2]
1.13	**1.68**	**31.0**	**1892**	**20.2**	**80.8**	**Si**	$\mathbf{Cs_{0.05}FA_{0.8}MA_{0.15}Br_{0.72}PbI_{2.28}}$	[115]
1.13	**1.68**	**31.0**	**1912**	**20.1**	**80.9**	**Si**	$\mathbf{Cs_{0.05}FA_{0.73}MA_{0.22}PbBr_{0.69}I_{2.31}}$	[116]
1.13	1.68	28.9	1850	19.8	78.9	Si	$CsFAPb(Br,I)_3{:}MA(Cl_{0.5}SCN_{0.5})_{28.9}$	[4]
1.13	1.68	27.9	1833	19.4	77.5	Si	$CsFAPb(Br,I)_3{:}MA(Cl_{0.5}SCN_{0.5})_{28.9}$	[4][a]
1.13	**1.69**	**33.1**	**1970**	**20.3**	**82.8**	**Si**	$\mathbf{Cs_{0.05}FA_{0.8}MA_{0.15}PbBr_{0.75}I_{2.25}}$	[117]
1.13	**1.69**	**31.6**	**1945**	**20.1**	**79.3**	**Si**	$\mathbf{Cs_{0.05}FA_{0.8}MA_{0.15}PbBr_{0.75}I_{2.25}}$	[117][a]
1.13	1.69	32.5	1980	20.2	81.2	Si	$Cs_{0.209}FA_{0.741}MA_{0.05}PbBr_{0.4275}Cl_{0.15}I_{2.4225}$	[4][a]
1.13	1.69	31.3	1910	20.5	79.8	Si	$Cs_{0.18}FA_{0.82}Pb(Br,I)_3$	[4][a]
1.13	**1.70**	**31.1**	**1880**	**20.0**	**82.6**	**Si**	$\mathbf{Cs_{0.05}FA_{0.8}MA_{0.15}PbBr_{0.75}I_{2.25}}$	[92]
1.13	**1.70**	**29.6**	**1861**	**20.6**	**77.4**	**Si**	$\mathbf{Cs_{0.05}FA_{0.8}MA_{0.15}PbBr_{0.75}I_{2.25}}$	[92][a]
1.13	**1.70**	**29.6**	**1848**	**20.1**	**79.6**	**Si**	$\mathbf{FAPbI_3}$	[118]
1.14	**1.67**	**31.1**	**1946**	**19.78**	**80.9**	**Si**	$\mathbf{Cs_{0.2}FA_{0.8}PbBr_{0.6}I_{2.4}}$	[119]
1.14	1.68	27.5	1779	19.6	78.9	Si	$Cs_{0.22}FA_{0.78}PbBr_{0.45}Cl_{0.09}I_{2.55}$	[3]
1.14	**1.69**	**31.2**	**1950**	**19.77**	**80.9**	**Si**	$\mathbf{Cs_{0.05}FA_{0.8}PbBr_{0.75}I_{2.25}}$	[120]
1.14	1.69	26.0	1780	18.2	80.2	Si	$Cs_{0.15}FA_{0.7055}MA_{0.1445}PbBr_{0.6}I_{2.4}$	[3]
1.15	1.62	20.9	1690	15.9	77.6	Si	$MAPbI_3$	[2]
1.15	1.68	25.4	1800	17.8	79.4	Si	$Cs_{0.15}FA_{0.71}MA_{0.14}PbBr_{0.6}I_{2.4}$	[2]
1.15	1.68	25.0	1770	18.4	77.0	Si	$Cs_{0.25}FA_{0.75}PbBr_{0.6}\ I_{2.4}$	[2]
1.16	1.62	19.2	1701	16.1	70.1	Si	$MAPbI_3$	[2]
1.17	1.63	26.4	1804	18.1	80.6	Si	$FA_{0.83}MA_{0.17}PbBr_{0.51}I_{2.49}$	[4]
1.17	1.63	23.7	1770	17.9	74.5	Si	$FA_{0.83}MA_{0.17}PbBr_{0.51}I_{2.49}$	[4][b]
1.17	1.63	19.5	1772	17.7	62.3	Si	$FA_{0.83}MA_{0.17}PbBr_{0.51}I_{2.49}$	[4][b]
							GaAs/perovskite	
1.42	1.85	24.3	2160	14.3	78.8	GaAs	$Cs_{0.16}FA_{0.80}MA_{0.04}PbBr_{1.50}I_{1.50}$	[2]
							CIGS/perovskite	
1.01	1.61	24.3	1570	21.0	73.6	$CuInSe_2$	$Cs_{0.05}FA_{0.85}MA_{0.1}PbI_{2.7}Br_{0.3}$	[3]

(Continues)

TABLE 8 | (Continued)

$E_{g,bottom}$ [eV]	$E_{g,middle}$, $E_{g,top}$ [eV]	PCE [%]	V_{oc} [mV]	J_{sc} [mA cm^{-2}]	FF [%]	Bottom absorber material	Middle, top absorber material[s]	Refs.
1.01	1.61	23.5	1590	19.4	75.5	$CuInSe_2$	$Cs_{0.05}FA_{0.85}MA_{0.1}PbI_{2.7}Br_{0.3}$	[3][a]
1.08	1.64	23.5	1700	19.5	71.0	$Cu(In,Ga)Se_2$	$Cs_{0.05}FA_{0.7885}MA_{0.1615}PbBr_{0.51}I_{2.49}$	[4]
1.08	**1.64**	**24.6**	**1762**	**19.3**	**72.5**	**$Cu(In,Ga)Se_2$**	[b]	[22][a]
1.10	1.65	22.4	1774	17.3	73.1	$Cu(In,Ga)Se_2$	$Cs_{0.09}FA_{0.77}MA_{0.14}PbBr_{0.42}I_{2.58}$	[2][a]
1.11	1.64	21.6	1580	18.0	76.0	$Cu(In,Ga)Se_2$	$Cs_{0.05}FA_{0.7885}MA_{0.1615}PbBr_{0.51}I_{2.49}$	[2]
1.11	1.65	23.3	1680	19.2	71.9	$Cu(In,Ga)Se_2$	$Cs_{0.05}FA_{0.7885}MA_{0.1615}PbBr_{0.51}I_{2.49}$	[2]
1.11	1.68	24.2	1770	18.8	71.2	$Cu(In,Ga)Se_2$	$Cs_{0.05}FA_{0.7315}MA_{0.2185}PbBr_{0.69}I_{2.31}$	[3]
1.13	1.63	18.1	1645	17.7	62.0	$Cu(In,Ga)Se_2$	$FA_{0.83}MA_{0.17}PbBr_{0.51}I_{2.49}$	[5]
1.14	**1.67**	**24.6**	**1760**	**17.9**	**78.0**	**$Cu(In,Ga)Se_2$**	**$Cs_{0.17}FA_{0.83}PbBr_{1.8}I_{1.2}$**	[45]
1.14	**1.67**	**23.2 (22.9)**[c]	**1748**	**17.7**	**75.2**	**$Cu(In,Ga)Se_2$**	**$Cs_{0.17}FA_{0.83}PbBr_{1.8}I_{1.2}$**	[45][a]
1.15	**1.69**	**28.1**	**1938**	**19.1**	**75.8**	**$Cu(In,Ga)Se_2$**	**$Cs_{0.2}DMA_{0.1}FA_{0.65}MA_{0.05}PbBr_{0.3}I_{2.7}$**	[44]
1.15	**1.69**	**27.2**	**1923**	**19.0**	**74.4**	**$Cu(In,Ga)Se_2$**	**$Cs_{0.2}DMA_{0.1}FA_{0.65}MA_{0.05}PbBr_{0.3}I_{2.7}$**	[44][a]
1.16	**1.67**	**22.8**	**1820**	**16.9**	**74.1**	**$Cu(In,Ga)Se_2$**	**$Cs_{0.05}FA_{0.73}MA_{0.22}PbBr_{0.69}I_{2.31}$**	[121]
						Perovskite/perovskite		
1.25	1.75	27.2	2110	16.1	80.3	$FA_{0.7}MA_{0.3}Pb_{0.5}Sn_{0.5}I_3$	$Cs_{0.3}FA_{0.7}PbBr_{1.2}I_{1.8}$	[5]
1.25	**1.77**	**27.4**	**2140**	**15.5**	**82.3**	**$FA_{0.7}MA_{0.3}Pb_{0.5}Sn_{0.5}I_3$**	**$Cs_{0.2}FA_{0.8}PbBr_{1.2}I_{1.8}$**	[122]
1.25	1.78	27.1	2200	15.3	80.8	$FA_{0.6}MA_{0.4}Pb_{0.4}\ Sn_{0.6}I_3$	$Cs_{0.3}DMA_{0.1}FA_{0.6}PbBr_{0.9}I_{2.1}$	[4]
1.25	**1.79**	**28.2**	**2140**	**15.9**	**83.1**	**$FA_{0.7}MA_{0.3}Pb_{0.5}Sn_{0.5}I_3$**	**$Cs_{0.2}FA_{0.8}PbBr_{1.2}I_{1.8}$**	[123]
1.25	**1.80**	**28.5**	**2150**	**16**	**82.8**	**$Cs_{0.1}FA_{0.6}MA_{0.3}Pb_{0.5}Sn_{0.5}I_3$**	**$Cs_{0.2}FA_{0.8}PbBr_{1.2}I_{1.8}$**	[124]
1.25	**1.80**	**28.9**	**2143**	**16.3**	**82.7**	**$FA_{0.6}MA_{0.4}Pb_{0.4}Sn_{0.6}I_3$**	**$Cs_{0.2}FA_{0.8}PbBr_{1.2}I_{1.8}$**	[125]
1.25	**1.80**	**28.0**	**2126**	**16.2**	**81.2**	**$FA_{0.6}MA_{0.4}Pb_{0.4}Sn_{0.6}I_3$**	**$Cs_{0.2}FA_{0.8}PbBr_{1.2}I_{1.8}$**	[125][a]
1.25	1.80	28.4	2111	16.5	81.5	$FA_{0.7}MA_{0.3}Pb_{0.5}Sn_{0.5}I_3$	$Cs_{0.2}FA_{0.8}PbBr_{1.14}I_{1.86}$	[4]
1.25	1.80	28.0	2125	16.4	80.3	$FA_{0.7}MA_{0.3}Pb_{0.5}Sn_{0.5}I_3$	$Cs_{0.2}FA_{0.8}PbBr_{1.14}I_{1.86}$	[4][a]
1.25	1.80	26.3 (26.4)[c]	2044	16.5	78.1	$FA_{0.7}MA_{0.3}Pb_{0.5}Sn_{0.5}I_3$	$Cs_{0.2}FA_{0.8}PbBr_{1.14}I_{1.86}$	[3][a,d]
1.25	**1.81**	**28.6**	**2155**	**16.1**	**82.7**	**$Cs_{0.1}FA_{0.6}MA_{0.3}Pb_{0.5}Sn_{0.5}I_3$**	**$Cs_{0.2}FA_{0.8}PbBr_{1.2}I_{1.8}$**	[81]
1.26	**1.77**	**27.7 (28.3)**[c]	**2180**	**16.3**	**78.0**	**$Cs_{0.1}FA_{0.6}MA_{0.3}Pb_{0.5}Sn_{0.5}I_3$**	**$Cs_{0.2}FA_{0.8}PbBr_{1.2}I_{1.8}$**	[49][a]
1.26	1.78	28.2	2110	16.7	80.2	$FA_{0.7}MA_{0.3}Pb_{0.5}Sn_{0.5}I_3$	$Cs_{0.2}FA_{0.8}PbBr_{1.2}I_{1.8}$	[5]
1.26	**1.79**	**29.6**	**2176**	**16.3**	**83.4**	**$Cs_{0.1}FA_{0.6}MA_{0.3}Pb_{0.5}Sn_{0.5}I_3$**	**$Cs_{0.2}FA_{0.8}PbBr_{1.2}I_{1.8}$**	[40]
1.26	**1.79**	**29.5 (28.7)**[c]	**2179**	**16.3**	**83.3**	**$Cs_{0.1}FA_{0.6}MA_{0.3}Pb_{0.5}Sn_{0.5}I_3$**	**$Cs_{0.2}FA_{0.8}PbBr_{1.2}I_{1.8}$**	[40][a]

(Continues)

TABLE 8 | (Continued)

$E_{g,bottom}$ [eV]	$E_{g,middle}$, $E_{g,top}$ [eV]	PCE [%]	V_{oc} [mV]	J_{sc} [mA cm^{-2}]	FF [%]	Bottom absorber material	Middle, top absorber material[s]	Refs.
1.26	**1.79**	**28.5**	**2170**	**16.4**	**80.2**	**$FA_{0.7}MA_{0.3}Pb_{0.5}Sn_{0.5}I_3$**	**$Cs_{0.2}FA_{0.8}PbBr_{1.2}I_{1.8}$**	[43]
1.26	**1.79**	**28.5 (28.2)**[c]	**2157**	**16.6**	**79.5**	**$FA_{0.7}MA_{0.3}Pb_{0.5}Sn_{0.5}I_3$**	**$Cs_{0.2}FA_{0.8}PbBr_{1.2}I_{1.8}$**	[43][a]
1.26	**1.80**	**28.9**	**2146**	**16.2**	**83.3**	**$Cs_{0.1}FA_{0.6}MA_{0.3}Pb_{0.5}Sn_{0.5}I_3$**	**$Cs_{0.2}FA_{0.8}PbBr_{1.2}I_{1.8}$**	[93]
1.26	**1.80**	**28.4**	**2149**	**16.2**	**81.5**	**$Cs_{0.1}FA_{0.6}MA_{0.3}Pb_{0.5}Sn_{0.5}I_3$**	**$Cs_{0.2}FA_{0.8}PbBr_{1.2}I_{1.8}$**	[93][a]
1.26	**1.81**	**29.1**	**2151**	**16.51**	**82.0**	**$FA_{0.7}MA_{0.3}Pb_{0.5}Sn_{0.5}I_3$**	**$Cs_{0.2}FA_{0.8}PbBr_{1.2}I_{1.8}$**	[41][a]
1.26	**1.82**	**26.0**	**2080**	**16.0**	**78.0**	**$Cs_{0.05}FA_{0.7}MA_{0.25}Pb_{0.5}Sn_{0.5}I_3$**	**$Cs_{0.2}FA_{0.8}PbBr_{1.2}I_{1.8}$**	[126]
1.26	1.82	26.3	2130	15.2	81.0	$Cs_{0.05}FA_{0.7}MA_{0.25}Pb_{0.5}Sn_{0.5}I_3$	$Cs_{0.2}FA_{0.8}PbBr_{1.2}I_{1.8}$	[4][a]
1.26	1.84	26.6	2119	15.2	82.4	$FA_{0.6}MA_{0.3}Cs_{0.1}Sn_{0.5}Pb_{0.5}I_3$	$FA_{0.8}Cs_{0.2}PbBr_{1.2}I_{1.8}$	[4][a,b]
1.27	1.72	22.9	1915	15.0	79.8	$FA_{0.6}MA_{0.4}Pb_{0.4}Sn_{0.6}I_3$	$Cs_{0.05}FA_{0.8}MA_{0.15}$ Pb $Br_{0.45}I_{2.55}$	[2]
1.27	**1.79**	**28.6**	**2131**	**16.1**	**83.5**	**$FA_{0.6}MA_{0.4}Pb_{0.4}Sn_{0.6}I_3$**	**$Cs_{0.2}FA_{0.8}PbBr_{1.2}I_{1.8}$**	[127]
1.27	**1.79**	**27.8**	**2033**	**16.2**	**81.0**	**$FA_{0.6}MA_{0.4}Pb_{0.4}Sn_{0.6}I_3$**	**$Cs_{0.2}FA_{0.8}PbBr_{1.2}I_{1.8}$**	[127][a]
1.27	1.81	25.1	2021	15.6	79.5	$FA_{0.7}MA_{0.3}Pb_{0.5}Sn_{0.5}I_3$	$Cs_{0.2}FA_{0.8}PbBr_{1.2}I_{1.8}$	[4]
1.27	**1.82**	**27.7**	**2110**	**16.5**	**79.8**	**$Cs_{0.05}FA_{0.7}MA_{0.25}Pb_{0.5}Sn_{0.5}I_3$**	**$Cs_{0.2}FA_{0.8}PbBr_{1.2}I_{1.8}$**	[128]
1.27	1.85	23.4	2000	15.0	77.8	$Cs_{0.17}FA_{0.83}Pb_{0.5}Sn_{0.5}I_3$	$Cs_{0.05}FA_{0.57}MA_{0.38}PbBr_{1.2}I_{1.8}$	[4]
1.28	1.73	23.1	1880	16.0	77.0	$Cs_{0.25}FA_{0.75}Pb_{0.5}Sn_{0.5}I_3$	$Cs_{0.3}DMA_{0.1}$ $FA_{0.6}PbBr_{0.6}I_{2.4}$	[2]
1.28	1.79	24.5	1800	17.16	79.3	$Cs_{0.025}FA_{0.475}MA_{0.5}Pb_{0.5}Sn_{0.5}Br_{0.075}$ $I_{2.925}$	$Cs_{0.2}FA_{0.8}PbBr_{1.2}I_{1.8}$	[4]
1.28	1.82	27.2	2160	15.6	81.0	$Cs_{0.1}FA_{0.7}MA_{0.2}Pb_{0.5}Sn_{0.5}I_3$	$Cs_{0.2}FA_{0.8}Pbr_{0.9}I_{2.1}$	[5]
1.29	**1.78**	**27.6**	**2143**	**16.0**	**80.7**	**$Cs_{0.1}FA_{0.6}MA_{0.3}Pb_{0.5}Sn_{0.5}I_3$**	**$Cs_{0.5}DMA_{0.1}FA_{0.4}PbBr_{0.15}I_{0.85}$**	[129]
1.31	**1.90**	**22.6**	**1900**	**14.6**	**81.4**	**$CsPb_{0.4}Sn_{0.6}I_3$**	**$CsPbBrI_2$**	[130]
1.31	**1.90**	**21.9**	**1895**	**14.5**	**80.0**	**$CsPb_{0.4}Sn_{0.6}I_3$**	**$CsPbBrI_2$**	[130][a]
						OPV/perovskite		
1.21	1.83	21.7	1880	15.7	73.5	PTB7-Th:BTPV-4Cl-eC9	$FA_{0.6}MA_{0.4}PbBr_{1.2}I_{1.8}$	[3]
1.25	1.91	15.0	1710	12.0	73.4	PTB7-Th:COi8DFIC:$PC_{71}BM$	$CsPbBrI_2$	[2]
1.33	**1.80**	**27.5**	**2140**	**15.4**	**83.7**	**PM6:P2EH-1V**	**$Cs_{0.25}FA_{0.75}PbBr_{1.2}I_{1.8}$**	[46]
1.33	**1.80**	**26.4**	**2127**	**15.0**	**82.5**	**PM6:P2EH-1V**	**$Cs_{0.25}FA_{0.75}PbBr_{1.2}I_{1.8}$**	[46][a]
1.34	**1.91**	**26.4**	**2160**	**15.4**	**79.4**	**PM6:BTPSe-Ph4F**	**$FA_{0.7}MA_{0.2}Rb_{0.1}PbBr_{1.5}I_{1.5}$**	[131]
1.34	**1.91**	**25.6**	**2157**	**15.4**	**77.2**	**PM6:BTPSe-Ph4F**	**$FA_{0.7}MA_{0.2}Rb_{0.1}PbBr_{1.5}I_{1.5}$**	[131][a]

(Continues)

TABLE 8 | (Continued)

$E_{g,bottom}$ [eV]	$E_{g,middle}$, $E_{g,top}$ [eV]	PCE [%]	V_{oc} [mV]	J_{sc} [mA cm^{-2}]	FF [%]	Bottom absorber material	Middle, top absorber material[s]	Refs.
1.35	1.91	23.2	2150	13.4	80.3	D18-Cl:N3:$PC_{61}BM$	$CsPbBr_{1.1}I_{1.9}$	[4]
1.35	1.91	21.7	2150	13.0	77.5	D18-Cl:N3:$PC_{61}BM$	$CsPbBr_{1.1}I_{1.9}$	[4][b]
1.36	**1.85**	**26.0**	**2210**	**14.6**	**80.8**	**PM6:BTP-eC9**	**$Cs_{0.25}FA_{0.75}PbBr_{1.5}I_{1.5}$**	[95]
1.37	**1.85**	**26.1**	**2210**	**14.4**	**81.8**	**PM6:BTP-eC9:L8-BO**	**$Cs_{0.1}FA_{0.8}MA_{0.1}PbBr_{1.5}I_{1.5}$**	[132]
1.37	**1.85**	**24.5**	**2216**	**13.7**	**80.7**	**PM6:BTP-eC9:L8-BO**	**$Cs_{0.1}FA_{0.8}MA_{0.1}PbBr_{1.5}I_{1.5}$**	[132][a]
1.38	**1.78**	**25.5**	**2150**	**14.7**	**81.0**	**PM6:BTP-eC9:$PC_{71}BM$**	**$Cs_{0.2}FA_{0.8}PbBr_{1.2}I_{1.8}$**	[133]
1.38	**1.84**	**26.1**	**2131**	**15.0**	**81.9**	**PM6:BTP-eC9**	**$Cs_{0.25}FA_{0.75}PbBr_{1.5}I_{1.5}$**	[98]
1.38	1.87	25.9	2120	14.7	83.0	D18-Cl:N3:$PC_{61}BM$	$Cs_{0.2}FA_{0.8}PbBr_{1.4}I_{1.6}$	[5]
1.38	1.87	24.7	2114	14.7	79.5	D18-Cl:N3:$PC_{61}BM$	$Cs_{0.2}FA_{0.8}PbBr_{1.4}I_{1.6}$	[5][a]
1.38	**1.88**	**25.9**	**2210**	**14.5**	**80.8**	**PM6:BTP-eC9**	**$CsPbBrI_2$**	[94]
1.38	**1.88**	**22.9**	**2111**	**14.5**	**74.6**	**PM6:BTP-eC9**	**$CsPbBrI_2$**	[94][a]
1.38	1.88	21.4	2078	13.2	77.9	PM6:CH1007	$CsPbBr_{1.2}I_{1.8}$	[4][a]
1.38	1.88	22.4	2095	13.9	77.0	PM6:CH1007	$CsPbBr_{1.2}I_{1.8}$	[4]
1.38	1.91	21.1	1960	13.3	80.9	PM6:Y6-BO	$CsPbBrI_2$	[2]
1.39	**1.82**	**25.1**	**2100**	**14.7**	**81.1**	**PM6:BTP-eC9:$PC_{71}BM$**	**$Cs_{0.1}FA_{0.8}MA_{0.1}PbBr_{1.2}I_{1.8}$**	[134]
1.39	**1.84**	**25.2**	**2142**	**14.3**	**82.2**	**PM6:D18:BTP-eC9**	**$Cs_{0.2}FA_{0.8}PbBr_{1.4}I_{1.6}$**	[135]
1.39	**1.87**	**26.1**	**2150**	**14.6**	**83.4**	**PM6:BTP-eC9:ICBA**	**$Cs_{0.2}FA_{0.8}PbBr_{1.4}I_{1.6}$**	[136]
1.39	**1.87**	**25.1**	**2103**	**14.4**	**83.0**	**PM6:BTP-eC9:ICBA**	**$Cs_{0.2}FA_{0.8}PbBr_{1.4}I_{1.6}$**	[136][a]
1.39	**1.90**	**24.4**	**2290**	**14.7**	**72.5**	**D18-Cl:L8-BO:BTP-eC9**	**$CsPbBrI_2$**	[47]
1.40	1.81	23.6	2063	14.8	77.2	PM6:Y6:$P_{71}CBM$	$Cs_{0.25}FA_{0.75}PbBr_{1.2}I_{1.8}$	[4]
1.40	1.81	22.5	2058	14.9	73.5	PM6:Y6:$P_{71}CBM$	$Cs_{0.25}FA_{0.75}PbBr_{1.2}I_{1.8}$	[4][a]
1.40	1.83	15.1	1850	11.5	71.0	PBDB-T:SN6IC-4F	$Cs_{0.1}FA_{0.54}MA_{0.36}PbBr_{1.4}I_{1.8}$	[2]
1.40	1.82	19.5	1925	13.1	77.2	PBDBT-2F:Y6:$PC_{71}BM$	$Cs_{0.18}FA_{0.8}MA_{0.02}PbBr_{1.2}I_{1.8}$	[2][a]
1.40	1.82	20.4	1902	13.1	81.5	PBDBT-2F:Y6:$PC_{71}BM$	$Cs_{0.18}FA_{0.8}MA_{0.02}PbBr_{1.2}I_{1.8}$	[2]
1.41	1.86	23.8	2140	14.1	79.0	PM6:Y6:$PC_{61}BM$	$Cs_{0.2}FA_{0.8}PbBr_{1.5}I_{1.5}$	[4]
1.41	**1.91**	**25.3**	**2230**	**15.0**	**75.8**	**D18-Cl:L8-BO:BTP-eC9**	**$CsPbBrI_2$**	[94]

(Continues)

TABLE 8 | (Continued)

$E_{g,bottom}$ [eV]	$E_{g,middle}$, $E_{g,top}$ [eV]	PCE [%]	V_{oc} [mV]	J_{sc} [mA cm^{-2}]	FF [%]	Bottom absorber material	Middle, top absorber material[s]	Refs.
1.42	**1.78**	**23.0**	**2147**	**12.8**	**84.0**	**PM6:Y6**	**$Cs_{0.2}FA_{0.8}PbBr_{1.2}I_{1.8}$**	[47]
						DSSC/perovskite		
1.59	1.93	10.5	1170	12.9	70.0	$FA_{0.85}MA_{0.15}PbBr_{0.45}I_{2.49}$	N719	[2]
						Triple-junction		
1.08	1.53, 1.89	22.2	2780	10.2	78.6	Si	$Cs_{0.1}FA_{0.85}MA_{0.05}PbI_3$, $MAPbBr_{1.05}Cl_{0.45}I_{1.5}$	[4]
1.11	1.58, 1.92	27.6	3132	11.6	76.2	Si	$Cs_{0.25}FA_{0.60}MA_{0.15}PbBr_{1.5}I_{1.35}OCN_{0.15}$, $Cs_{0.25}FA_{0.75}PbBr_{1.5}I_{0.5}$	[5]
1.11	1.58, 1.92	27.1	3145	11.1	77.7	Si	$Cs_{0.25}FA_{0.60}MA_{0.15}PbBr_{1.5}I_{1.35}OCN_{0.15}$, $FA_{0.75}Cs_{0.25}PbBr_{1.5}$ $I_{0.5}$	[5][a]
1.12	**1.52, 1.97**	**28.7**	**3080**	**11.9**	**78.2**	**Si**	**$Cs_{0.05}FA_{0.9}Rb_{0.05}PbI_3$, $Cs_{0.4}FA_{0.7}PbBr_{1.8}I_{1.2}$**	[50]
1.12	1.57, 1.88	24.4	2840	11.6	74.0	Si	$FAPbI_3$, $Cs_{0.2}FA_{0.8}PbBr_{1.5}I_{1.5}$	[5]
1.13	1.54, 1.91	20.1	2740	8.5	86.0	Si	$Cs_{0.1}FA_{0.9}PbI_3$, $Cs_{0.2}FA_{0.8}PbBr_{1.65}I_{1.35}$	[3]
1.18	**1.58, 1.92**	**27.0**	**3160**	**10.2**	**83.6**	**Si**	**$Cs_{0.08}FA_{0.9}Rb_{0.02}PbI_3$, $Cs_{0.16}FA_{0.8}Rb_{0.04}PbBr_{1.65}I_{1.35}$**	[51]
1.18	**1.58, 1.92**	**23.0 (23.3)**[c]	**3050**	**9.8**	**76.7**	**Si**	**$Cs_{0.08}FA_{0.9}Rb_{0.02}PbI_3$, $Cs_{0.16}FA_{0.8}Rb_{0.04}PbBr_{1.65}I_{1.35}$**	[51][a,b]
1.23	1.57, 1.78	16.8	2780	7.4	81	$FA_{0.66}MA_{0.34}Pb_{0.5}Sn_{0.5}I_3$	$FA_{0.66}MA_{0.34}$ Pb $Br_{0.15}I_{2.85}$, $Cs_{0.1}FA_{0.594}MA_{0.306}PbBrI_2$	[3]
1.25	1.61, 1.97	25.1	3330	9.7	78.0	$Cs_{0.05}FA_{0.7}MA_{0.25}Pb_{0.5}Sn_{0.5}I_3$	$Cs_{0.05}FA_{0.9}MA_{0.05}PbBr_{0.45}I_{2.55}$, $Cs_{0.15}FA_{0.85}PbBr_{1.8}I_{1.2}$	[5]
1.25	1.61, 1.97	23.9	3267	9.1	80.3	$Cs_{0.05}FA_{0.7}MA_{0.25}Pb_{0.5}Sn_{0.5}I_3$	$Cs_{0.05}FA_{0.9}MA_{0.05}PbBr_{0.45}I_{2.55}$, $Cs_{0.15}FA_{0.85}PbBr_{1.8}I_{1.2}$	[5][a]
1.26	**1.61, 1.97**	**28.4 (28.2)**[c]	**3370**	**10.3**	**81.0**	**$Cs_{0.1}FA_{0.6}MA_{0.3}Pb_{0.5}Sn_{0.5}I_3$**	**$Cs_{0.1}FA_{0.9}PbBr_{0.45}I_{2.55}$, $Cs_{0.15}FA_{0.85}PbBr_2I_1$**	[49]
1.26	**1.61, 1.97**	**27.2 (28.0)**[c]	**3430**	**10.2**	**78.0**	**$Cs_{0.1}FA_{0.6}MA_{0.3}Pb_{0.5}Sn_{0.5}I_3$**	**$Cs_{0.1}FA_{0.9}PbBr_{0.45}I_{2.55}$, $Cs_{0.15}FA_{0.85}PbBr_2I_1$**	[49][a]
1.26	**1.61, 1.97, 2.26**[d]	**27.9 (27.4)**[c]	**4870**	**7.0**	**81.0**	**$Cs_{0.1}FA_{0.6}MA_{0.3}Pb_{0.5}Sn_{0.5}I_3$**	**$Cs_{0.1}FA_{0.9}PbBr_{0.45}I_{2.55}$, $Cs_{0.15}FA_{0.85}PbBr_2I_1$, $FAPbBr_3$**	[49]
1.26	1.65, 2.06	19.9	2793	8.8	80.7	$FA_{0.7}MA_{0.3}Pb_{0.5}Sn_{0.5}I_3$	$Cs_{0.05}FA_{0.95}PbBr_{0.45}$ $I_{2.55}$, $Cs_{0.2}FA_{0.8}PbBr_{2.1}I_{0.9}$	[3]
1.26	1.6, 1.99	23.3	3181	9.61	76.2	$Cs_{0.05}FA_{0.7}MA_{0.25}Pb_{0.5}Sn_{0.5}I_{3\text{-}0.05}SnF$	$Cs_{0.05}FA_{0.9}MA_{0.05}PbBr_{0.3}I_{2.7}$, $Cs_{0.85}Rb_{0.15}PbBr_{1.25}I_{1.75}$	[4][a]
1.26	1.6, 1.99	24.3	3215	9.71	77.9	$Cs_{0.05}FA_{0.7}MA_{0.25}Pb_{0.5}Sn_{0.5}I_{3\text{-}0.05}SnF$	$Cs_{0.05}FA_{0.9}MA_{0.05}PbBr_{0.3}I_{2.7}$, $Cs_{0.85}Rb_{0.15}PbBr_{1.25}I_{1.75}$	[4]

[a]Certified power conversion efficiency.
[b]Notable exception included as a large-area highlight, and/or a PCE highlight without the absorber material information.
[c]In parentheses, the certified efficiency from MPP tracking.
[d]Notable exception quadruple junction (top sub-cell bandgap).

TABLE 9 | Monolithic multijunction (non-perovskite) solar cells, including organic and dye-sensitized sub-cells, with the highest efficiency: performance parameters as a function of the device bandgap energies (from the EQE spectra) of the sub-cells.

$E_{g,bottom}$ [eV]	$E_{g,top}$ [eV]	PCE [%]	V_{oc} [mV]	J_{sc} [mA cm^{-2}]	FF [%]	Bottom absorber	Top absorber	Refs.
						OPV/OPV		
1.21	1.58	19.0	1690	15.0	74.8	PTB7-Th:BTPSeV-4F	PM6:O1-Br	[4]
1.23	1.66	16.4	1650	14.5	68.5	PTB7-Th:BTPV-4F:$PC_{71}BM$	PM6:m-DTC-2F	[2]
1.24	1.72	17.3	1640	14.4	73.3	PTB7-Th:O6T-4F:$PC_{71}BM$	PBDB-T:F-M	[2]
1.31	1.64	15.9	1660	14.1	68.0	PM6:SFT8-4F	PCE-10:BT-CIC:BEIT-4F	[2]
1.32	1.65	15.0	1600	13.6	69.0	PTB7-Th:PCDTBT:IEICO-4F	PBDB-T-2F:TfIF-4FIC	[2]
1.32	1.74	19.6	1910	14.2	72.4	PBDB-TF:BTP-eC11	PBDB-TF:ITCC	[2]
1.35	**1.74**	**21.5**	**1903**	**14.3**	**79.2**	**PBDB-TF:BTA-4F**	**PB3:FTCC-Br**	[48]
1.35	**1.74**	**21.2**	**1902**	**14.0**	**79.7**	**PBDB-TF:BTA-4F**	**PB3:FTCC-Br**	[48][a]
1.36	1.73	18.7	1883	14.0	70.9	PM6:CH1007:$PC_{71}BM$	D18:F-ThBr	[3]
1.37	1.73	15.2	1610	12.9	73.0	PM6:Y6	PV2000:PCBM	[2]
1.37	1.77	20.3	2020	13.2	76.0	BTP-eC9:AITC:PBDB-TCI	AITC:PFBCPZ	[4]
1.37	1.77	20.6	2020	13.3	76.6	BTP-eC9:AITC:PBDB-TCI	AITC:PFBCPZ	[4]
1.38	1.80	20.3	2010	13.1	76.8	PBDB-TF:GS-ISO	PBDM-TF:BTp-eC9	[3]
1.38	1.80	20.3	2010	13.1	76.8	PBDB-TF:GS-ISO	PBDM-TF:BTp-eC9	[3]
1.39	1.78	19.6	2030	13.0	74.2	PBDB-TF:HDO-4Cl:BTP-eC9	PB2:GS-ISO	[4]
1.40	1.71	20.0	1960	13.5	75.9	PB4:FTCC-Br	PBQx-TCl:PBDB-TF:eC9-2Cl	[4]
1.42	1.79	15.0	1590	13.3	71.0	PCE-10:BTCIC	DTDCPB:C_{70}	[2]
1.45	1.76	17.9	2000	11.7	76.3	PM6:PY-IT	PM7:PIDT	[4]
1.48	1.74	14.1	1710	11.7	70.0	PTB7-Th: NOBDT	PBDB-T: F-M	[2]
						OPV/a-Si		
1.33	1.78	15.1	1610	13.2	71.0	PTB7-Th:IEICO-4F	a-Si	[2]
						Si/DSSC		
1.11	1.84	14.7	580	40.9	62.0	Si	N719	[2]
1.24	1.67	17.2	1360	18.1	69.3	Si	SGT-021	[2]
						CIGS/DSSC		
1.21	1.82	13.0	1170	14.6	77.0	Cu(In,Ga)Se_2	N719	[2]
1.22	1.90	12.4	1435	14.1	61.0	Cu(In,Ga)Se_2	N719	[2]
1.22	1.82	15.1	1450	14.1	74.0	Cu(In,Ga)Se_2	N719	[2]
						DSSC/DSSC		
1.40	1.98	11.4	1400	12.2	66.7	DX1	N719	[2]
1.44	1.95	10.4	1450	10.8	67	N719	Black dye	[2]
1.67	1.98	12.3	1825	10.3	65	SGT-121/HC-A1	SGT-021/HC-A4	[3]
1.78	2.37	7.1	1420	7.2	69	N719	D131	[2]

TABLE 10 | Monolithic multijunction (non-perovskite) inorganic absorber-based solar cells with the highest efficiency: performance parameters as a function of the device bandgap energies (from the EQE spectra) of the sub-cells.

$E_{g,bottom}$ [eV]	$E_{g,middle}$, $E_{g,top}$, [eV]	PCE [%]	V_{oc} [mV]	J_{sc} [mA cm^{-2}]	FF [%]	Bottom absorber	Middle, top absorber[s]	Refs.
						GaAs/GaInP		
1.35	1.90	32.9	2500	15.4	85.7	GaAs	GaInP	[2]
1.41	1.88	32.8	2568	14.66	87.7	GaAs	GaInP	[2]
1.41	1.92	27.4	2400	13.1	88.0	GaAs	GaInP	[2]
1.42	1.85	31.6	2538	14.2	87.7	GaAs	GaInP	[2]
						Si/GaAsP		
1.17	1.90	23.4	1732	17.34	77.7	Si	GaAsP	[2]
						nc-Si/a-Si		
1.36	1.93	11.8	1428	12.27	67.5	nc-Si	a-Si	[2]
						Si/Se		
1.13	1.98	2.7	1403	5.7	34.2	Si	Se	[5]
						Triple-junction cells		
0.92	1.33,1.88	39.5	3000	15.4	85.3	InGaAs	GaAs, InGaP	[3]
0.98	1.41, 1.89	37.7	3014	14.6	86.0	InGaAs	GaAs, InGaP	[3]
1.09	1.42, 1.92	19.1	2510	9.9	77.0	GaAsBi	GaAs, AlGaAs	[4]
1.13	1.48, 1.93	35.9	3248	13.1	84.3	Si	GaInAsP, InGaP	[3]
1.01	1.50, 1.92	28.1	2952	11.7	81.1	CIGS	AlGaAs/GaInP	[3]
1.30	1.27, 2.03	14.0	1922	9.9	73.4	nc-Si	nc-Si, a-Si	[3]

7.2 | Best Performing Flexible Research Solar Cells Tables

TABLE 11 | Flexible perovskite single-junction solar cells with the highest efficiency: performance parameters as a function of photovoltaic bandgap energy (from the EQE spectrum).

E_g [eV]	PCE [%]	V_{oc} [mV]	J_{sc} [mA cm^{-2}]	FF [%]	Absorber perovskite	Refs.
1.44	8.5	650	20.8	62.9	$FAGe_{0.1}Sn_{0.9}I_3$	[3]
1.52	**24.2**	**1181**	**25.3**	**81**	**$FAPbI_3$**	[55]
1.53	24.5	1150	25.5	83.5	$FAPbI_3$	[5][a]
1.53	25.1	1180	25.3	84.1	$FAPbI_3$	[5][b]
1.53	24.9	1180	25.3	83.4	$FAPbI_3$	[5][a]
1.53	**25.2**	**1177**	**25.7**	**83.8**	**$FAPbI_3$**	[53]
1.53	**25.5**	**1191**	**25.5**	**84.0**	**$Cs_{0.05}FA_{0.86}MA_{0.9}PbBr_{0.3}I_{2.7}$**	[52]
1.53	**25.4**	**1190**	**25.5**	**83.9**	**$Cs_{0.05}FA_{0.86}MA_{0.9}PbBr_{0.3}I_{2.7}$**	[52][a]
1.54	24.5	1170	25.0	83.7	$Cs_{0.05}FA_{0.84}MA_{0.11}PbBr_{0.12}I_{2.88}$	[5][b]
1.54	**25.3**	**1210**	**25.5**	**81.6**	**$Cs_{0.05}$ $FA_{0.90}$ $MA_{0.05}$ PbI_3**	[54]
1.54	**24.6**	**1190**	**25.2**	**81.2**	**$Cs_{0.05}$ $FA_{0.90}$ $MA_{0.05}$ PbI_3**	[54][a]
1.55	23.4	1164	24.8	80.9	$Cs_{0.05}FA_{0.931}MA_{0.019}PbBr_{0.06}I_{2.94}$	[4][a]

(Continues)

TABLE 11 | (Continued)

E_g [eV]	PCE [%]	V_{oc} [mV]	J_{sc} [mA cm^{-2}]	FF [%]	Absorber perovskite	Refs.
1.55	**24.9**	**1161**	**25.9**	**82.7**	**$Cs_{0.05}FA_{0.95}PbI_3$**	[59]
1.55	**25.4**	**1193**	**25.6**	**84.0**	**$Cs_{0.05}FA_{0.86}MA_{0.9}PbBr_{0.3}I_{2.7}$**	[137]
1.55	**25.1**	**1192**	**25.4**	**82.7**	**$Cs_{0.05}FA_{0.86}MA_{0.9}PbBr_{0.3}I_{2.7}$**	[137][a]
1.56	19.9	1109	23.2	77.3	$Cs_{0.05}$ $FA_{0.747}MA_{0.153}Rb_{0.05}PbBr_{0.15}I_{2.85}$	[2][a]
1.56	19.9	1192	21.9	76.3	$FA_{0.95}MA_{0.05}PbBr_{0.15}I_{2.85}$	[2][a]
1.56	**24.4**	**1174**	**25.4**	**81.7**	**$(FAPbI_3)_{1-x}(MAPbBr_3)_x$**	[138]
1.56	**24.5**	**1174**	**24.5**	**81.7**	**$Rb_{0.05}Cs_{0.05}MA_{0.05}FA_{0.85}Pb(I_{0.95}Br_{0.05})_3$**	[139]
1.57	19.7	990	24.3	81.9	$MAPbI_3$	[5]
1.57	22.1	1200	22.8	80.9	$Cs_{0.05}FA_{0.90}MA_{0.05}PbBr_{0.15}I_{2.85}$	[4]
1.57	19.5	1110	23.1	76.0	$Cs_{0.03}FA_{0.945}MA_{0.025}PbBr_{0.075}I_{2.925}$	[2]
1.57	19.5	1105	23.1	76.1	$CsFAMAPb(Br,I)_3$	[4]
1.57	**23.9**	**1162**	**25.2**	**81.4**	**$Cs_{0.05}(FA_{0.92}MA_{0.03})Pb(I_{0.96}Br_{0.04})_3$**	[56]
1.57	**24.5**	**1161**	**25.3**	**78.9**	**$FA_{0.93}MA_{0.07}PbI_3$**	[140]
1.58	19.2	1120	21.7	78.9	$Cs_{0.08}FA_{0.87}MA_{0.05}PbBr_{0.12}I_{2.88}$	[2]
1.59	**24.6**	**1176**	**25.5**	**84.0**	**$Cs_{0.05}FA_{0.92}MA_{0.03}PbBr_{0.12}I_{2.88}$**	[141]
1.59	**24.1**	**1166**	**25.4**	**83.4**	**$Cs_{0.05}FA_{0.92}MA_{0.03}PbBr_{0.12}I_{2.88}$**	[141][a]
1.60	20.6	1110	23.0	80.7	CsFAMAPbBrI	[3]
1.60	20.5	1140	23.5	76.5	$Cs_{0.04}FA_{0.86}MA_{0.1}PbBr_{0.29}I_{2.71}$	[3]
1.60	17.8	1060	21.8	77.3	CsFAMAPbBrI	[3][b]
1.61	20.1	1150	22.4	78.0	$MAPbI_3$: $Cs_{0.12}MA_{0.88}(MBA)_2Pb_7I_{22}$	[5][b]
1.61	17.3	1062	21.7	74.9	$Cs_{0.05}FA_{0.81}MA_{0.14}PbBr_{0.45}I_{2.55}$	[2][a]
1.61	19.1	1135	21.2	79.2	$Cs_{0.05}FA_{0.75}K_{0.04}MA_{0.15}Rb_{0.01}PbBr_{0.51}I_{2.49}$	[2]
1.62	20.1	1150	22.4	78.0	$Cs_{0.04}FA_{0.8064}MA_{0.1536}PbBr_{0.48}I_{2.52}$	[2]
1.62	18.0	1120	22.3	72.1	$Cs_{0.06}FA_{0.79}MA_{0.15}PbBr_{0.45}I_{2.55}$	[2]
1.63	**13.0**	**1060**	**19.7**	**62.0**	**$Cs_{0.08}FA_{0.78}MA_{0.16}PbBr_{0.48}I_{2.52}$**	[142]
1.63	14.9	1030	21.5	67.3	$MAPbI_3$	[3]
1.63	10.4	1030	19.2	52.8	$FA_{0.85}MA_{0.15}PbBr_{0.45}I_{2.55}$	[2]
1.65	11.2	940	18.4	64.9	$MAPbI_3$	[2]
1.65	7.9	1090	10.8	70.7	$FA_{0.5}MA_{0.5}PbBr_{0.5}I_{2.5}$	[2]
1.66	20.0	1200	20.4	81.9	$Cs_{0.05}FA_{0.732}MA_{0.218}PbBr_{0.69}I_{2.31}$	[5][b]
1.74	**13.9**	**1110**	**18.9**	**65.9**	**$CsPbI_3$**	[57]
1.79	14.3	1090	18.5	70.8	$CsPbBr_{0.19}I_{2.81}$	[5][b]
1.80	**15.0**	**1120**	**18.5**	**72.3**	**$CsPbBr_{0.19}I_{2.81}$**	[143]
2.27	6.8	1400	7.4	66.1	$FAPbBr_3$	[5][b]

[a]Certified power conversion efficiency.

[b]Notable exceptions included as materials and/or large-area highlights.

TABLE 12 | Flexible organic single-junction solar cells with the highest efficiency: performance parameters as a function of photovoltaic bandgap energy (from the EQE spectrum).

E_g [eV]	PCE [%]	V_{oc} [mV]	J_{sc} [mA cm^{-2}]	FF [%]	Absorber blend	Refs.
1.27	7.4	708	15.9	65.2	PTB7-Th:COi 8DFIC:$PC_{71}BM$	[2]
1.32	10.6	690	24.3	63.2	PTB7-Th:IEICO-4F	[2]
1.34	**19.5**	**912**	**26.5**	**80.1**	**D18:L8-BO**	[60]
1.34	**18.7**	**907**	**26.1**	**79.1**	**D18:L8-BO**	[60][a]
1.34	**18.6**	**908**	**26.5**	**77.3**	**D18:L8-BO**	[26]
1.36	16.6	821	26.8	75.4	PM6:BTP-4Cl-12	[3]
1.37	16.1	840	25.0	76.7	PM6:N3:$PC_{71}BM$	[2]
1.37	15.8	851	25.1	73.9	D18:Y6	[5][a,b]
1.37	**18.3**	**829**	**28.2**	**78.4**	**PM6:BTA-E3**	[96]
1.38	16.2	840	25.4	76.0	PM6:BTP-eC9:$PC_{71}BM$	[5]
1.38	12.0	827	21.6	67.4	PM6:BTP-4Cl-12	[3][a]
1.38	17.5	835	27.4	76.7	PM6:BTP-eC9:$PC_{71}BM$	[3]
1.39	16.1	820	25.9	75.8	PM6:BTP-eC9:$PC_{71}BM$	[2]
1.39	15.9	864	25.0	73.5	D-18-Cl:G19:Y6	[3]
1.39	15.7	830	25.4	74.5	PM6:BTP-eC9	[4]
1.39	14.4	830	25.4	68.3	PM6:BTP-eC9	[4][b]
1.39	17.9	768	27.3	85.3	D18:N3:DOY-C4	[5]
1.39	18.2	865	27.4	76.5	PM6:BTP-eC9	[5]
1.39	17.0	874	26.4	73.6	PM6:BTP-eC9	[5]
1.39	13.0	780	24.9	67.2	PM6:BTP-eC9	[5][b]
1.39	17.5	860	27.0	75.4	PM6:BTP-eC9	[5]
1.39	**17.2**	**841**	**27.2**	**75.0**	**PM6:BTP-eC9**	[144]
1.40	17.2	870	25.5	77.3	PM6:L8-BO	[4][b]
1.40	17.4	869	25.5	78.5	PM6:L8-BO	[4]
1.40	16.1	860	25.9	74.7	PM6:Y6	[2]
1.40	15.2	832	25.1	73.0	PM6:Y6	[2]
1.40	17.1	830	27.4	74.9	PM6:BTP-eC9:$PC_{71}BM$	[3]
1.40	**18.7**	**876**	**27.8**	**77.1**	**PM6:L8-BO**	[145]
1.41	15.2	830	25.0	73.3	PM6:Y6	[3]
1.41	15.1	847	24.9	71.6	PM6:Y6:C6	[2]
1.41	**18.5**	**905**	**26.1**	**78.3**	**PM6:L8-BO:ZY-4Cl**	[146]
1.42	16.6	860	25.9	74.7	PM6:Y6	[3]
1.42	**18.6**	**880**	**27.5**	**76.7**	**PM6:L8-BO:BTP-eC9**	[147]
1.42	**18.8**	**849**	**27.9**	**80.5**	**PM6:D18:BTP-eC9**	[62]
1.42	**18.6**	**847**	**27.7**	**80.3**	**PM6:D18:BTP-eC9**	[62][a]
1.43	16.5	925	23.6	75.6	PBQx-TF:PBDB-TF:PY-IT	[4]
1.44	10.7	943	17.7	64.3	D18:(40)-b-PYIT	[4]
1.44	10.4	848	17.0	72.2	PM6:Y6	[2]
1.44	**17.8**	**900**	**25.3**	**78.0**	**PBET-TF**	[148]
1.45	**19.4**	**950**	**25.5**	**79.9**	**PM6:PBQx-TF:PY-IT**	[61]

(Continues)

TABLE 12 | (Continued)

E_g [eV]	PCE [%]	V_{oc} [mV]	J_{sc} [mA cm^{-2}]	FF [%]	Absorber blend	Refs.
1.45	**19.1**	**946**	**25.2**	**79.7**	**PM6:PBQx-TF:PY-IT**	[61][a]
1.45	16.6	860	25.5	75.8	PM6:L8-BO	[4]
1.45	14.3	920	21.6	71.8	PBQx-TF:DYBT-C4	[5]
1.48	**19.0**	**940**	**26.3**	**77.0**	**PM6:4Y-BO**	[149]
1.53	**17.0**	**865**	**25.7**	**76.5**	**PM6:DSY-C10**	[144]
1.55	12.0	840	19.5	73.3	PM6:IT-4F	[2]
1.56	11.6	820	19.6	72.2	PM6:IT-4F	[2]
1.56	12.1	826	20.9	70.1	PM6:IT-4F	[2]
1.61	10.9	900	18.7	64.8	PBDB-T:ITIC	[2]
1.63	9.2	770	16.0	74.7	PTB7-Th:$PC_{71}BM$	[2]
1.65	9.3	820	16.5	68.7	J51:ITIC	[2]
1.65	8.2	890	13.4	68.6	PBDB-T:ITIC	[2]
1.82	7.2	925	10.9	71.3	JP02	[2]
2.01	3.7	592	10.4	59.2	P3HT:PCBM	[2]

[a]Certified power conversion efficiency;
[b]Notable exceptions included as a material and/or large-area cell highlight.

TABLE 13 | Flexible dye-sensitized single-junction solar cells with the highest efficiency: performance parameters as a function of device absorber bandgap energy (from the EQE spectrum).

E_g [eV]	PCE [%]	V_{oc} [mV]	J_{sc} [mA cm^{-2}]	FF [%]	Sensitizing dye	Refs.
1.65	4.1	770	9.9	53.9	N719	[2]
1.67	12.5	777	21.1	76.5	N719	[5][b]
1.74	4.6	750	10.5	58.0	N719	[2]
1.75	**8.9**	**759**	**17.2**	**68.1**	**N719**	[150]
1.75	**8.6**	**760**	**15.4**	**72.8**	**N719**	[151]
1.75	7.6	732	15.0	69.2	N719	[2][a]
1.78	7.5	725	15.4	67.5	N719	[2]
1.79	6.5	729	13.2	68.0	N719	[2]
1.80	6.3	732	13.1	66.0	N719	[2]
1.81	6.3	754	12.3	67.9	$(JH\text{-}1)_{0.6}(SQ2)_{0.4}$	[2]
183	5.0	735	10.0	67.8	N719	[2]
1.88	6.0	750	11.2	71.0	N719	[2]
1.90	4.2	680	10.7	57.7	N719	[2]
1.94	4.2	710	10.3	57.2	N719	[2]
1.95	4.9	702	11.2	62.3	N719	[2]
2.02	3.9	720	11.9	45.2	N719	[3]
2.12	5.4	680	10.4	76.3	N719	[2]

[a]Certified power conversion efficiency.

TABLE 14 | Flexible Monolithic Multijunction Solar Cells With the Highest Efficiency: Performance Parameters as a Function of Photovoltaic Bandgap Energies (From the EQE spectrum) of each Sub-cell. For Triple-junction Devices the Middle and Top Sub-cell Values Are Listed With a Comma Separator.

$E_{g,bottom}$ [eV]	$E_{g,top}$ [eV]	PCE [%]	V_{oc} [mV]	J_{sc} [mA cm^{-2}]	FF [%]	Bottom absorber material	Top absorber material [s]	Refs.
						Double junction cells		
1.20	1.68	23.4	1733	17.2	78.9	c-Si	$Cs_{0.05}FA_{0.731}MA_{0.219}PbBr_{0.69}I_{2.31}$	[5]
1.12	**1.68**	**26.4**	**1830**	**17.9**	**80.7**	**c-Si SHJ**	$\mathbf{Cs_{0.05}FA_{0.69}MA_{0.21}PbBr_{0.69}I_{2.31}}$	[152]
1.12	**1.68**	**29.9**	**1890**	**19.5**	**80.9**	**c-Si**	$\mathbf{Cs_{0.15}FA_{0.85}Pb\ Br_{0.36}I_{2.64}}$	[63][a]
1.20	1.62	18.1	1645	17.7	62.0	$Cu(In,Ga)Se_2$	$FA_{0.83}MA_{0.17}PbBr_{0.51}I_{2.49}$	[5]
1.12	**1.64**	**22.8**	**1752**	**17.9**	**75.2**	**CIGS**	$\mathbf{Cs_{0.05}FA_{0.79}MA_{0.16}\ Pb\ Br_{0.51}I_{2.49}}$	[153][a]
1.12	**1.64**	**22.8**	**1820**	**16.8**	**74.1**	**CIGS**	$\mathbf{Cs_{0.05}(FA_{0.77}MA_{0.23})_{0.95}Pb(I_{0.77}Br_{0.23})_3}$	[121]
1.12	**1.65**	**23.8**	**1753**	**17.6**	**77.2**	**CIGS**	$\mathbf{Cs_{0.05}(FA_{0.77}MA_{0.23})_{0.95}Pb(I_{0.77}Br_{0.23})_3}$	[45][a]
1.12	**1.65**	**24.6**	**1760**	**17.9**	**78.9**	**CIGS**	$\mathbf{Cs_{0.05}FA_{0.73}MA_{0.22}PbBr_{0.69}I_{2.31}}$	[45]
1.12	**1.60**	**21.3**	**1750**	**17.8**	**75.0**	**CIGS**	$\mathbf{Cs_{0.05}FA_{0.80}MA_{0.15}PbBr_{1.2}I_{2.8}}$	[154]
1.25	1.78	24.7	2000	15.8	78.3	$FA_{0.7}MA_{0.3}Pb_{0.5}Sn_{0.5}I_3$	$Cs_{0.2}FA_{0.8}PbBr_{1.05}I_{1.95}$	[3]
1.25	1.78	24.4	2016	15.6	77.3	$FA_{0.7}MA_{0.3}Pb_{0.5}Sn_{0.5}I_3$	$Cs_{0.2}FA_{0.8}PbBr_{1.05}I_{1.95}$	[3][a]
1.26	1.79	23.8	2100	15.1	75.1	$FA_{0.6}MA_{0.4}Pb_{0.4}Sn_{0.6}I_3$	$Cs_{0.12}FA_{0.8}MA_{0.08}PbBr_{1.2}I_{1.8}$	[3]
1.27	1.81	23.8	2012	15.5	76.1	$FA_{0.7}MA_{0.3}Pb_{0.5}Sn_{0.5}I_3$	$Cs_{0.2}FA_{0.8}PbBr_{1.2}I_{1.8}$	[4]
1.28	1.73	21.3	1820	15.6	75.0	$Cs_{0.25}FA_{0.75}Pb_{0.5}Sn_{0.5}I_3$	$Cs_{0.3}DMA_{0.1}FA_{0.6}PbBr_{0.6}I_{2.4}$	[2]
1.28	**1.84**	**27.5**	**2108**	**14.9**	**87.5**	$\mathbf{Cs_{0.2}FA_{0.8}Pb_{0.5}Sn_{0.5}I_3}$	$\mathbf{Cs_{0.25}FA_{0.75}Pb\ Br_{1.2}I_{2.8}}$	[64]
1.30	**1.85**	**24.4**	**1974**	**15.9**	**77.8**	$\mathbf{Cs_{0.2}FA_{0.8}\ Pb_{0.7}Sn_{0.3}I_3}$	$\mathbf{C_{s0.17}FA_{0.83}Pb\ Br_{1.2}I_{2.8}}$	[155]
1.30	**1.85**	**24.0**	**1962**	**15.9**	**77.4**	$\mathbf{Cs_{0.2}FA_{0.8}\ Pb_{0.7}Sn_{0.3}I_3}$	$\mathbf{C_{s0.17}FA_{0.83}Pb\ Br_{1.2}I_{2.8}}$	[155][a]
1.40	1.82	13.6	1800	11.1	68.3	PBDB-T:SN6IC-4F	$Cs_{0.1}FA_{0.54}MA_{0.36}PbBr_{1.2}I_{1.8}$	[2]
1.41	1.86	30.4	2547	14.3	84.7	GaAs	InGaP	[2]
1.41	1.92	27.4	2400	13.1	88.0	GaAs	InGaP	[2]
						Triple junction cells		
1.00	1.41, 1.91	30.2	3043	16.1	84.5	$Ga_{0.73}In_{0.27}As$	GaAs, $Ga_{0.51}In_{0.49}P$	[4][b]

[a]Certified power conversion efficiency.

[b]*J–V* measured under AM0 136.7 mW cm^{-2}.

TABLE 15 | Flexible emerging inorganic single-junction solar cells with the highest efficiency: performance parameters as a function of device absorber bandgap energy (from the EQE spectrum).

E_g [eV]	PCE [%]	V_{oc} [mV]	J_{sc} [mA cm^{-2}]	FF [%]	Absorber material	Refs.
1.04	4.4	394	23.9	46.4	$Cu_2Cd_xZn_{1-x}Sn(S,Se)_4$	[3]
1.06	12.2	525	36.6	63.5	$Cu_2ZnSn(S,Se)_4$	[5]
1.07	4.9	358	28.7	47.3	$Cu_2ZnSn(S,Se)_4$	[3]
1.09	8.7	401	36.5	59.4	$Cu_2ZnSn(S,Se)_4$	[4]
1.10	**11.2**	**410**	**37.4**	**73.0**	**$Cu_2ZnSn(S,Se)_4$**	[156]
1.12	**10.3**	**465**	**34.3**	**64.7**	**$Cu_2ZnSn(S,Se)_4$**	[157]
1.13	10.2	463	35.7	62.0	$Cu_2ZnSn(S,Se)_4$	[3]
1.15	10.1	503	29.6	67.9	$Cu_2ZnSn(S,Se)_4$	[5]
1.16	11.2	539	33.1	62.8	$Cu_2ZnSn(S,Se)_4$	[2]
1.32	8.23	479	26.5	64.9	Sb_2Se_3	[5]
1.32	8.43	452	29.0	64.3	Sb_2Se_3	[5]
1.32	8.42	470	31.3	57.2	Sb_2Se_3	[5]
1.32	8.03	492	26.2	62.3	Sb_2Se_3	[5]
1.52	0.6	204	7.6	35.5	Cu_2ZnSnS_4	[2]
1.59	6.5	601	22.6	48.0	CZTSSe	[3]
1.80	3.8	650	11.6	49.5	Sb_2S_3	[4]

TABLE 16 | Flexible single-junction solar cells with the highest efficiency among established inorganic technologies: performance parameters as a function of device absorber bandgap energy (from the EQE spectrum).

E_g [eV]	PCE [%]	V_{oc} [mV]	J_{sc} [mA cm^{-2}]	FF [%]	Absorber material/technology	Refs.
1.10	26.8	751	41.5	86.1	Si	[5]
1.11	11.5	526	33.8	64.6	$Cu(In,Ga)(S,Se)_2$	[3]
1.14	17.0	656	36.6	70.8	Si	[2]
1.15	18.9	693	35.8	76.3	$Cu(In,Ga)Se_2$	[4]
1.17	18.9	608	39.5	63.0	Si	[2]
1.17	12.0	580	35.8	58.4	$Cu(In,Ga)Se_2$	[2]
1.18	17.6	698	33.9	74.4	$Cu(In,Ga)Se_2$	[4]
1.20	20.4	736	35.1	78.9	$Cu(In,Ga)Se_2$	[2][a]
1.20	17.6	630	38.9	72.4	$Cu(In,Ga)Se_2$	[5]
1.22	18.7	720	35.0	74.4	$Cu(In,Ga)Se_2$	[2]
1.32	8.4	550	24.3	63.0	Si	[2]
1.42	22.1	980	27.1	83.4	GaAs	[2]
1.45	13.5	786	22.1	77.7	GaAs	[3]
1.45	12.6	829	23.6	64.3	CdTe	[4]
1.46	14.1	821	24.3	70.3	CdTe	[3][a]
1.46	16.4	831	25.5	77.4	CdTe	[2]
1.49	11.5	821	22.0	63.9	CdTe	[2]
1.79	8.8	888	14.3	70	a-Si:H	[2]
1.88	8.2	820	15.6	64.0	a-Si:H	[2]

[a]Certified power conversion efficiency.

7.3 | Best Performing Transparent and Semitransparent Research Solar Cells Tables

TABLE 17 | (Semi-)transparent perovskite solar cells with the highest efficiency: performance parameters as a function of average visible transmittance and photovoltaic bandgap energy (from the EQE spectrum). For the tandem cells, the bandgap energies and absorber materials for the bottom and top sub-cells are separated with a comma in that order.

AVT [%]	E_g [eV]	*LUE* [%]	*PCE* [%]	V_{oc} [mV]	J_{sc} [mA cm^{-2}]	*FF* [%]	Absorber	Refs.
1	**1.61**	**0.17**	**17.9**	**1050**	**21.8**	**78.0**	**$Cs_{0.05}FA_{0.7885}MA_{0.1615}PbBr_{0.51}I_{2.49}$**	[158]
2	1.65	0.25	15.0	1091	18.2	75.5	$Cs_{0.09}FA_{0.77}MA_{0.14}PbBr_{0.42}I_{2.58}$	[159]
2	**1.69**	**0.50**	**20.4**	**1230**	**19.8**	**83.8**	**$Cs_{0.25}FA_{0.75}PbBr_{0.6}I_{2.4}$**	[160]
3	**1.80**	**0.45**	**17.2**	**1240**	**17.4**	**79.9**	**$Cs_{0.25}FA_{0.75}PbBr_{1.2}I_{1.8}/CF_3PEAI$**	[161]
3	1.67	0.49	16.3	1099	18.9	78.3	$Cs_{0.25}FA_{0.75}PbBr_{0.6}I_{2.4}$	[3]
3	1.53	0.37	12.2	1017	17.5	68.5	$MAPbI_3$	[2]
5	1.80	0.69	15.1	1290	15.0	77.9	$Cs_{0.12}FA_{0.8}MA_{0.08}PbBr_{1.2}I_{1.8}$	[162]
5	1.60	1.14	19.1	1120	23.2	73.4	$MAPbI_3$	[3]
5	1.60	0.83	16.5	1080	20.6	74.2	$MAPbI_3$	[2]
5	1.61	0.60	12.0	960	19.2	65.3	$MAPb(Cl,I)_3$	[2]
5	1.65	0.56	11.2	940	18.4	64.9	$MAPbI_3$	[2]
7	1.62	1.28	18.3	1100	21.9	75.8	$MAPbBr_{0.12}I_{2.88}$	[4]
7	1.55	0.95	13.6	988	20.4	67.5	$MAPbI_3$	[2]
9	1.63	1.60	17.8	1120	19.3	82.7	$Cs_{0.13}FA_{0.87}PbBr_{0.39}I_{2.61}$	[3]
10	1.78	1.13	11.3	1190	15.0	63.1	$CsPbI_3$	[4]
10	1.59	1.75	17.5	1070	22.4	73.1	$MAPbI_3$	[2]
10	**1.77**	**1.82**	**18.5**	**1300**	**16.8**	**84.6**	**$Cs_{0.2}FA_{0.8}PbBr_{1.2}I_{1.8}$**	[122]
12	1.27, 1.80	1.80	15.0	1940	11.4	68.0	$Cs_x(FA_{0.83}MA_{0.17})_{1-x}Pb_{0.5}Sn_{0.5}I_3$, $Cs_{0.2}FA_{0.8}PbBr_{1.2}I_{1.8}$	[4]
12	1.60	1.58	13.2	1000	19.5	67.8	$MAPbI_3$	[2]
13	1.67	1.94	14.9	1100	19.8	68.4	$MAPbBr_{0.5}I_{2.5}$	[2]
13	1.88	1.72	13.2	1298	13.8	74.1	$Cs_{0.25}FA_{0.75}PbBr_{1.5}I_{1.5}$	[3]
14	1.55	1.04	7.3	1037	13.4	52.5	$MAPbI_3$	[2]
15	1.61	1.79	11.9	1000	17.8	66.3	$MAPbI_3$	[2]
15	1.67	2.06	13.7	1097	17.1	73.1	$Cs_{0.05}FA_{0.79}MA_{0.16}PbBr_{0.51}I_{2.49}$	[163]
16	1.76	2.19	13.7	1120	16.7	73.4	$MAPbBrI_2$	[2]
17	1.65	2.18	12.8	1040	16.6	74.1	$Cs_{0.05}FA_{0.8075}MA_{0.1425}PbBr_{0.45}I_{2.55}$	[2]
18	1.73	2.50	14.1	1230	15.9	72.3	$Cs_{0.1}FA_{0.9}PbBrI_2$	[5]
18	1.77	2.20	12.2	1110	15.1	72.7	$MAPbBrI_2$	[2]
18	1.53	1.64	9.1	1017	14.6	61.5	$MAPbI_3$	[2]
19	1.62	2.46	12.8	1030	16.5	74.9	$MAPb(Cl,I)_3$	[2]
21	1.60	1.80	8.5	964	13.1	66.8	$MAPb(Cl,I)_3$	[2]
21	1.57	1.67	8.1	1030	11.2	70.2	$MAPb(Cl,I)_3$	[2]
22	1.63	2.65	2.28	1070	12.2	78.1	$MAPbI_3$	[2]
23	1.96	2.76	12.0	1289	12.7	73.6	$Cs_{0.25}FA_{0.75}PbBr_{1.5}I_{1.5}$	[3]

(Continues)

TABLE 17 | (Continued)

AVT [%]	E_g [eV]	*LUE* [%]	*PCE* [%]	V_{oc} [mV]	J_{sc} [mA cm^{-2}]	*FF* [%]	Absorber	Refs.
23	1.62	2.61	11.3	1040	15.1	72.3	$MAPbI_3$	[2]
24	1.87	2.25	9.4	1120	13.6	61.6	$MAPbBr_{1.5}I_{1.5}$	[2]
26	1.62	3.02	11.7	990	15.9	74.6	$MAPb(Cl,I)_3$	[2]
27	1.60	3.26	12.1	1000	18.3	66.2	$MAPbI_3$	[2]
29	1.57	2.27	7.8	970	11.6	69.6	$MAPb(Cl,I)_3$	[2]
30	1.65	2.22	7.4	1010	11.8	62.2	$Cs_{0.05}FA_{0.8075}MA_{0.1425}PbBr_{0.45}I_{2.55}$	[2]
31	1.84	3.31	10.7	1.24	11.6	73.9	$Cs_{0.25}FA_{0.75}PbI_{2.01}Br_{0.99}$	[3]
31	1.62	3.34	10.8	1010	14.7	73.0	$MAPb(Cl,I)_3$	[2]
31	1.27, 1.80	2.88	9.3	1940	7.9	61.0	$Cs_x(FA_{0.83}MA_{0.17})_{1-x}Pb_{0.5}Sn_{0.5}I_3$, $Cs_{0.2}FA_{0.}8PbBr1_{.2}I_{1.8}$	[4]
31	1.69	3.69	11.9	1050	16.3	69.4	$MAPbBr_{0.5}I_{2.5}$	[2]
35	1.63	3.64	10.3	1000	13.6	75.6	$MAPb(Cl,I)_3$	[2]
36	1.79	3.71	10.3	1080	14.6	65.5	$MAPbBr\ I_2$	[2]
41	1.90	3.61	8.8	1110	12.8	62.2	$MAPbBr_{1.5}I_{1.5}$	[2]
41	1.63	1.85	4.5	880	8.2	63.0	$MAPbI_3$	[2]
42	1.64	3.57	8.5	960	12.6	73.5	$MAPb(Cl,I)_3$	[2]
46	1.57	1.66	3.6	1030	5.4	64.4	$MAPb(Cl,I)_3$	[2]
51	**2.65**	**1.55**	**3.07**	**1160**	**3.47**	**76.1**	**$Cs_2AgBiBr_6$**	[73]
52	1.88	2.13	4.1	1125	5.8	63.0	$Cs_{0.25}FA_{0.75}PbBr_{1.5}I_{1.5}$	[3]
54	2.27	3.64	6.8	1400	7.4	65.7	$FAPbBr_3$	[5]
66	2.62	0.73	1.1	1000	2.1	52.9	$Cs_2AgBiBr_6$	[2]
68	2.35	5.30	7.8	1554	6.7	72.0	$FAPbBr_{2.43}Cl_{0.57}$	[2]
71	2.28	5.67	8.1	1640	6.7	74.0	$FAPbBr_3$	[5]
72	2.62	1.08	1.5	960	2.1	74.3	$Cs_2AgBiBr_6$	[2]
72	3.03	0.14	0.2	1110	0.6	35.4	$MAPbCl_3$	[2]
73	2.62	1.17	1.6	970	2.2	73.1	$Cs_2AgBiBr_6$	[2]
73	2.84	0.37	0.5	1260	0.9	44.9	$MAPbBr_{0.6}Cl_{2.4}$	[2]
74	2.62	1.11	1.5	970	2.2	71.1	$Cs_2AgBiBr_6$	[2]

TABLE 18 | (Semi-)transparent organic solar cells with the highest efficiency: performance parameters as a function of average visible transmittance and photovoltaic bandgap energy (from the EQE spectrum).

AVT [%]	E_g [eV]	*LUE* [%]	*PCE* [%]	V_{oc} [mV]	J_{sc} [mA cm^{-2}]	*FF* [%]	Active material	Refs.
1	1.41	0.13	13.2	852	22.0	70.3	D18-Cl:Y6:$PC_{71}BM$	[3]
1	1.41	0.13	12.8	851	21.4	70.3	D18-Cl:Y6:$PC_{71}BM$	[3]
2	1.66	0.15	7.6	770	15.6	63.3	PBDTTT-C-T:$PC_{71}BM$	[2]
3	1.40	0.40	12.6	800	24.5	64.5	PM6:Y6	[2]
4	1.38	0.65	15.6	837	24.7	75.6	PM6:BTP-eC9	[164]
5	**1.42**	**0.54**	**11.4**	**835**	**22.4**	**60.8**	**PM6:BTP-eC9**	[70]
8	1.41	1.02	12.7	852	21.1	70.4	D18-Cl:Y6:$PC_{71}BM$	[3]
9	1.42	1.17	13.0	855	21.7	70.3	D18-Cl:Y6:$PC_{71}BM$	[3]
9	1.42	1.28	14.2	854	23.0	72.3	PM6:Y6	[2]

(Continues)

TABLE 18 | (Continued)

AVT [%]	E_g [eV]	*LUE* [%]	*PCE* [%]	V_{oc} [mV]	J_{sc} [mA cm^{-2}]	*FF* [%]	Active material	Refs.
10	1.39	1.41	14.9	847	23.1	75.8	D18: N3	[4]
11	**1.41**	**1.72**	**15.8**	**860**	**23.5**	**77.9**	**PM6:L8-BO**	[71]
11	1.66	0.78	7.1	760	14.5	64.4	PBDTTT-C-T:$PC_{71}BM$	[2]
13	1.42	1.73	13.3	853	21.7	71.9	PM6:Y6	[2]
14	1.45	1.55	11.1	727	21.4	71.3	PTB7-Th:FNIC2	[2]
15	1.52	1.34	8.9	772	18.3	63.0	PTB7-Th:FNIC1	[2]
17	1.39	2.14	12.6	810	21.2	73.2	PM6:Y6	[2]
18	1.39	2.10	11.7	810	20.7	69.6	PM6:Y6	[2]
19	1.42	2.61	13.6	830	23.4	70.2	PM6:Y7	[3]
19	1.42	2.35	12.4	852	20.4	71.4	PM6:Y6	[2]
20	1.37	2.31	14.0	820	23.0	74.3	PM6:Y6:SN3	[3]
20	1.39	2.80	14.6	860	22.8	74.7	PM6/ICBA:Y6	[3]
20	1.23	2.40	11.6	661	25.6	68.2	PTB7-Th:ATT-9	[3]
21	1.39	2.21	10.5	800	19.3	68.3	PM6:Y6	[2]
21	1.39	3.32	16.1	859	24.6	76.1	PM6-Ir1:BTP-eC9:$PC_{71}BM$	[3]
21	1.42	2.82	13.4	831	21.8	73.9	PM6:PCE10-2F:Y6	[4]
22	1.41	2.81	12.8	834	20.9	73.7	PM6:BTP-eC9	[165]
23	1.41	2.90	12.9	831	20.9	74.3	D18:N3	[4]
24	1.39	2.62	10.8	830	18.2	71.6	PBT1-C-2Cl: Y6	[4]
25	**1.41**	**3.26**	**13.3**	**851**	**21.1**	**74.3**	**PTzBI-Cl:BTR-Cl:DT-Y6**	[166]
25	1.34	2.75	11.0	750	20.9	70.0	PCE-10:A078	[2]
25	1.40	2.55	10.2	736	20.3	68.3	PTB7-Th:FOIC	[2]
25	1.43	3.03	12.1	760	23.9	66.6	PM6:Y6	[3]
25	1.45	3.44	13.6	895	19.6	77.1	DA:PM6:L8-BO:Y5	[5]
26	1.40	3.35	12.9	825	21.6	72.4	PM6:Y6	[2]
26	1.43	2.31	8.77	839	19.1	54.7	PM6:BTP-eC9	[167]
27	**1.35**	**3.38**	**12.5**	**790**	**21.9**	**72.4**	**PM6:S9SBO-F:Y6-O**	[168]
28	**1.45**	**3.89**	**14.0**	**890**	**21.2**	**74.6**	**PM6:BO-4C:L8-BO**	[169]
28	1.66	1.57	5.6	760	11.9	61.9	PBDTTT-C-T:$PC_{71}BM$	[2]
30	1.41	3.03	10.1	880	16.8	67.8	PBOF:eC9:LB-BO	[4]
30	1.35	3.24	10.8	718	21.9	68.7	PTB7-Th:IEICO-4F	[2]
31	1.39	3.72	12.0	758	22.8	69.7	PCE10-BDT2F-0.8:Y6	[3]
32	1.36	4.86	15.2	880	22.6	76.8	PM6:BTP-eC9:L8-BO	[170]
32	1.41	2.31	7.15	801	14.3	62.5	PM6:Y6-BO	[4]
32	1.42	3.58	11.2	849	17.0	77.6	PM6:m-BTP-PhC6:BO-Cl	[3]
33	**1.43**	**4.04**	**12.3**	**869**	**18.9**	**74.7**	**PM6:L8-BO:BTP-eC9**	[171]
33	1.39	4.08	12.3	781	22.0	71.3	PM6:PCE 10–2F:Y6	[4]
34	1.40	3.09	9.1	733	18.5	67.1	PTB7-Th:FOIC	[2]

(Continues)

TABLE 18 | (Continued)

AVT [%]	E_g [eV]	*LUE* [%]	*PCE* [%]	V_{oc} [mV]	J_{sc} [mA cm^{-2}]	*FF* [%]	Active material	Refs.
36	1.37	2.48	8.8	680	18.0	71.9	PCE-10:BT-CIC:TT-FIC	[2]
36	1.86	3.33	6.9	890	11.6	66.5	PSEHTT:ICBA	[2]
36	1.24	2.26	9.4	658	20.7	68.7	PTB7-Th:ATT-9	[5]
37	**1.41**	**4.03**	**10.9**	**868**	**16.8**	**75.0**	**PM6:BTP-eC9:L8-BO**	[172]
37	1.86	2.25	6.1	890	10.2	66.8	PSEHTT:ICBA	[2]
39	1.40	3.82	9.8	851	15.3	75.4	PM6:BTP-eC9:L8-BO	[5]
39	1.40	4.99	12.8	849	19.0	79.2	PBDB-TF:L8-BO:BTP-eC9	[3]
39	1.86	1.91	4.9	880	8.3	67.9	PSEHTT:ICBA	[2]
42	**1.42**	**4.28**	**10.2**	**770**	**17.8**	**74.5**	**PCE10:eC9-2Cl**	[68]
43	1.34	3.48	8.1	730	16.3	68.1	PCE-10:A078	[2]
43	1.40	3.90	9.0	850	14.0	75.7	PM6:BTP-eC9:L8-BO	[5]
44	1.37	3.52	8.0	680	16.2	72.6	PCE-10:BT-CIC:TT-FIC	[2]
44	1.39	3.62	8.2	806	15.1	67.2	PBT1-C-2Cl:Y6	[4]
44	1.40	2.95	6.7	600	18.6	60.2	PDTTP-TBT:Y6-BO:$PC_{61}BM$	[5]
44	**1.40**	**4.16**	**9.5**	**846**	**14.8**	**75.4**	**PM6:BTP-eC9:L8-BO**	[72]
44	1.39	2.95	12.6	840	19.8	75.8	PM6:BTP-eC9:L8-BO	[5]
45	**1.39**	**6.02**	**13.3**	**868**	**20.1**	**76.3**	**D18:BTP-eC9:BTO-BO**	[66]
45	**1.40**	**4.91**	**10.8**	**808**	**18.6**	**72.0**	**PCE10-2F/4FY**	[69]
46	1.39	5.10	11.2	803	19.3	72.0	DA:PCE10-2F/Y6:Y5	[5]
46	1.34	4.97	10.8	750	20.4	70.6	PCE-10:A078	[2]
47	1.40	5.30	11.3	854	17.9	74.1	PM6: BTP-eC9:L8-BO	[173]
47	1.39	5.35	11.4	854	18.0	74.5	PM6:BTP-eC9:L8-BO	[3]
47	1.34	3.34	7.1	730	14.3	68.0	PCE-10:A078	[2]
47	1.86	1.12	2.4	860	4.1	68.2	PSEHTT:ICBA	[2]
49	1.37	3.53	7.2	670	14.8	72.6	PCE-10:BT-CIC:TT-FIC	[2]
49	1.41	2.96	6.0	851	11.1	63.8	FC-S1:PM6:Y6-BO	[4]
50	**1.38**	**6.05**	**12.2**	**880**	**18.1**	**76.7**	**PBOF:eC9:$PC_{61}BM$**	[65]
50	1.40	4.16	8.3	746	16.7	66.8	PTB7-Th:FOIC:$PC_{71}BM$	[2]
50	1.39	4.75	9.5	786	16.9	71.4	PCE10-2F:Y6	[174]
51	1.24	3.73	7.3	645	17.9	63.6	PTB7-Th:ATT-9	[5]
51	1.40	3.76	7.4	749	14.7	66.7	PTB7:FOIC:PC71BM	[2]
53	1.86	0.95	1.8	890	3.8	54.8	PSEHTT:ICBA	[2]
53	1.32	3.02	5.7	750	10.6	69.5	DPP2T:IEICO-4F	[2]
60	1.33	2.34	3.9	749	7.34	70.2	DPP2T:IEICO-4F	[2]
62	1.33	3.66	5.9	690	12.9	66.0	PTB7-Th:6TIC-4F	[2]
71	1.33	2.87	4.1	703	9.5	61.0	PTB7-Th:IEICO-4F	[5]
80	1.36	1.91	2.4	705	5.7	59.3	PTB7-Th:IEICO-4F	[5]

TABLE 19 | (Semi-)transparent dye-sensitized solar cells with the highest efficiency: performance parameters as a function of average visible transmittance and photovoltaic bandgap energy (from the EQE spectrum).

AVT [%]	E_g [eV]	*LUE* [%]	*PCE* [%]	V_{oc} [mV]	J_{sc} [mA cm^{-2}]	*FF* [%]	Sensitizing dye	Refs.
1	2.00	0.05	5.2	780	12.4	53.7	N719	[2]
5	1.80	0.55	11.0	871	16.8	75.2	C268+Y1	[3]
9	2.00	0.41	4.5	780	10.3	56.0	N719	[2]
9	1.82	0.39	4.3	720	9.9	60.0	N719+SDA	[2]
10	2.01	0.52	5.2	770	11.9	57.0	N719	[2]
10	2.00	0.49	4.9	765	11.4	56.1	N719	[2]
13	1.68	1.31	10.1	851	14.9	80.2	SGT-021	[2]
14	1.68	1.39	9.9	850	14.9	78.5	SGT-021	[2]
15	1.68	1.44	9.6	850	14.7	77.2	SGT-021	[2]
17	1.68	1.67	9.8	855	15.1	75.5	SGT-021	[2]
23	1.82	0.97	4.2	650	9.9	64.0	N719+SDA	[2]
23	2.01	0.83	3.6	650	8.2	68.0	N719	[2]
25	1.82	0.65	2.6	650	5.6	71.0	N719+SDA	[2]
27	1.77	0.99	3.7	521	10.7	65.8	NPI	[2]
30	2.19	0.45	1.5	640	3.3	70.0	N719	[2]
31	2.23	1.98	6.4	698	13.5	67.9	TPA-1 (EtOH)	[2]
33	2.30	2.02	6.1	711	12.5	68.3	TPA-2 (EtOH)	[2]
36	2.23	2.20	6.1	766	14.5	54.7	TPA-1 (EtOH)	[2]
37	2.46	1.30	3.5	648	8.0	67.5	Cz-2	[2]
38	2.31	2.16	5.7	769	13.6	54.2	TPA-2 (EtOH)	[2]
69	1.39	2.13	3.1	422	11.2	65.6	VG20-C_{16}	[2]
75	1.53	1.88	2.5	408	10.9	56.2	TB207	[3]
76	1.41	1.75	2.3	406	8.6	65.9	VG20-C_{16}	[2]

TABLE 20 | Semitransparent emerging inorganic solar cells with the highest efficiency: performance parameters as a function of average visible transmittance and photovoltaic bandgap energy (from the EQE spectrum).

AVT [%]	E_g [eV]	*LUE* [%]	*PCE* [%]	V_{oc} [mV]	J_{sc} [mA cm^{-2}]	*FF* [%]	Absorber/technology	Refs.
1	1.46	0.03	3.0	475	14.6	42.8	$Cu_2ZnSn(S,Se)_4$	[2]
2	**1.57**	**0.13**	**8.3**	**647**	**20.0**	**63.7**	**$Sb_2(S,Se)_3$**	[175]
8	1.83	0.27	3.4	679	12.1	42.0	Sb_2S_3	[2]

TABLE 21 | Semitransparent solar cells among established inorganic technologies with the highest efficiency: performance parameters as a function of average visible transmittance and photovoltaic bandgap energy (from the EQE spectrum).

AVT (%)	E_g (eV)	*LUE* (%)	*PCE* (%)	V_{oc} (mV)	J_{sc} (mA cm^{-2})	*FF* (%)	Absorber/technology	Refs.
2	1.23	0.20	10.0	640	23.3	66.9	CIGS	[2]
9	1.30	0.88	9.8	630	20.9	74.1	CIGS	[2]
9	1.28	0.59	6.5	597	22.9	46.5	CIGS	[2]
16	1.83	1.20	7.5	810	14.2	65.3	a-Si:H	[2]
17	1.83	1.31	7.7	810	14.1	67.3	a-Si:H	[2]
18	2.05	1.07	5.9	720	14.1	58.3	a-SiGe:H	[2]
19	1.87	1.38	7.3	820	13.1	67.6	a-Si:H	[2]
19	1.34	1.24	6.5	580	17.5	63.5	CIGS	[2]
20	1.64	0.34	1.7	495	8.9	40.8	CIGS	[2]
22	2.05	1.20	5.5	760	12.3	58.6	a-Si:H	[2]
23	1.92	1.38	6.0	830	10.6	68.2	a-Si:H	[2]
24	1.68[a]	1.66	6.9	920	10.7	70.3	a-Si:H	[2]
26	1.50	1.53	5.9	710	14.6	57.4	CIGS	[2]
37	1.54	0.15	0.4	101	14.7	27.2	CdTe	[2]
45	2.16	0.50	1.1	596	3.9	47.7	a-Si:H	[2]

[a]E_g taken from the absorbance spectrum

TABLE 22 | Transparent photovoltaic devices with the highest efficiency including transparent luminescent solar concentrators: performance parameters (measured under the standard of Yang et al.) [18] as a function of the average visible transmittance and photovoltaic bandgap energy (from the EQE spectrum) [15].

AVT (%)	E_g (eV)	*LUE* (%)	*PCE* (%)	V_{oc} (mV)	J_{sc} (mA cm^{-2})	*FF* (%)	Luminophore(s)/absorber	Refs.
73	1.50	0.88	1.2	990	1.5	81.3	CO_i8DFIC/GaAs	[2]
75	1.64	2.26	3.0	1020	3.8	77.7	$Cs_2Mo_6I_8(CF_3CF_2COO)_6$:BODIPY/GaAs	[3]
84	2.81	0.37	0.4	520	1.3	65.1	$(TBA)_2Mo_6Cl_{14}$ /Si	[3]
84	2.60	0.65	0.8	4810	0.2	79.2	Si-QDs/Si	[5]
86	1.52	0.34	0.4	500	1.2	66.7	Cy7-NHS/Si	[3]
88	**2.53**	**0.60**	**0.68**	**1001**	**1.08**	**62.5**	**HBTM/Si**	[74]
89	2.94	1.86	2.1	500	5.7	73.3	Si-CDs/Si	[4]
90	**2.61**	**0.86**	**0.96**	**500**	**3.6**	**53.0**	**$MAPbBr_3$/Si**	[75]

7.4 | Operational Stability Tables of Emerging Research Solar Cells

TABLE 23 | Perovskite solar cells with the highest operational (MPP) stability test energy yield for 200 and 1000 hours under simulated 1 sun illumination as a function of the device photovoltaic bandgap energy (from the EQE spectrum).

E_g (eV)	0 h PCE (%)	200 h PCE (%)	1 000 h PCE (%)	E_{200h} (Wh·cm^{-2})	E_{1000h} (Wh·cm^{-2})	t_{95} (h)	Absorber	Comments	Refs.
1.40	9.4	9.4	9.2	1.9	9.3	>500	$FASnI_3$+$NaBH_4$+DipI	AM1.5G, N_2, 70°C	[3]
1.45	13.8	14.1	13.0	2.8	13.6	520	$FASnI_3$	AM1.5G, air	[3]
1.50	**25.5**	**24.7**	**23.2**	**5.0**	**24.3**	**583**	**$FAPbI_3$**	**AM1.5G, N_2, 25°C,**	[85]
1.51	22.8	21.9	20.0	4.5	21.2	285	$Cs_{0.025}FA_{0.90}MA_{0.075}PbI_3$	AM1.5G, 40°C, 50% RH, encapsulation	[5]
1.52	25.4	25.1	24.4	5.0	24.8	1262	$Cs_{0.05}FA_{0.95}PbI_3$	AM1.5G, N_2, 25°C	[5]
1.52	**26.0**	**24.9**	**—**	**5.1**	**—**	**415**	**$FAPbI_3$**	**w-LED, N_2, 45°C**	[86]
1.53	24.3	23.8	—	4.8	—	>495	$FAPbI_3$	AM1.5G, 45°C	[5]
1.53	**26.2**	**25.6**	**25.1**	**5.1**	**25.4**	**1759**	**$FAPbI_3$**	**AM1.5G**	[53]
1.53	**25.8**	**25.5**	**24.1**	**5.1**	**25.1**	**914**	**$Cs_{0.05}FA_{0.85}MA_{0.1}PbI_3$**	**AM1.5G, N_2, 25°C**	[176]
1.54	24.8	24.1	23.0	4.9	23.6	477	$Cs_{0.05}FA_{0.931}MA_{0.019}$ Pb $Br_{0.06}I_{2.94}$	AM1.5G, N_2, 65°C	[5]
1.54	24.3	24.6	24.5	5.0	24.5	>3000	$Cs_{0.17}FA_{0.83}PbI_3$	AM1.5G, N_2	[177]
1.54	**25.5**	**27.3**	**23.3**	**5.4**	**25.7**	**874**	**$Cs_{0.05}FA_{0.9}MA_{0.05}PbI_3$**	**w-LED, air, 25°C, 60% RH, encapsulation**	[178]
1.54	**26.3**	**25.9**	**25.0**	**5.13**	**25.6**	**>850**	**$Cs_{0.05}FA_{0.9}MA_{0.05}Pb_{95}Br_{0.15}I_{2.85}$**	**AM1.5G, N_2, 55°C, encapsulation**	[179]
1.54	**25.1**	**24.9**	**25.0**	**5.0**	**24.8**	**>1800**	**$Cs_{0.05}FA_{0.85}MA_{0.1}PbBr_{0.09}I_{2.91}$**	**AM1.5G, air, 60°C**	[79]
1.55	25.5	24.2	22.2	4.9	23.7	198	$FA_{0.97}MA_{0.03}PbBr_{0.09}I_{2.91}$	AM1.5G, 65°C, encapsulation	[5]
1.55	25.0	23.8	—	4.8	—	216	$Cs_{0.1}FA_{0.9}PbI_3$	w-LED, 30°C, encapsulation	[5]
1.55	**25.5**	**26.3**	**26.1**	**5.2**	**26.2**	**>2000**	**$CsFAMAPbCl_xI_{3-x}$**	**w-LED, air, 45°C, 60% RH, encapsulation**	[80]

(Continues)

TABLE 23 | (Continued)

E_g (eV)	0 h PCE (%)	200 h PCE (%)	1 000 h PCE (%)	E_{200h} (Wh·cm^{-2})	E_{1000h} (Wh·cm^{-2})	t_{95} (h)	Absorber	Comments	Refs.
1.55	**25.4**	**25.0**	**—**	**5.0**	**—**	**610**	**$CsFAMAPbCl_xI_{3-x}$**	**AM1.5G, air, 85°C, 60% RH, encapsulation**	[80]
1.55	**25.2**	**24.8**	**23.4**	**5.0**	**24.2**	**680**	**$FAPbI_3$**	**w-LED, N_2, 25°C**	[180]
1.55	**24.0**	**23.8**	**—**	**4.8**	**—**	**891**	**$FA_{0.3}MA_{0.7}PbI_3$**	**AM1.5G, air, 85°C, 50% RH, encapsulation**	[181]
1.56	**24.3**	**24.1**	**—**	**4.8**	**—**	**680**	**$FA_{1-x}MA_xPbBr_{3x}I_{3-3x}$**	**AM1.5G, N_2, 45°C**	[138]
1.56	24.3	23.0	—	4.7	—-	139	$Cs_{0.01}FA_{0.9603}MA_{0.0297}PbBr_{0.09}I_{2.91}$	w-LED, 40°C, encapsulation	[5]
1.57	**26.67**	**23.82**	**23.56**	**4.85**	**24**	**1135**	**$Cs_{0.05}FA_{0.85}MA_{0.1}PbI_3$**	**AM1.5G, air, 25°C, 50% RH**	[182]
1.57	**26.1**	**25.5**	**24.8**	**5.2**	**25.4**	**744**	**$Cs_{0.05}FA_{0.90}MA_{0.05}PbBr_{0.15}$ $I_{2.85}$**	**AM1.5G, air, 65°C, 50% RH**	[90]
1.58	23.1	22.9	—	4.6	—	>250	$Cs_{0.05}FA_{0.9}MA_{0.05}$ Pb $Br_{0.26}I_{2.74}$	N_2	[3]
1.59	21.2	21.1	21.3	4.2	21.2	>1000	$CsFAMAPbI_3$	AM1.5G, Air, 45°C	[2]
1.60	22.0	22.2	20.2	4.4	21.4	691	$Cs_{0.05}FA_{0.874}MA_{0.076}PbBr_{0.18}I_{2.76}$	AM1.5G, encapsulation, 55°C	[4]
1.61	18.1	11.9	13.6	2.6	13.0	10	$Gua_{0.25}MA_{0.75}PbI_3$	AM1.5G, Ar, 60°C	[2]
1.63	21.0	19.7	—	3.9	19.6	14	$Cs_{0.05}FA_{0.81}MA_{0.14}PbBr_{0.45}I_{2.55}$/FGCs	AM1.5G, N_2, 60°C	[2]
1.64	20.1	17.8	—	3.6	—	2	$Cs_{0.1}$ $FA_{0.747}MA_{0.153}PbBr_{0.51}I_{2.49}$	N_2, 25°C	[2]
1.66	13.0	14.5	12.9	2.8	14.0	>1000	$Cs_{0.17}FA_{0.83}PbBr_{0.51}I_{2.49}$	AM1.5G, 40% RH, 35°C	[2]
1.67	**19.8**	**18.0**	**—**	**3.5**	**—**	**11**	**$Cs_{0.22}FA_{0.75}MA_{0.03}PbBr_{0.45}Cl_{0.09}I_{2.46}$**	**w-LED, N_2, 45°C**	[183]
1.69	6.8	6.7	—	1.3	—	389	$CsGe_{0.5}Sn_{0.5}I_3$	AM1.5G, N_2, 45°C	[2]
1.70	**21.8**	**20.2**	**—**	**4.1**	**—**	**>500**	**$CsPbI_3$**	**Encapsulation, air, AM1.5G, 25°C, 50% RH**	[184]
1.78	16.8	17.1	17.1	3.4	17.1	>2000	$CsPbBr_xI_{3-x}$	AM1.5G, air 30–40% RH, 35°C	[4]
1.79	19.0	18.9	—	3.8	—	>700	$Cs_{0.2}FA_{0.8}PbBr_{1.2}I_{1.8}$	AM1.5G, encapsulation	[4]

Abbreviations: RH, relative humidity.; UV-f, ultraviolet light filter; w-LED, white-light spectrum light-emitting diode source.

TABLE 24 | Organic and dye-sensitized solar cells with the highest operational (mpp) stability test energy yield for 200 and 1000 h under simulated 1 sun illumination as a function of the device photovoltaic bandgap energy (from the EQE spectrum).

E_g (eV)	0 h PCE (%)	200 h PCE (%)	1 000 h PCE (%)	E_{200h} (Wh·cm^{-2})	E_{1000h} (Wh·cm^{-2})	t_{95} (h)	Active material or dye	Comments	Refs.
1.40	18.8	16.4	14.6	3.4	15.6	46	PM6:BTP-eC9	w-LED, air	[4]
1.43	17.7	16.1	14.7	3.3	7.9	49	PM6:PY-1S1Se:PY-2Cl	AM1.5G, air	[4]
1.44	**17.8**	**17.3**	**16.8**	**3.5**	**17.1**	**714**	**PM6:L8-BO**	**w-LED, N_2**	[77]
1.44	**19.6**	**18.3**	**—**	**3.8**	**—**	**150**	**D18:L8-BO**	**AM1.5G, air, 25% RH, 25°C**	[185]
1.65	11.2	11.0	9.7	2.2	10.4	398	SGT-021/HC-A6+ThCA	AM1.5G, 25°C, air, 50% RH	[5]

Abbreviation: w-LED, white-light spectrum light-emitting diode source.

TABLE 25 | Multijunction solar cells with the highest operational (MPP) stability test energy yield for 200 and 1000 h under simulated/equivalent 1 sun illumination as a function of the device photovoltaic bandgap energies (from the EQE spectra).

Bottom E_g (eV)	Top E_g (eV)	0 h PCE (%)	200 h PCE (%)	1000 h PCE (%)	E_{200h} (Wh cm^{-2})	E_{1000h} (Wh cm^{-2})	t_{95} (h)	Bottom absorber material	Top absorber material	Comments	Refs.
								Perovskite/perovskite			
1.25	1.80	27.4	28.4	—	5.6	—	511	$FA_{0.7}MA_{0.3}Pb_{0.5}Sn_{0.5}I_3$	$Cs_{0.2}FA_{0.8}PbBr_{1.14}I_{1.86}$	AM1.5G, air 30–50% RH, 35°C	[4]
1.25	1.80	25.6	26.4	—	5.2	—	497	$Cs_{0.2}FA_{0.8}PbBr_{01.14}I_{1.86}$	$FA_{0.7}MA_{0.3}Pb_{0.5}Sn_{0.5}I_3$	AM1.5G, air 30–50% RH, 35°C	[3]
1.25	**1.77**	**29.3**	**25.88**	**23**	**5.29**	**24.8**	**23**	**$FA_{0.8}Cs_{0.2}Pb(I_{0.6}Br_{0.4})_3$**	**$FA_{0.65}MA_{0.3}Cs_{0.05}Pb_{0.5}Sn_{0.5}I_3$**	**AM1.5G, air 40% RH, 25°C**	[186]
1.26	1.80	24.1	23.5	23.2	4.8	23.7	988	$FA_{0.7}MA_{0.3}Pb_{0.5}Sn_{0.5}I_3$	$CsPbBr_xI_{3-x}$	AM1.5G, air 30–50% RH, 35°C	[4]
1.26	1.80	26.9	24.6	—	5.1	—	92	$Cs_{0.1}FA_{0.6}MA_{0.3}Pb_{0.5}Sn_{0.5}I_3$	$Cs_{0.2}FA_{0.8}$ Pb $Br_{1.2}I_{1.8}$	AM1.5G, air 25–35°C	[4]
1.26	**1.61[m], 1.99**	**26.5**	**24.0**	**—**	**4.9**	**—**	**908**	**$Cs_{0.1}FA_{0.6}MA_{0.3}Sn_{0.5}Pb_{0.5}I_3$**	**$Cs_{0.1}FA_{0.9}PbBr_{0.45}$ $I_{2.55}$ [m], $Cs_{0.2}FA_{0.8}PbBr_{1.2}$ $I_{1.8}$**	**AM1.5G, air, 45% RH**	[49]
1.27	**1.82**	**27.1**	**26.3**	**—**	**5.40**	**—**	**261**	**$Cs_{0.05}FA_{0.7}MA_{0.25}Pb_{0.5}Sn_{0.5}I_3$**	**$Cs_{0.2}FA_{0.8}PbBr_{1.2}$ $I_{1.8}$**	**AM1.5G, air, 25°C, 85% RH, encapsulation**	[128]
								GaAs/perovskite			
1.42	1.85	24.1	23.9	—	4.76	—		GaAs	$FA_{0.80}MA_{0.04}Cs_{0.16}PbBr_{1.5}I_{1.5}$	air 20–25% RH, AM1.5G, room T, UV-f	[2]
								CIGS/perovskite			
1.10	1.65	22.0	19.9	—	4.1	—	32	CIGS	$Cs_{0.09}FA_{0.77}MA_{0.14}PbBr_{0.42}I_{2.58}$	air 20% RH, 30°C	[2]
1.14	**1.67**	**24.1**	**22.8**	**—**	**4.6**	**—**	**166**	**CIGS**	**$Cs_{0.17}FA_{0.83}PbBr_{1.8}I_{1.2}$**	**AM1.5G, air, 25°C,40% RH**	[45]
1.15	**1.69**	**23.6**	**24.8**	**—**	**4.9**	**—**	**>420**	**CIGS**	**$Cs_{0.2}DMA_{0.1}FA_{0.65}MA_{0.05}PbBr_{0.3}I_{2.7}$**	**AM1.5G, air, 25°C,50% RH**	[44]

(Continues)

TABLE 25 | (Continued)

Bottom E_g (eV)	Top E_g (eV)	0 h PCE (%)	200 h PCE (%)	1000 h PCE (%)	E_{200h} (Wh cm^{-2})	E_{1000h} (Wh cm^{-2})	t_{95} (h)	Bottom absorber material	Top absorber material	Comments	Refs.
								Si/perovskite			
1.11	**1.68**	**33.3**	**31.5**	**27.3**	**6.4**	**30.1**	**183**	**Si**	**$Cs_{0.05}FA_{0.8}MA_{0.15}PbBr_{0.72}I_{2.28}$**	**AM1.5G, air, 25°C,50% RH**	[78]
1.13	1.68	24.0	22.8	21.5	4.6	22.4	503	Si	$CsFAPb(Br,I)_3$:$MA(Cl_{0.5}SCN_{0.5})$	w-LED, air, 40% RH, 25°C	[4]
1.18	**1.58,[m] 1.92**	**25.2**	**24.6**	**—**	**5.0**	**—**	**295**	**Si**	**$Cs_{0.08}FA_{0.9}Rb_{0.02}PbI_3$,[m] $Cs_{0.16}FA_{0.8}Rb_{0.04}PbBr_{1.65}I_{1.35}$**	**AM1.5G, air, 25°C, encapsulation**	[51]
								Organic/perovskite			
1.38	**1.88**	**24.5**	**22.8**	**—**	**4.7** [94]	**—**	**85**	**PM6:BTP-eC9**	**$CsPbBrI_2$**	**AM1.5G, air, 25°C, 50% RH, encapsulation**	[94]
1.40	1.81	21.1	19.9	—	4.0	—	69	PM6:Y6:P_{71}CBM	$Cs_{0.25}FA_{0.75}PbBr_{1.2}I_{1.8}$	AM1.5G, N_2, encapsulation	[187]

Abbreviations: m), superscript indicating middle sub-cell in triple junction devices; RH, relative humidity; UV-f, ultraviolet light filter; w-LED, white-light spectrum light-emitting diode source.

Acknowledgements

C.J.B. gratefully acknowledges financial support through the "Aufbruch Bayern" initiative of the state of Bavaria (EnCN and SFF), the Bavarian Initiative "Solar Technologies go Hybrid" (SolTech), the DFG—SFB953 (project no. 182849149), and DFG—INST 90/917-1 FUGG. R. R. L. gratefully acknowledges support from the National Science Foundation under grant CBET-1702591. C. S. gratefully acknowledges financial support by the Vector Foundation. L.A.C acknowledges the European Union's Framework Programme for Research and Innovation Horizon Europe (2021-2027) under the Marie Sklodowska-Curie Grant Agreement No. 101068387 "EFESO". K.F. acknowledges the support from JST ASPIRE for Rising Scientists (JPMJAP2336). A.O.A. and B.E. received funding from the European Research Council under the European Union's Horizon 2020 research and innovation program under Grant Agreement No. 947221. We also acknowledge Simon Stier for his work as software developer of the emerging-pv.org website and database, and all the contributions to the database updating; particularly the effort by Wei Yu. We also thank Dr. Xiangchuan Meng, Prof. Xiaotian Hu, Prof. Xiaodong Li, Prof. Chao Liang, and Prof. Xiaopeng Zheng for their further data contribution.

Conflicts of Interest

R.R.L. is a co-founder, director, and a part-owner of Ubiquitous Energy, Inc., a company working to commercialize transparent photovoltaic technologies. All other authors declare no conflicts of interest.

Data Availability Statement

The data that support the findings of this study are available from the corresponding author upon reasonable request.

References

1. O. Almora, D. Baran, G. C. Bazan, et al., "Device Performance of Emerging Photovoltaic Materials (Version 1)," *Advanced Energy Materials* 11 (2021): 2002774.

2. O. Almora, D. Baran, G. C. Bazan, et al., "Device Performance of Emerging Photovoltaic Materials (Version 2)," *Advanced Energy Materials* 11 (2021): 2102526.

3. O. Almora, D. Baran, G. C. Bazan, et al., "Device Performance of Emerging Photovoltaic Materials (Version 3)," *Advanced Energy Materials* 13, (2022): 2203313.

4. O. Almora, C. I. Cabrera, S. Erten-Ela, et al., "Device Performance of Emerging Photovoltaic Materials (Version 4)," *Advanced Energy Materials* 14 (2024): 2303173.

5. O. Almora, G. C. Bazan, C. I. Cabrera, et al., "Device Performance of Emerging Photovoltaic Materials (Version 5)," *Advanced Energy Materials* 15 (2025): 2404386.

6. Emerging PV, https://emerging-pv.org, accessed: August 30, 2025.

7. W. Shockley and H. J. Queisser, "Detailed Balance Limit of Efficiency of p-n Junction Solar Cells," *Journal of Applied Physics* 32 (1961): 510.

8. A. S. Brown and M. A. Green, "Radiative Coupling as a Means to Reduce Spectral Mismatch in Monolithic Tandem Solar Cell Stacks Theoretical Considerations," presented at *Conference Record of the Twenty-Ninth IEEE Photovoltaic Specialists Conference, 2002*, New Orleans, LA, USA, 19–24 May 2002, 2002.

9. A. S. Brown and M. A. Green, "Detailed Balance Limit for the Series Constrained Two Terminal Tandem Solar Cell," *Physica E: Low-dimensional Systems and Nanostructures* 14 (2002): 96.

10. L. Sun, K. Fukuda, R. Guo, et al., "A Flexible Photovoltaic Fatigue Factor for Quantification of Mechanical Device Performance," *Advanced Functional Materials* 35 (2025): 2422706.

11. J. M. Jailani, A. Luu, E. Salvosa, et al., "Accurate Performance Characterization, Reporting, and Benchmarking for Indoor Photovoltaics," *Joule* 9 (2025): 102126.

12. R. L. Z. Hoye, G. Koutsourakis, M. Freitag, et al., "Reaching a Consensus on Indoor Photovoltaics Testing," *Joule* 9 (2025): 102127.

13. A. Chakraborty, G. Lucarelli, V. Singh, et al., "Best Practices for Measuring Indoor Photovoltaic Devices," *Nature Energy* (2025).

14. K. Fukuda, L. Sun, B. Du, et al., "A Bending Test Protocol for Characterizing the Mechanical Performance of Flexible Photovoltaics," *Nature Energy* 9 (2024): 1335.

15. O. Almora, C. I. Cabrera, J. Garcia-Cerrillo, T. Kirchartz, U. Rau, and C. J. Brabec, "Quantifying the Absorption Onset in the Quantum Efficiency of Emerging Photovoltaic Devices," *Advanced Energy Materials* 11 (2021): 2100022.

16. L. Krückemeier, U. Rau, M. Stolterfoht, and T. Kirchartz, "How to Report Record Open-Circuit Voltages in Lead-Halide Perovskite Solar Cells," *Advanced Energy Materials* 10 (2020): 1902573.

17. J.-F. Guillemoles, T. Kirchartz, D. Cahen, and U. Rau, "Guide for the Perplexed to the Shockley–Queisser Model for Solar Cells," *Nature Photonics* 13 (2019): 501–505.

18. C. Yang, D. Liu, M. Bates, M. C. Barr, and R. R. Lunt, "How to Accurately Report Transparent Solar Cells," *Joule* 3 (2019): 1803.

19. C. J. Traverse, R. Pandey, M. C. Barr, and R. R. Lunt, "Emergence of Highly Transparent Photovoltaics for Distributed Applications," *Nature Energy* 2 (2017): 849–860.

20. Y. Yang, "The Original Design Principles of the Y-Series Nonfullerene Acceptors, from Y1 to Y6," *ACS Nano* 15 (2021): 18679.

21. S. Rühle, "Tabulated Values of the Shockley–Queisser Limit for Single Junction Solar Cells," *Solar Energy* 2016, 130, 139.

22. M. A. Green, E. D. Dunlop, M. Yoshita, et al., "Solar Cell Efficiency Tables (Version 66)," *Progress in Photovoltaics: Research and Applications* 33 (2025): 795.

23. Z. Qu, Y. Zhao, F. Ma, et al., "Enhanced Charge Carrier Transport and Defects Mitigation of Passivation Layer for Efficient Perovskite Solar Cells," *Nature Communications* 15 (2024): 8620.

24. X. Wang, J. Li, R. Guo, et al., "Regulating Phase Homogeneity by Self-assembled Molecules for Enhanced Efficiency and Stability of Inverted Perovskite Solar Cells," *Nature Photonics* 18 (2024): 1269.

25. N.-G. Park and S. G. Mhaisalkar, "Mini-Review on Detailed Synthetic Methods of Lead Halide Perovskite Powders, Single Crystals, and Thin Films," *Energy & Fuels* 39 (2025): 5133.

26. C. Li, Y. Cai, P. Hu, et al., "Organic Solar Cells with 21% Efficiency Enabled by a Hybrid Interfacial Layer with Dual-component Synergy," *Nature Materials* 24 (2025): 1626.

27. L. Wang, C. Chen, Z. Gan, et al., "Diluted Ternary Heterojunctions to Suppress Charge Recombination for Organic Solar Cells with 21% Efficiency," *Advanced Materials* 37 (2025): 2419923.

28. G. Yao, Z. Wu, D. Kou, et al., "Phase Evolution Extension of Cu 2 ZnSn(S,Se) 4 Absorber Boosting the Efficiency of Kesterite Solar Cells to 14.99%.99%," *ACS Energy Letters* 10 (2025): 2761.

29. Y. Zhao, W. Xu, J. Wen, et al., "Innovative in Situ Passivation Strategy for High-Efficiency Sb2(S,Se)3 Solar Cells," *Advanced Materials* 36 (2024): 2410669.

30. C. Liu, A. Gong, C. Zuo, et al., "Heterojunction Lithiation Engineering and Diffusion-induced Defect Passivation for Highly Efficient Sb2(S,Se)3 Solar Cells," *Energy & Environmental Science* 17 (2024): 8402.

31. J. Dong, Q. Gao, L. Wu, et al., "Carrier Management through Electrode and Electron-selective Layer Engineering for 10.70% Efficiency Antimony Selenosulfide Solar Cells," *Nature Energy* 10 (2025): 857.

32. J. T. Oh, Y. Wang, C. Rodà, et al., "Post-deposition in Situ Passivation of AgBiS2 Nanocrystal Inks for High-efficiency Ultra-thin Solar Cells," *Energy & Environmental Science* 17 (2024): 8885.

33. I. Hadar, T.-B. Song, W. Ke, and M. G. Kanatzidis, "Modern Processing and Insights on Selenium Solar Cells: the World's First Photovoltaic Device," *Advanced Energy Materials* 9 (2019): 1802766.

34. Q. Liu, X. Wang, Z. Li, et al., "Standing 1D Chains Enable Efficient Wide-Bandgap Selenium Solar Cells," *Advanced Materials* 37 (2025): 2410835.

35. U. Rau, B. Blank, T. C. M. Müller, and T. Kirchartz, "Efficiency Potential of Photovoltaic Materials and Devices Unveiled by Detailed-Balance Analysis," *Physical Review Applied* 7 (2017): 044016.

36. R. S. Nielsen, M. Schleuning, O. Karalis, et al., "Increasing the Collection Efficiency in Selenium Thin-Film Solar Cells Using a Closed-Space Annealing Strategy," *ACS Applied Energy Materials* 2024, 7, 5209.

37. C. I. Cabrera and O. Almora, "More Junctions Is Not Always Better: Mapping Optimal Bandgap Partners for Tandem and Triple-junction Solar Cells," *EES Solar* 1 (2025): 554.

38. L. Jia, S. Xia, J. Li, et al., "Efficient Perovskite/Silicon Tandem with Asymmetric Self-assembly Molecule," *Nature* 644 (2025): 912.

39. O. Er-raji, C. Messmer, R. R. Pradhan, et al., "Electron Accumulation across the Perovskite Layer Enhances Tandem Solar Cells with Textured Silicon," *Science* 390 (2025): adx1745.

40. J. Wang, S. Hu, H. Zhu, et al., "Mercapto-functionalized Scaffold Improves Perovskite Buried Interfaces for Tandem Photovoltaics," *Nature Communications* 16 (2025): 4917.

41. Z. Liu, R. Lin, M. Wei, et al., "All-perovskite Tandem Solar Cells Achieving >29% Efficiency with Improved (100) Orientation in Wide-bandgap Perovskites," *Nat Mater* 24 (2025): 252.

42. M. A. Green, E. D. Dunlop, M. Yoshita, et al., "Solar Cell Efficiency Tables (Version 64)," *Progress in Photovoltaics: Research and Applications* 32 (2024): 425.

43. Y. Wang, R. Lin, C. Liu, et al., "Homogenized Contact in all-perovskite Tandems Using Tailored 2D Perovskite," *Nature* 635 (2024): 867–873.

44. F. Pei, S. Lin, Z. Zhang, et al., "Inhibiting Defect Passivation Failure in Perovskite for Perovskite/Cu(In,Ga)Se2 Monolithic Tandem Solar Cells with Certified Efficiency 27.35%.35%," *Nature Energy* 10 (2025): 824–835.

45. Z. Ying, S. Su, X. Li, et al., "Antisolvent Seeding of Self-assembled Monolayers for Flexible Monolithic Perovskite/Cu(In,Ga)Se2 Tandem Solar Cells," *Nature Energy* 10 (2025): 737–749.

46. Z. Jia, X. Guo, X. Yin, et al., "Efficient near-infrared Harvesting in Perovskite–organic Tandem Solar Cells," *Nature* 643 (2025): 104–110.

47. J. Tian, C. Liu, K. Forberich, et al., "Overcoming Optical Losses in Thin Metal-based Recombination Layers for Efficient n-i-p Perovskite-organic Tandem Solar Cells," *Nature Communications* 16 (2025): 154.

48. J. Wang, J. Li, Y. Wang, et al., "Tandem Organic Solar Cells with 21.5% Efficiency," *Advanced Materials* 37 (2025): 10378.

49. S. Hu, J. Wang, P. Zhao, et al., "Steering Perovskite Precursor Solutions for Multijunction Photovoltaics," *Nature* 639 (2025): 93–101.

50. F. Xu, E. Aydin, I. Yavuz, et al., "Stabilized Perovskite Phases Enabling Efficient Perovskite/Perovskite/Silicon Triple-junction Solar Cells," *Nature Materials* (2025).

51. J. Zheng, G. Wang, L. Duan, et al., "Tailoring Nanoscale Interfaces for Perovskite–perovskite–silicon Triple-junction Solar Cells," *Nature Nanotechnology* 20 (2025): 1648–1655.

52. Z. Chu, B. Fan, W. Shi, et al., "Synergistic Macroscopic–Microscopic Regulation: Dual Constraints of the Island Effect and Coffee-Ring Effect in Printing Efficient Flexible Perovskite Photovoltaics," *Advanced Functional Materials* 35 (2025): 2424191.

53. X. Tang, C. Yang, Y. Xu, et al., "Enhancing the Efficiency and Stability of Perovskite Solar Cells via a Polymer Heterointerface Bridge," *Nature Photonics* 19 (2025): 701.

54. H. Liang, W. Zhu, Z. Lin, et al., "Enhancing Efficiency and Stability of Inverted Flexible Perovskite Solar Cells via Multi-Functionalized Molecular Design," *Angewandte Chemie International Edition* 64 (2025): 202501267.

55. Z. Cai, Z. Yao, Z. Xing, et al., "A Buried Interface Fastening Approach for Efficient and Flexible Perovskite Photovoltaics," *Advanced Functional Materials* 35 (2025): 2505921.

56. L. Ning, Z. Yao, L. Zha, et al., "High-Oriented SnO 2 Nanocrystals for Air-Processed Flexible Perovskite Solar Cells with an Efficiency of 23.87%.87%," *Advanced Materials* 37 (2025): 2418791.

57. X. Guo, W. Zhang, H. Yuan, et al., "Low-Temperature Processed CsPbI 3 for Flexible Perovskite Solar Cells through Cs—I Bond Weakening," *Advanced Energy Materials* 15 (2025): 2404293.

58. F. Yang, Y. Ruan, S. Li, et al., "A Flowing Liquid Phase Induces the Crystallization Processes of Cesium Lead Triiodide for 21.85%-efficiency Solar Cells and Low-energy Loss," *Energy & Environmental Science* 18 (2025): 1232.

59. X. Li, B. Ding, J. Huang, et al., "Visible Light-Triggered Self-Welding Perovskite Solar Cells and Modules," *Advanced Materials* 37 (2025): 2410338.

60. J.-D. Chen, H. Ren, F.-M. Xie, et al., "Harnessing Plasmon-exciton Energy Exchange for Flexible Organic Solar Cells with Efficiency of 19.5%.5%," *Nature Communications* 16 (2025): 3829.

61. H. Li, J. Le, H. Tan, et al., "Synergistic Multimodal Energy Dissipation Enhances Certified Efficiency of Flexible Organic Photovoltaics beyond 19%," *Advanced Materials* 37 (2025): 2411989.

62. J. Xia, J. Zhu, H. Chen, et al., "Smart Targeting Layer on Silver Nanowire Electrodes Achieving Efficiency Breakthroughs in ITO-Free Conventional Flexible Organic Solar Cells," *Angewandte Chemie International Edition* 64 (2025): 202501270.

63. Y. Sun, F. Li, H. Zhang, et al., "Flexible Perovskite/Silicon Monolithic Tandem Solar Cells Approaching 30% Efficiency," *Nature Communications* 16 (2025): 5733.

64. M. Li, H. Gao, L. Li, et al., "In Situ Coating Strategy for Flexible all-perovskite Tandem Modules," *Nature Photonics* 19 (2025): 1255.

65. J. Yu, J. Pu, D. Xie, et al., "Semitransparent Organic Photovoltaics with Wide Geographical Adaptability as Sustainable Smart Windows," *Nature Communications* 16 (2025): 7421.

66. J. Ding, H. Mou, H. Chen, et al., "Manipulating Molecular Stacking for Semitransparent Organic Photovoltaics Achieving Light Utilization Efficiency >6%," *Advanced Materials* 37 (2025): 2420439.

67. E. J. Stallknecht, C. K. Herrera, C. Yang, et al., "Designing Plant–transparent Agrivoltaics," *Scientific Reports* 13 (2023): 1903.

68. C. Han, Z. Jin, C. Shen, et al., "Green-Solvent-Processed Scalable Semi-Transparent Organic Solar Modules with 9.4% Efficiency and 42% Visible Transparency for Energy-Generating Windows," *Advanced Energy Materials* 15 (2025): 2501682.

69. S. Yang, X. Huang, Y. Cho, et al., "Efficient Semitransparent Organic Solar Modules with Exceptional Diurnal Stability through Asymmetric Interaction Induced by Symmetric Molecular Structure," *Angewandte Chemie International Edition* 64 (2025): 202424287.

70. K. Khandelwal, S. Biswas, and G. D. Sharma, "Advancements in Colorful Semitransparent Organic Solar Cells: Enhancing Aesthetic Appeal and Efficiency," *Solar RRL* 9 (2025): 2400676.

71. B. Deng, Y. Li, Z. Lu, et al., "The Art and Science of Translucent Color Organic Solar Cells," *Nature Communications* 16 (2025): 597.

72. J. Wu, M. Cao, X. Liu, et al., "PDINN Sandwiched Silver Nanowires for Solution-processed Semitransparent Organic Photovoltaics with over 4%

Light Utilization Efficiency and Nearly 100% Bifaciality Factor," *Journal of Energy Chemistry* 104 (2025): 1–9.

73. J. Barichello, G. Shankar, P. Mariani, A. Di Carlo, and F. Matteocci, "Unveiling the Potential of $Cs_2AgBiBr_6$ Perovskites for next-generation See-Through Photovoltaics," *Mater Today Energy* 46 (2024): 101725.

74. P. Chonlateeroj, S. Arunlimsawat, P. Janthakit, et al., "Excited-state Intramolecular Proton Transfer Derivatives as Self-absorption Free Luminophores for Luminescent Solar Concentrators," *Mater Chem Front* 9 (2025): 695.

75. P. Xia, Y. Chen, E. Zhang, et al., "Luminescent Solar Concentrators with Tunable Radiative Cooling and Self-Powered Heating for Synergizing Energy Harvesting and Room Temperature Regulation," *Adv Funct Mater* n/a (2025): 2504934.

76. M. V. Khenkin, E. A. Katz, A. Abate, et al., "Consensus Statement for Stability Assessment and Reporting for Perovskite Photovoltaics Based on ISOS Procedures," *Nature Energy* 5 (2020): 35.

77. B. Liu, O. J. Sandberg, J. Qin, et al., "Inverted Organic Solar Cells with an in Situ-derived SiOxNy Passivation Layer and Power Conversion Efficiency Exceeding 18%," *Nature Photonics* 19 (2025): 195.

78. J. Liu, Y. He, L. Ding, et al., "Perovskite/Silicon Tandem Solar Cells with Bilayer Interface Passivation," *Nature* 635 (2024): 596.

79. H. Zhu, B. Shao, Z. Shen, et al., "In Situ Energetics Modulation Enables High-efficiency and Stable Inverted Perovskite Solar Cells," *Nature Photonics* 19 (2025): 28.

80. W. Wu, H. Gao, L. Jia, et al., "Stable and Uniform Self-assembled Organic Diradical Molecules for Perovskite Photovoltaics," *Science* 389 (2025): 195.

81. J. Zhu, X. Huang, Y. Luo, et al., "Self-assembled Hole-selective Contact for Efficient Sn-Pb Perovskite Solar Cells and all-perovskite Tandems," *Nature Communications* 16 (2025): 240.

82. Y. Zhang, C. Li, H. Zhao, et al., "Synchronized Crystallization in Tin-lead Perovskite Solar Cells," *Nature Communications* 15 (2024): 6887.

83. M.-H. Lee, M. S. Kim, Y. J. Lee, et al., "Suppressing Hole Accumulation through Sub-Nanometer Dipole Interfaces in Hybrid Perovskite/Organic Solar Cells for Boosting near-Infrared Photon Harvesting," *Advanced Materials* 36 (2024): 2411015.

84. M. Pitaro, L. Di Mario, J. Pinna, et al., "Bulk Defects Passivation of Tin Halide Perovskite by Tin Thiocyanate," *Carbon Energy* 7 (2025): 710.

85. B. Li, Y. Yao, C. Kan, et al., "Promising Excitonic Absorption for Efficient Perovskite Solar Cells," *Joule* 9 (2025): 101780.

86. Q. Li, H. Liu, C.-H. Hou, et al., "Harmonizing the Bilateral Bond Strength of the Interfacial Molecule in Perovskite Solar Cells," *Nature Energy* 9 (2024): 1506.

87. Y. Wang, C. Lu, M. Liu, et al., "Solvent-assisted Reaction for Spontaneous Defect Passivation in Perovskite Solar Cells," *Nature Photonics* 19 (2025): 985.

88. Z. Qin, M. Chen, Z. Zhang, Y. Wang, and L. Han, "Eliminating High-dimensional Defects by Upward Unidirectional Crystallization for Efficient and Stable Inverted Perovskite Solar Cells," *Energy & Environmental Science* 18 (2025): 2264.

89. L. Ye, J. Wu, S. Catalán-Gómez, et al., "Superoxide Radical Derived Metal-free Spiro-OMeTAD for Highly Stable Perovskite Solar Cells," *Nature Communications* 15 (2024): 7889.

90. S. Yin, X. Luo, F. Tang, et al., "A Green-solvent-processable Polymer Hole Transport Material for Achieving 26.31% Efficiency in Inverted Perovskite Solar Cells," *Energy & Environmental Science* 18 (2025): 4153.

91. J. Zhang, R. Dai, J. Yang, et al., "Regulation of Crystallization by Introducing a Multistage Growth Template Affords Efficient and Stable Inverted Perovskite Solar Cells," *Energy & Environmental Science* 18 (2025): 3235.

92. Y. Luo, Y. Tian, K. Zhao, et al., "Inductive Effects in Molecular Contacts Enable Wide-bandgap Perovskite Cells for Efficient Perovskite/TOPCon Tandems," *Nature Communications* 16 (2025): 4516.

93. C. Shi, J. Wang, X. Lei, et al., "Modulating Competitive Adsorption of Hybrid Self-assembled Molecules for Efficient Wide-bandgap Perovskite Solar Cells and Tandems," *Nature Communications* 16 (2025): 3029.

94. Y. Han, J. Fu, Z. Ren, et al., "Inorganic Perovskite/Organic Tandem Solar Cells with 25.1% Certified Efficiency via Bottom Contact Modulation," *Nature Energy* 10 (2025): 513.

95. Z. Song, J. Wang, Y. Bao, et al., "Optimization of Crystallization Dynamics in Wide-bandgap Bromine–iodine Perovskite Films for High-performance Perovskite–organic Tandem Solar Cells," *Energy & Environmental Science* 18 (2025): 4883.

96. H. He, X. Li, J. Zhang, et al., "Dynamic Hydrogen-bonding Enables High-performance and Mechanically Robust Organic Solar Cells Processed with Non-halogenated Solvent," *Nature Communications* 16 (2025): 787.

97. H. Chen, Y. Huang, R. Zhang, et al., "Organic Solar Cells with 20.82% Efficiency and High Tolerance of Active Layer Thickness through Crystallization Sequence Manipulation," *Nature Materials* 24 (2025): 444.

98. X. Sun, F. Wang, G. Yang, et al., "From 20% Single-junction Organic Photovoltaics to 26% Perovskite/Organic Tandem Solar Cells: Self-assembled Hole Transport Molecules Matter," *Energy & Environmental Science* 18 (2025): 2536.

99. J. Dong, Y. Li, C. Liao, et al., "Dielectric Constant Engineering of Nonfullerene Acceptors Enables a Record Fill Factor of 83.58% and a High Efficiency of 20.80% in Organic Solar Cells," *Energy & Environmental Science* 18 (2025): 4982.

100. Y. Jiang, K. Liu, F. Liu, et al., "20.6% Efficiency Organic Solar Cells Enabled by Incorporating a Lower Bandgap Guest Nonfullerene Acceptor without Open-Circuit Voltage Loss," *Advanced Materials* 37 (2025): 2500282.

101. Y. Xie, J. Tian, X. Yang, et al., "Thiophene Expanded Self-Assembled Monolayer as Hole Transport Layer for Organic Solar Cells with Efficiency of 20.78%.78%," *Advanced Materials* 37 (2025): 02485.

102. J. Zhou, X. Zhou, H. Jia, et al., "20.0% efficiency of Ternary Organic Solar Cells Enabled by a Novel Wide Band Gap Polymer Guest Donor," *Energy & Environmental Science* 18 (2025): 3341.

103. Y. Fu, L. Xu, Y. Li, et al., "Enhancing Inter-domain Connectivity by Reducing Fractal Dimensions: The Key to Passivating Deep Traps in Organic Photovoltaics," *Energy & Environmental Science* 17 (2024): 8893.

104. C. Li, G. Yao, X. Gu, et al., "Highly Efficient Organic Solar Cells Enabled by Suppressing Triplet Exciton Formation and Non-radiative Recombination," *Nature Communications* 15 (2024): 8872.

105. N. Wei, H. Lu, Y. Wei, et al., "Constructing a Dual-fiber Network in High Efficiency Organic Solar Cells via Additive-induced Supramolecular Interactions with both Donor and Acceptor," *Energy & Environmental Science* 18 (2025): 2298.

106. C. Sun, J. Wang, F. Bi, et al., "Non-fused Core-linked Star-shaped Oligomer Acceptors for Stable Binary Organic Solar Cells with over 19% Efficiency," *Energy & Environmental Science* 18 (2025): 862–873.

107. Z. Zhao, S. Chung, L. Tan, et al., "Molecular Order Manipulation with Dual Additives Suppressing Trap Density in Non-fullerene Acceptors Enables Efficient Bilayer Organic Solar Cells," *Energy & Environmental Science* 18 (2025): 2791.

108. J. Liu, R. Wang, L. Li, et al., "Fine-tuning central Extended Unit Symmetry via Atom-level Asymmetric Molecular Design Enables Efficient Binary Organic Solar Cells," *Energy & Environmental Science* 18 (2025): 4470.

109. X. Liang, X. Wang, Q. Chang, et al., "Reduction of Bulk and Interface Defects via Photo-annealing Treatment for High-efficiency Antimony Selenide Solar Cells," *Energy & Environmental Science* 17 (2024): 9499.

110. T. Wu, S. Chen, Z. Su, et al., "Heat Treatment in an Oxygen-rich Environment to Suppress Deep-level Traps in Cu2ZnSnS4 Solar Cell with 11.51% Certified Efficiency," *Nature Energy* 10 (2025): 630.

111. A. S. Subbiah, S. Mannar, V. Hnapovskyi, et al., "Efficient Blade-coated Perovskite/Silicon Tandems via Interface Engineering," *Joule* 9 (2025): 101767.

112. Z. Li, Z. Wei, X. Sun, et al., "Nanocrystal-Nucleus Template Strategy for Efficient Wide-Bandgap Perovskite Solar Cells with Enhanced Homogeneity and Energy-Level Alignment," *Advanced Materials* 37 (2025): 2509202.

113. Z. Liu, S. Yang, Y. Tian, et al., "Homogeneity Regulation in Sequential Fabricated Perovskite Film for Industrial-Scale Deposition of Fully-Textured Perovskite/Silicon Tandem Cells," *Advanced Materials* (2025): 11177.

114. C. Kan, P. Hang, S. Wang, et al., "Efficient and Stable Perovskite-silicon Tandem Solar Cells with Copper Thiocyanate-embedded Perovskite on Textured Silicon," *Nature Photonics* 19 (2025): 63–70.

115. Z. Zhang, Y. Feng, J. Ding, et al., "Rationally Designed Universal Passivator for High-performance Single-junction and Tandem Perovskite Solar Cells," *Nature Communications* 16 (2025): 753.

116. X. Liu, M. Rienäcker, M. Gholipoor, et al., "Charge Carrier Management for Highly Efficient Perovskite/Si Tandem Solar Cells with Poly-Si Based Passivating Contacts," *Energy & Environmental Science* 18 (2025): 5599.

117. R. Li, D. Zhang, J. Wei, et al., "n-type Regulation of 2D Perovskite Interlayers for Efficient Perovskite-silicon Tandem Solar Cells," *Joule* 9 (2025): 102141.

118. B. P. Kore, O. Er-raji, O. Fischer, et al., "Efficient Fully Textured Perovskite Silicon Tandems with Thermally Evaporated Hole Transporting Materials," *Energy & Environmental Science* 18 (2025): 354.

119. W. Wang, H. Liang, Y. Ding, et al., "Super -Hydrophilic SAMs via Chlorine Substituted all-Hydrophilic Molecule Modification for Monolithic Perovskite-Silicon Tandem Solar Cells," *Advanced Energy Materials* (2025): 02222.

120. H. Du, J. Li, Z. Ma, et al., "Suppressing Halide Segregation via Dual-Anchoring Strategy for 31.20% Perovskite/Silicon Tandem Solar Cells," *Advanced Energy Materials* (2025): 03565.

121. L. Tang, H. Yan, L. Zeng, et al., "Record-Efficient Flexible Monolithic Perovskite–CIGS Tandem Solar Cell with V OC Exceeding 1.8 V on Polymer Substrate," *Advanced Energy Materials* 15 (2025): 2403682.

122. H. Guan, S. Fu, G. Zeng, et al., "Efficient 1.77 eV-bandgap Perovskite and all-perovskite Tandem Solar Cells Enabled by Long-alkyl Phosphonic Acid," *Energy & Environmental Science* 17 (2024): 8219.

123. W. Chen, S. Zhou, H. Cui, et al., "Universal in Situ Oxide-based ABX3-structured Seeds for Templating Halide Perovskite Growth in all-perovskite Tandems," *Nature Communications* 16 (2025): 1894.

124. J. Wang, B. Jiao, R. Tian, et al., "Less-acidic Boric Acid-functionalized Self-assembled Monolayer for Mitigating NiOx Corrosion for Efficient all-perovskite Tandem Solar Cells," *Nature Communications* 16 (2025): 4148.

125. Y. Zhao, T. Ma, X. Yin, et al., "Interface Parallel Dipole Regulation in all-perovskite Tandem Solar Cells," *Energy & Environmental Science* 18 (2025): 8527.

126. J. Wang, B. Branco, W. H. M. Remmerswaal, et al., "Performance and Stability Analysis of all-perovskite Tandem Photovoltaics in Light-driven Electrochemical Water Splitting," *Nature Communications* 16 (2025): 174.

127. Y. Liu, T. Ma, C. Wang, et al., "Synergistic Immobilization of Ions in Mixed Tin-lead and all-perovskite Tandem Solar Cells," *Nature Communications* 16 (2025): 3477.

128. Z. Wei, Q. Zhou, X. Niu, et al., "Surpassing 90% Shockley–Queisser VOC Limit in 1.79 eV Wide-bandgap Perovskite Solar Cells Using Bromine-substituted Self-assembled Monolayers," *Energy & Environmental Science* 18 (2025): 1847.

129. C. Ge, Q. Xu, D. Liu, et al., "Light Radiation Annealing Enables Unidirectional Crystallization of Vacuum-assisted Sn–Pb Perovskites for Efficient Tandem Solar Cells," *Energy & Environmental Science* 18 (2025): 430.

130. C. Duan, K. Zhang, Z. Peng, et al., "Durable All-inorganic Perovskite Tandem Photovoltaics," *Nature* 637 (2025): 1111.

131. X. Jiang, S. Qin, L. Meng, et al., "Isomeric Diammonium Passivation for Perovskite–organic Tandem Solar Cells," *Nature* 635 (2024): 860–866.

132. Y. An, N. Zhang, Q. Liu, et al., "Balancing Carrier Transport in Interconnection Layer for Efficient Perovskite/Organic Tandem Solar Cells," *Nature Communications* 16 (2025): 2759.

133. M. Chen, Y. Li, Z. Zeng, et al., "Regulating the Crystallization of Mixed-halide Perovskites by Cation Alloying for Perovskite–organic Tandem Solar Cells," *Energy & Environmental Science* 17 (2024): 9580.

134. Z. He, R. Yu, Y. Dong, R. Wang, Y. Zhang, and Z. A. Tan, "Minimized Optical/Electrical Energy Loss for 25.1% Monolithic Perovskite/Organic Tandem Solar Cells," *Nature Communications* 16 (2025): 1773.

135. J. Zheng, W. Chen, Z. Wang, et al., "Selective Crystallization Delay in Wide-Bandgap Perovskites Enables Initial Homogeneous Phase for Square Centimeter Perovskite/Organic Tandem Solar Cells," *Advanced Materials* 37 (2025): 10437.

136. Q. Ye, B. Fan, Y. Zhou, et al., "Competitive Crystallization Modulated Phase-Homogeneous Wide-Bandgap Perovskites for Monolithic Perovskite-Organic Tandem Solar Cells," *Advanced Materials* 37 (2025): 11781.

137. C. Wang, C. Gong, W. Ai, et al., "A Wenzel Interfaces Design for Homogeneous Solute Distribution Obtains Efficient and Stable Perovskite Solar Cells," *Advanced Materials* 37 (2025): 2417779.

138. Z. Li, C. Jia, Z. Wan, et al., "Boosting Mechanical Durability under High Humidity by Bioinspired Multisite Polymer for High-efficiency Flexible Perovskite Solar Cells," *Nature Communications* 16 (2025): 1771.

139. Z. Xu, R. Yu, T. Xue, et al., "Stress Release via Thermodynamic Regulation towards Efficient Flexible Perovskite Solar Cells," *Energy & Environmental Science* 18 (2025): 4324.

140. Z. Li, C. Jia, H. Wu, et al., "In-Situ Cross-Linked Polymers for Enhanced Thermal Cycling Stability in Flexible Perovskite Solar Cells," *Angewandte Chemie International Edition* 64 (2025): 202421063.

141. W. Zhang, J. Liu, W. Song, et al., "Chemical Passivation and Grain-boundary Manipulation via in Situ Cross-linking Strategy for Scalable Flexible Perovskite Solar Cells," *Science Advances* 11 (2025): adr2290.

142. Z. Skafi, L. A. Castriotta, B. Taheri, et al., "Flexible Perovskite Solar Cells on Polycarbonate Film Substrates," *Advanced Energy Materials* 14 (2024): 2400912.

143. H. Liu, Z. Zhang, J. Xu, et al., "Selective Chemical Etching to Remove 0D Cs 4 Pb(IBr) 6 from Mixed-Dimensional Perovskite Surface Achieving High Efficiency Flexible All-Inorganic Perovskite Solar Cells with Superior Mechanical Durability," *Advanced Energy Materials* 14 (2024): 2402142.

144. Q. Ye, W. Song, Y. Bai, et al., "The Butterfly-effect of Flexible Linkers in Giant-molecule Acceptors: Optimized Crystallization and Aggregation for Enhancing Mechanical Durability and Approaching 19% Efficiency in Binary Organic Solar Cells," *Energy & Environmental Science* 18 (2025): 4373.

145. Z. Xiao, J. Liu, X. Chen, et al., "Ultra-flexible Organic Solar Cells Based on Eco-friendly Cellulose Substrate with Efficiency Approaching 19%," *Journal of Materials Chemistry A* 13 (2025): 2301.

146. R. Ding, S. Wang, Z. Yang, et al., "Ternary Strategy for Energy Loss Suppression toward Efficient Rigid and Flexible Organic Solar Cells," *Journal of Materials Chemistry A* 13 (2025): 33356.

147. S. Zeng, H. Li, S. Liu, et al., "Interface Design Based on Strain Isolation Theory with an Optimized Neutral Mechanical Plane Enables Highly

Ductile and Flexible Organic Photovoltaics," *Energy & Environmental Science* 18 (2025): 2318.

148. J.-W. Lee, E. S. Oh, S. Lee, et al., "Strain-induced Power Output Enhancement in Intrinsically Stretchable Organic Solar Cells," *Joule* 9 (2025): 101792.

149. J. Wang, C. Sun, Y. Li, et al., "Polymer-Like Tetramer Acceptor Enables Stable and 19.75% Efficiency Binary Organic Solar Cells," *Nature Communications* 16 (2025): 1784.

150. M. M. A. Mahmoud, N. Fayzullaev, R. A. Ibrahem, et al., "Fabrication of CF/WS_2/MoS_2 Composite Counter Electrodes for Enhancing Efficiency in fiber-shaped Dye-sensitized Solar Cells (FDSSCs)," *Journal of Alloys and Compounds* 1010 (2025): 177276.

151. A. Ahmad, B. M. Alshehri, P. Kanjariya, et al., "Newly Formed Carbon Nanotubes as Counter Electrodes for Wire-shaped Dye-sensitized Solar Cells (WDSSCs)," *Nanotechnology* 36 (2025): 105602.

152. H. Shishido, R. Sato, D. Ieki, et al., "High-Efficiency Perovskite/Silicon Tandem Solar Cells with Flexibility," *Solar RRL* 9 (2025): 2400899.

153. I. Jeong, T. K. Lee, H. Van Tran, et al., "Flexible and Lightweight Perovskite/Cu(In,Ga)Se_2 Tandem Solar Cells," *Joule* 9 (2025): 101794.

154. W. Tian, L. Yao, E. Bi, et al., "Inert Interlayer Secures Flexible Monolithic Perovskite/CIGS Tandem Solar Cells with Efficiency beyond 21%," *ACS Energy Letters* 10 (2025): 562–568.

155. L. Geng, Y. Ma, Y. Sun, et al., "Bilateral Anchoring for Enhanced Mechanical Stability and Efficiency in Flexible All-Perovskite Tandem Solar Cells," *Advanced Materials* 37 (2025): 2419018.

156. Y. Zhang, Q. Sun, W. Xie, et al., "Flexible CZTSSe Solar Cells with 11.21% Efficiency Enabled by O-doped CZTSSe/CdS Heterojunction," *Journal of Energy Chemistry* 105 (2025): 806–813.

157. H. Xu, R. Meng, X. Xu, et al., "Facile Tailor on the Surface of Mo Foil toward High-Efficient Flexible CZTSSe Solar Cells," *Small Methods* 9 (2025): 2401084.

158. D. De Luca, J. S. Lee, H. A. Dewi, et al., "Buffer-Layer-Free Semitransparent Perovskite Solar Cells with Soft Sputtered Electrodes Optimized via Design of Experiments," *ACS Energy Letters* 10 (2025): 2236.

159. Q. Han, Y.-T. Hsieh, L. Meng, et al., "High-performance Perovskite/Cu(In,Ga)Se2 Monolithic Tandem Solar Cells," *Science* 361 (2018): 904–908.

160. S. Du, Y. Guo, C. Wang, et al., "Improving Crystallization of Wide-Bandgap Lead Halide Perovskite for all-perovskite Tandems," *Advanced Energy Materials* 15 (2025): 2404180.

161. H. Shi, T. Xie, D. Li, et al., "Defect Passivation Engineering for Achieving 4.29% Light Utilization Efficiency MA-free Wide-bandgap Semi-transparent Perovskite Solar Cells," *Chemical Engineering Journal* 500 (2024): 156962.

162. H. Lai, J. Luo, Y. Zwirner, et al., "High-Performance Flexible All-Perovskite Tandem Solar Cells with Reduced VOC -Deficit in Wide-Bandgap Subcell," *Advanced Energy Materials* 12 (2022): 2202438.

163. S. Lie, A. Bruno, L. H. Wong, and L. Etgar, "Semitransparent Perovskite Solar Cells with >13% Efficiency and 27% Transperancy Using Plasmonic Au Nanorods," *ACS Applied Materials & Interfaces* 14 (2022): 11339.

164. Y. Li, J. Wang, C. Yan, et al., "Optical and Electrical Losses in Semitransparent Organic Photovoltaics," *Joule* 8 (2024): 527–541.

165. J. Huang, Z. Lu, J. He, et al., "Intrinsically Stretchable, Semitransparent Organic Photovoltaics with High Efficiency and Mechanical Robustness via a Full-solution Process," *Energy & Environmental Science* 16 (2023): 1251.

166. J. Xie, J. Zhao, Z. Zhou, et al., "Multifunctional Ternary Semitransparent Organic Solar Cell Module with Area above 100 cm2 and Average Visible Transmittance above 30%," *Energy & Environmental Science* 17 (2024): 7681.

167. K. Khandelwal, S. Biswas, and G. D. Sharma, "Advancing Multifunctional Semitransparent Organic Solar Cells through Strategic Optical Layer Integration," *ACS Applied Energy Materials* 7 (2024): 7085.

168. N. Zhang, Z. Zhou, Y. An, et al., "Modeling-Guided Design of Semitransparent Organic Photovoltaics with Improved Energy Harvesting and Saving Capabilities," *Advanced Energy Materials* (2024): 2404129.

169. W. Xu, H. Zhou, H. Tian, et al., "Achieving Light Utilization Efficiency of 3.88% and Efficiency of 14.04% for Semitransparent Layer-by-layer Organic Solar Cells by Diluting Donor Layer," *Chemical Engineering Journal* 508 (2025): 161148.

170. T. Xu, B. Deng, Y. Zhao, et al., "High-Throughput Computing Guided Low/High Index Optical Coupling Layer for Record-Performance Semitransparent Organic Solar Cells," *Advanced Energy Materials* 13 (2023): 2301367.

171. Z. You, J. Wen, W. Liu, et al., "Transparent and Conductive Polyimide-Ionene Hybrid Interlayers for High Performance and Cost-Effective Semitransparent Organic Solar Cells," *Advanced Materials* 37 (2025): 2500450.

172. M. Zhao, J. Wu, H. Tang, et al., "A Novel Ultra-Thin and Smooth Sm:Ag Composite Electrode with High Visible Transmittance Enables Efficient Color-Neutral Semitransparent Organic Solar Cells," *Advanced Optical Materials* 12 (2024): 2401776.

173. Z. Wu, B. Shi, J. Yu, et al., "Human-friendly Semitransparent Organic Solar Cells Achieving High Performance," *Energy & Environmental Science* 17 (2024): 6013.

174. X. Huang, Y. Cheng, Y. Fang, et al., "A Molecular Weight-regulated Sequential Deposition Strategy Enabling Semitransparent Organic Solar Cells with the Light Utilization Efficiency of over 5%," *Energy & Environmental Science* 15 (2022): 4776.

175. J. Yang, J. Li, Y. Gu, et al., "Amorphous Indium–zinc Oxide Layer with Transport and Protective Dual-function for High-efficiency Semitransparent and Tandem Sb 2 (S,Se) 3 Solar Cells," *Energy & Environmental Science* 18 (2025): 4833.

176. T. Zhang, T. Liu, X. Wang, et al., "Surface Lattice Engineering Enables Efficient Inverted Perovskite Solar Cells," *Advanced Energy Materials* 15 (2025): 2403554.

177. H. Xu, Z. Liang, J. Ye, et al., "Constructing Robust Heterointerfaces for Carrier Viaduct via Interfacial Molecular Bridges Enables Efficient and Stable Inverted Perovskite Solar Cells," *Energy & Environmental Science* 16 (2023): 5792.

178. K. Feng, G. Wang, Q. Lian, et al., "Non-fullerene Electron-transporting Materials for High-performance and Stable Perovskite Solar Cells," *Nature Materials* 24 (2025): 770.

179. H. Chen, Q. Cao, X. Pu, et al., "Strong Coupling of NiOx and Self-Assembled Molecules via Inserted Reductant for High-Performance Inverted Perovskite Solar Cells," *Advanced Materials* 37 (2025): 10553.

180. S. Luo, S. Cao, T. Zheng, et al., "Melamine Holding PbI2 with Three "Arms": An Effective Chelation Strategy to Control the Lead Iodide to Perovskite Conversion for Inverted Perovskite Solar Cells," *Energy & Environmental Science* 18 (2025): 2436.

181. Y. Zhao, Y. Liu, Z. Ren, et al., "Enhanced Interface Adhesion with a Polymeric Hole Transporter Enabling High-performance Air-processed Perovskite Solar Cells," *Energy & Environmental Science* 18 (2025): 1366.

182. Z. Lv, Z. Wang, G. Liu, et al., "Pre-Anchored Ionic Bond Mediators Enabling Controllable Monolayer Assembly for High-Performance Perovskite Solar Cells and Modules," *Advanced Materials* (2025): 13600.

183. L. Zheng, M. Wei, F. T. Eickemeyer, et al., "Strain-induced Rubidium Incorporation into Wide-bandgap Perovskites Reduces Photovoltage Loss," *Science* 388 (2025): 88.

184. S. Yang, M. Wu, X. Lei, et al., "Ultra-High 1.27 V V_{OC} of Pure $CsPbI_3$ Perovskite Solar Cells with an Efficiency of 21.8%," *ACS Energy Lett* 9 (2024): 4817.

185. K. Sun, Y. Wang, G. Zhang, et al., "20.64% Efficient and Stable Binary Organic Solar Cells via Thermodynamic-Engineered Interlayer Diffusion and Exciton Generation," *Advanced Materials* (2025): 09806.

186. S. Li, X. Yang, S. Cheng, et al., "Solvent Engineering Enables Tin-lead Perovskite Films with Long Carrier Diffusion Lengths and Reduced Tin Segregation," *Nature Communications* 16 (2025): 8072.

187. W. Chen, Y. Zhu, J. Xiu, et al., "Monolithic Perovskite/Organic Tandem Solar Cells with 23.6% Efficiency Enabled by Reduced Voltage Losses and Optimized Interconnecting Layer," *Nature Energy* 7 (2022): 229–237.

Supporting Information

Additional supporting information can be found online in the Supporting Information section.

Supporting File: aenm70490-sup-0001-SuppMat.docx